ORGANIC SEMICONDUCTOR SENSORS FOR DETECTING AIRBORNE CHEMICALS

by

Benjamin R. Bunes

A dissertation submitted to the faculty of
The University of Utah
in partial fulfillment of the requirements for the degree of

Doctor of Philosophy

Department of Materials Science and Engineering

The University of Utah

August 2015

The University of Utah Graduate School

STATEMENT OF DISSERTATION APPROVAL

The dissertation of **Benjamin R. Bunes**

has been approved by the following supervisory committee members:

Ling Zang	, Chair	**6/15/2015** Date Approved
Feng Liu	, Member	**6/18/2015** Date Approved
Rajesh Menon	, Member	**6/15/2015** Date Approved
Marc Porter	, Member	**6/15/2015** Date Approved
Michael Scarpulla	, Member	**6/15/2015** Date Approved

and by **Feng Liu** , Chair/Dean of

the Department/College/School of **Materials Science and Engineering**

and by David B. Kieda, Dean of The Graduate School.

ABSTRACT

Organic semiconductors offer tremendous potential for detecting airborne chemicals. Planar, π-conjugated molecules, such as perelyene diimide derivatives, are especially appealing because they can form nanofibers through self-assembly. Depositing these structures onto a substrate creates a porous network. This network is easily penetrable and offers a large surface area for interaction with the target chemical, leading to enhanced sensitivity when used as a gas sensor. Furthermore, the π-conjugation provides electronic conductivity, which enables the use of these materials as chemiresistors. Finally, because the building blocks are organic molecules, there are virtually limitless structural possibilities; molecules can be engineered to interact with a specific chemical by modifying the side groups. Using these materials, our group has demonstrated vapor-phase detection of explosives, chemical warfare agents, narcotics, and toxic gases at concentrations extending into the low parts per trillion range.

While organic semiconductors have many strengths, major barriers have limited their utility to the lab. First, the conductivity is intrinsically low. Oftentimes, it is too low to be read by commercial electronics (picoampere scale). Secondly, because of the random way the nanofibers deposit, device-to-device variation is difficult to control. In this dissertation, we will discuss early-stage work to address these issues. Three strategies were investigated and will be presented: 1) integrating sensor molecules with conductive materials, 2) integrating sensor molecules with conductive devices, and 3) controlled deposition to align the nanofibers across the electrode gap. In the first strategy, we explore the fundamental properties of the sensing material interface

with carbon nanotubes. The formation of charge transfer complexes and unexpected charge transfer were observed. Next, sensor molecules were used to gate field effect transistors. The result is a sensitive, selective device compatible with production-scale manufacturing. Finally, we will discuss nanofiber alignment using dielectrophoresis. Removing the randomness from deposition is a potential means to reduce device-to-device variation while increasing the conductivity. These investigations may produce a route from the lab to the real world for sensors based on organic semiconductors.

CONTENTS

LIST OF FIGURES

LIST OF TABLES

ACKNOWLEDGMENTS

First and foremost, I would like to thank Prof. Ling Zang for all of his support and advice over the past six years. I would also like to thank the rest of the Zang Lab, including: Dr. Xioamei Yang, Dr. Yanke Che, Dr. Zengxing Zhang, Dr. Chengyi Zhang, Dr. Ligui Li, Dr. Jimin Han, Dr. Helin Huang, Dr. Miao Xu, Bennion Redd, Daniel L. Jacobs, Yaqiong Zhang, Chen Wang, Na Wu, Ryan Snowball, Marc Warren, Cole Castleton, and Trevor Knowlton. I would especially like to thank Zengxing for all of the time he spent training me on the methods and equipment used in this work.

I would also like to thank my advisory committee for all of their suggestions and assistance. Prof. Feng Lui, Prof. Rajesh Menon, Prof. Marc Porter, and Prof. Michael Scarpulla – thank you!

Additionally, the NASA team has been tremendously helpful. I would like to thank my collaborators, Dr. Azlin Biaggi-Labiosa and Dr. Jing Li. During my visits at the NASA Glenn and Ames Research Centers, a large number of people provided assistance, including Gordon Berger, Dr. Gary Hunter, Dr. Larry Matus, David Spry, Dr. Ami Hannon, and Dr. Meyya Meyyappan. I would also like to thank the Claudia Meyer and the NSTRF team for all of their hard work administrating my fellowship. Finally, I am grateful to Katie Kragh-Buetow and Adriana Popa for sharing their experience with me as interns at the NASA Glenn Research Center and NASA Ames Research Center, respectively.

The staff members of the Nanofab, Micron Microscopy Core, and Dixon Laser Institute also contributed greatly to this work. Specifically, I would like to thank Brian Baker, Steve Pritchett, Charles Fisher, Tony Olsen, Dr. Ian Harvey, Dr. Brian

van Devener, Dr. Randy Polson, and Dr. Matt DeLong.

Much of this work was performed in collaboration with Vaporsens. Specifically, I would like to thank Paul Slattum for his help synthesizing molecules and Paul Allen for developing the hardware for my sensors. Ben Rollins also deserves special credit for providing me with some very interesting opportunities, including presenting at CES 2015! I would also like to thank Josh Heiner, Scott Coburn, Charles McGuire, Rich Sisson, Greger Andersson, and Dr. Yin Sun.

I would also like to thank the Nano Institute of Utah, particularly Dr. Michael Granger, BJ Warner, Margaret Tennant, and Kathy Winkley for the various help they have provided including everything from assistance in the lab to grant administration.

The MSE Department Office staff has been very helpful. Thank you, Josh Hansen, Ashley Quimby, and Marilyn Bishop. I would also like to thank other department faculty members who have helped me along the way, including Prof. Ashutosh Tiwari, Prof. Gerald Stringfellow, and Prof. Taylor Sparks.

Of course, all of this started long before I joined the University of Utah. I would like to thank Jim Libous, Dr. Mark Hakey, Dr. Steve Holmes, Dr. John Arnold, and Dr. Dave Horak at IBM for providing me my first exposure to nanotechnology. I would also like to thank Prof. Palma Catravas, Prof. Mike Hagerman, and Prof. Kelly Black for giving me my first experiences in academic research.

Funding for this work was provided by the National Aeronautics and Space Administration Office of the Chief Technologist (NNX12AM67H) through the Space Technology Research Fellowship, the National Science Foundation Integrative Graduate Education and Research Traineeship (DGE 0903715), and the Wayne Brown Fellowship. Additional support was provided by the Department of Homeland Security (2009-ST-108-LR0005), National Science Foundation (CHE 0931466), and Utah Science, Technology, and Research initiative.

Finally, I would like to thank my family for their continued love and support

throughout my long educational journey. Thank you, Mom, Dad, Bruce, and Candi! And I extend a special thanks to my lovely girlfriend, Kelley Kowalski.

CHAPTER 1

SENSORS FOR AIRBORNE CHEMICALS

Detecting airborne chemicals is a global challenge. From locating illicit materials to monitoring air pollution, this field has the potential to improve lives everywhere. Other benefits include low-cost medical diagnostics and improved food security. However, approaching these applications is difficult. The major challenge is the complexity of the environment. Air itself is a mixture of gases, but there are also many interferents from manmade sources capable of producing false positives. A sensor used to identify a house in which methamphetamine is produced must not be triggered by a freshly-fertilized lawn, for example (methamphetamine and ammonia give similar responses on many sensors). Thus, selectivity is a critical parameter preventing wide-spread sensor use. Improvement of chemical sensors will have a very profound effect on the world.

1.1 Industry Needs

The industry needs for chemical sensing are vast and vary greatly. The defense industry requires extreme sensitivity to detect low vapor-pressure explosives (parts per quadrillion to parts per trillion), while only parts per million sensitivity is required for most safety applications. Detection accuracy is incredibly important for medical diagnostics, but less so for security. The requirements for a number of industries are presented here, although it is admittedly incomplete. These industry examples were selected to provide the reader a sense of practical applications for the work described in this dissertation.

Since developing new sensors has the potential to improve lives on the global scale, there is tremendous market potential. In fact, the total sensor market is $52.9B, largely comprised of the defense and security, air quality, and food and safety industries (Figure 1.1). This market is quite large, providing strong economic incentive for this work.

1.1.1 Defense and Security

Explosives detection is of critical importance to the United States and its allies. Overseas, the number of military casualties from explosive devices is staggering. As of 2007, 63% of American fatalities in Iraq and 41% of those in Afghanistan resulted from explosive devices. In addition to explosives, soldiers also face chemical warfare agents. Although they are no longer in use by most national militaries, militant

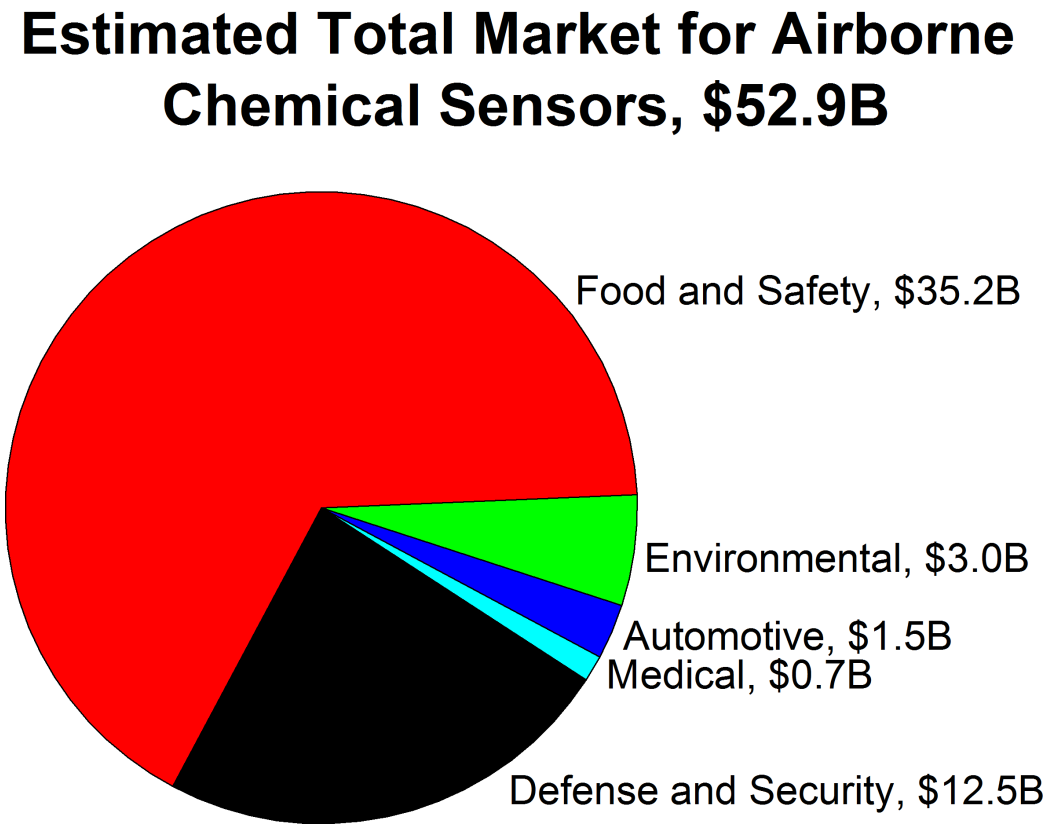

Figure 1.1. Total market size for various industries with a high demand for chemical sensors.

organizations such as the Islamic State, al Qaeda, and the Taliban will use them if they can be acquired. Detecting these materials is a major priority for the Department of Defense. Explosives detection is a $0.8B market [1].

In addition to explosives, narcotics detection is a major challenge. For example, methamphetamine is currently being smuggled into the United States at record levels. Right now, illicit drugs are detected largely by tracking the raw materials. However, possessing the raw materials is not illegal and may not provide sufficient grounds for a warrant to be issued. Therefore, there is significant interest in being able to detect narcotics or intermediaries in their manufacturing process. In fact, the Defense Threat Reduction Agency recently awarded two Utah companies, Vaporsens and Torion, $2.4M to develop a sensor system with these capabilities. The market for narcotics detection is approximately $2.6B [2].

Civilians are also threatened by explosive devices. Any major event can be a target. For example, there was an attempted attack using explosives at the Christmas tree lighting ceremony in Portland, Oregon, in 2010. Populated buildings can also be a major target, as seen in the famous Oklahoma City Bombing in 1995, which claimed 168 lives. Public transportation is particularly vulnerable, with over 1200 attacks recorded over the past 40 years – one every ten days! These can be major attacks, including those in Madrid (2004, 192 fatalities), London (2005, 52 fatalities), Mumbai (2006, 209 fatalities), and Moscow (2010, 40 fatalities). Securing public transportation is estimated to be an $7.3B market [3]. With similar needs, airport security is a $1.8B market [4].

1.1.2 Automotive

A major need in the automotive industry is ability to monitor air quality in the passenger cabin. Independent studies have shown concentrations of carbon monoxide, hydrocarbons, volatile organic compounds (VOCs), and nitrogen oxides (NO_x) exist at levels higher than the standards set by the Occupational Safety and Health

Administration (OSHA). In addition to toxicity, these gases can cause drowsiness, which imposes additional danger to the driver and anyone nearby. However, cabin air monitoring is not available in many vehicles, particularly those manufactured in the United States. Those that do have monitoring use sensors based on metal oxides. These sensors have several major drawbacks, which will be described in Section 1.2.8.2. The automobile cabin air monitoring market is around $1.5B [5].

1.1.3 Environmental Monitoring

Air pollution is an increasing concern. While developed nations are working diligently to reduce industrial emissions, many developing nations have deteriorating air quality, such as China and India. Rapid industrialization with a lack of environmental protection laws is a major contributor. Poor air quality contributes to numerous health issues, including asthma, chronic bronchitis, and lung cancer. While pollution is currently monitored by counting soot particles, there is little monitoring of chemicals. Hazardous chemicals in air pollution include carbon monoxide, nitrogen oxides, hydrogen cyanide, and hydrogen sulfide. The market for air pollution monitoring is an estimated $3B [5].

1.1.4 Food and Safety

With increasing population, efficient use of food is more important than ever. In the United States, roughly 30% of all food produced is lost to spoilage. Making matters worse, when food spoils, it releases ethylene, which is itself a spoiling agent. The ethylene released from spoiled food can cause nearby foods to go bad. Detecting ethylene early would enable spoiling foods to be removed before they can threaten the total supply. The market for food spoilage sensors is estimated to be $30.4B [6].

Many gas sensors in use today are applied to industrial safety. Toxic industrial chemicals (TICs) – including hydrogen sulfide, chlorine, and carbon monoxide – are heavily regulated. Most sensors currently in use are based on inexpensive electrochemical cells. While these sensors are effective, their sensitivity is inadequate. Typically,

the detection limit for a given sensor is equal to the OSHA exposure limit for a particular chemical. There is no warning that gases are approaching a dangerous level. When toxic gases are detected, the affected area must be evacuated because there is inadequate time to mitigate the hazard. This costs companies significant productivity and presents potential danger to employees. The current market for TIC sensors is $1.7B [7].

Indoor air quality is a growing concern. With increasing building efficiency, indoor air quality is degrading. Because of better sealing, the air turnover rate in a modern building is a mere 20% of the rate in older buildings. Furthermore, urbanization is increasing the population density; more people are living in closer quarters. Since most indoor air pollution is caused by human activities, such as cooking, increased housing density (*i.e.*, high-rise apartments and condominiums) exacerbates the situation. Pollutants including carbon monoxide, sulfur oxides, nitrogen oxides, VOCs, hydrogen cyanide, and hydrogen sulfide pose a serious threat to all of a building's occupants. This market is estimated to be $3.1B today, increasing to $5.6B by 2020 [5].

1.1.5 Aerospace

The aerospace industry is poised for major expansion over the next few decades. While air travel is a popular form of long-distance travel, the burgeoning space tourism market promises to make space travel nearly as routine. With increasing flight durations, air quality monitoring becomes more important. A variety of toxic gases can accumulate, including hydrogen cyanide, hydrogen sulfide, and nitrogen dioxide. These chemicals are dangerous in concentrations as low as 5 ppm. Detecting these chemicals is critical for the safety of the aircraft, crew, and passengers. The aerospace market for sensors is expected to be small due to low volumes, valued at $300,000 [5].

1.1.6 Medical

Chemical sensors may also have a major impact in medical diagnostics. Certain diseases change the chemical composition of an infected person's breath. For example, diabetics show an elevated concentration of acetone. A breath test represents a potential low-cost, rapid method to test patients for various medical issues. Diseases with known breath signatures include diabetes, lung cancer, colorectal cancer, breast cancer, liver disease, and tuberculosis [8]. Medical diagnostics is a market valued at $0.7B today and is expected to increase tenfold by 2020 [9].

1.2 Current Techniques

With a large number of potential applications and intriguing market opportunities, it is not surprising that a large number of sensing techniques have been developed. These techniques range from modified tools commonly used in analytic chemistry to novel nanomaterials and nanodevices. While some techniques have achieved commercial success, such as handheld ion mobility spectrometers in the defense industry and electrochemical cells for occupational safety, no appropriate sensors exist for a number of other applications. Here, various sensing techniques will be introduced, along with their strengths and shortcomings.

1.2.1 Canines

Dogs are considered the gold standard for chemical detection, particularly in the defense and law enforcement fields. The canine nose has evolved to become extremely sensitive and selective. While their sensing performance is nearly ideal, dogs have three major drawbacks. The first is cost. It costs approximately $6000 to train a dog to detect specific chemicals and roughly $2000 to care for and handle dogs annually, plus the cost of the handler [10]. This cost makes dogs the most expensive out of all the sensing techniques described here. Another issue is that it is not possible to know what the dogs are actually detecting. For example, an impurity might be what the

dog identifies as the target instead of the desired material. Consequently, an explosive may go undetected if it was manufactured using a different reagent than that used to produce the material used to train the dog [11]. Finally, dogs are only capable of working for a limited time and under limited conditions. Dogs fatigue easily and require frequent breaks to remain effective. High temperatures prevents dogs from detecting illicit materials. If a dog pants, it is only breathing through its mouth; it cannot smell anything [12]. These weaknesses provide opportunities for low cost sensors capable of operating under a variety of conditions.

1.2.2 Mass Spectrometry

Mass spectrometry (MS) is a widely-used analytic chemistry technique. It is used to determine the molecular mass and quantity of a substance. Molecules are ionized, accelerated with an electric field, and then separated by their mass/charge ratio with an electric or magnetic field. The field causes the paths of the ionized molecules to bend, with larger molecules less affected than smaller molecules. These molecules are then counted by a detector with spatial resolution and the mass is calculated [13]. MS is both sensitive and selective. However, it is very expensive and difficult to miniaturize, which limits its use to a few niche applications, such as air quality monitoring on the International Space Station. Even a small, portable MS can cost upwards of $100,000.

1.2.3 Ion Mobility Spectrometry

Ion mobility spectrometry (IMS) is an adaptable gas sensing technique that has been applied to a variety of situations. These include security systems in use at airports (*i.e.*, the "puffer" machine and the instruments that analyze swabs taken from passengers or luggage). There are also portable versions used for detecting explosives. IMS operates on a principle similar to MS. Molecules are ionized and accelerated in an electric field toward a detector. In this case, rather than separating molecules

with a magnetic field, molecules of different masses are separated by transit time. Lighter ions reach the detector sooner than heavier ions [14]. While this technique is simple and portable, there are a number of issues. Selectivity tends to be poor, which led to the quick demise of the "puffer" systems used in airports; the false positive rate was too high for this application [15]. The portable systems tend to have poor sensitivity to gases and are generally used with swabs. Oftentimes, the user (typically a soldier with a high school education rather than a trained analytical chemist) will introduce too much material, which saturates the detector. Clearing out the detector can take over three hours, which is long enough to drain the system's batteries [16]. The system is useless for the duration. Finally, the cost of a portable unit is high at around $35,000 [17].

1.2.4 Infrared Spectroscopy

Infrared spectroscopy techniques use an infrared laser to probe the vibrational modes of atoms in a molecule [18, 19]. The main advantage of these methods is that they provide stand-off detection, which is valuable when searching for explosives. Optical techniques have been demonstrated to identify explosives from 1 km away [20]. While this is impressive, such a technique is difficult to implement. The reason for this is the small spot size of the laser, typically 50-100 μm. Such a small size requires the user to know where the sample is prior to searching. While this may be effective in certain applications, it will be extraordinarily difficult to use in applications such as security or law enforcement where sensors are needed to aid in finding the desired materials. The sensitivity of infrared spectrometry is also low, so it is generally used to detect bulk materials.

1.2.5 Microelectromechanical Sensors

Microelectromechanical systems (MEMS) are a rapidly growing industry, particularly for motion sensors. Many MEMS devices have been developed into chemical

sensors with promising results. For example, sensors based on cantilevers can be sensitive enough to detect sub-attogram quantities [21]. These cantilevers oscillate at a fundamental frequency and when a molecule is adsorbed, this frequency changes [22]. The major challenge with MEMS sensors is selectivity. The sensors have no intrinsic selectivity; anything adsorbed will change the oscillation frequency. Some improvement was achieved through surface functionalization [23], but selectivity is still insufficient for practical use. MEMS sensors for airborne chemicals are far from commercial success.

1.2.6 Amplified Fluorescence Polymers

Amplified fluorescence polymers (AFP) represent another highly sensitive class of sensor. In fact, AFP demonstrated sensitivity to trinitrotoluene down to the parts per quadrillion level [24]. While fluorescence sensors have been studied for decades, AFP's superb sensitivity comes from its amplification. Traditional fluorescence sensors are based on organic molecules. When illuminated with sufficiently energetic light, these molecules absorb a photon, form an exciton, and emit light as that exciton recombines. When the analyte is present, it will either transfer an electron to the highest occupied molecular orbital (HOMO) of the excited sensor molecule or accept an excited electron from the lowest unoccupied molecular orbital (LUMO) of the sensor molecule. Both of these processes quench fluorescence. It also only allows one sensor molecule to be quenched by each analyte molecule; sensitivity is limited because this is a stoichiometric process.

In the case of AFP, the sensor molecules are polymerized. The resultant conjugated structure enables exciton diffusion. When an analyte molecule is adsorbed, it quenches the fluorescence of each sensor mer within the exciton diffusion length, typically about 5 nm. Thus, a single analyte molecule can quench hundreds of sensor molecules, leading to enhanced sensitivity [25]. Further sensitivity improvement can be achieved by increasing the exciton diffusion length [26], which will be discussed

further in Chapter 2. AFP is commercially successful; it is the technology used in the FIDO produced by FLIR. While the FIDO is currently a top seller in the defense industry, it is very expensive due to its costly optical components (such as the photomultiplier tube). Retail price is generally around $21,000 [17]. Selectivity is also an issue because any reducing species can quench the fluorescence, leading to false positives. Displacing AFP from the defense industry requires equivalent, or better, sensitivity and selectivity at a reduced cost.

1.2.7 Electrochemical Cells

Electrochemical cells are widely used, particularly for monitoring toxic industrial chemicals. They are inexpensive, compact, and consume little power. A typical configuration includes two electrodes in an electrolyte. A voltage is applied between the reference and working electrode. When the gas molecule is present, it will oxidize at the working electrode, which generates a current. The reduction reaction occurs at the counter electrode [27]. While electrochemical cells are widely used, they are far from optimal. Selectivity can be an issue. Sensitivity tends to be at the parts per million level [28]. For toxic gases, detection limits tend to be at the OSHA standard, so workers cannot receive warning of rising gas levels until they are exposed to a dangerous concentration. This means an area must be evacuated when a dangerous chemical is detected. Increased sensitivity could warn workers of the presence of the chemical, allowing them to fix the problem before it reaches a dangerous level. Not only is this safer, but it also eliminates downtime due to evacuations. They are in use essentially because they are the only means of complying with federal standards at an acceptable cost. A more sensitive or less expensive alternative can displace this technology.

1.2.8 Chemiresistors

Chemical sensing resistors, or chemiresistors, have the potential to displace these techniques as a low-cost, high-sensitivity alternative. The low cost results from reduced cost of the supporting hardware. While AFP requires expensive components, such as photomultiplier tubes, chemiresistors can be used with cheap integrated circuits. The all-electronic approach also has the benefit of increased robustness, as movement will impact on the sensor signal less than it would in an optical system. Creating an array is also simplified, which improves selectivity. Here, we will discuss four materials commonly used as chemiresistors: polymers that swell when exposed to an analyte, metal oxides, carbon allotropes, and dichalcogenides. A fifth material class, organic semiconductors, will be discussed in Chapter 2.

1.2.8.1 Polymer Swelling

Polymer swelling is a simple technique based on a blend of an electrically insulating polymer with a conductive material. The polymer is selected to be miscible with a target analyte. When the analyte is introduced, the polymer swells, breaking conductive pathways through the conductive material [29]. Selectivity tends to be poor because many analytes tend to be soluble in a given polymer. This can be improved by using an array [30]. However, the major challenge is device uniformity. Sensors deposited from the same batch of material following the same procedure will yield very different products. Conductivity can vary over several orders of magnitude. This variation necessitates individual training for each sensor array [31]. Individual training is costly, time consuming, and prevents the user from changing sensors in the field. Nevertheless, this technology is currently featured in the Cyranose by Smiths Detection.

1.2.8.2 Metal Oxides

Metal oxides, such as SnO_2, TiO_2, CuO, and ZnO, represent a widely-studied class of chemiresistive materials. They are particularly appealing because they can

form nanowires and/or porous structures, which improve sensitivity by increasing the surface area to volume ratio (Figure 1.2). Sensing occurs through charge transfer between the metal oxide and the analyte. Charge transfer changes the charge carrier density, which changes the conductivity [32]. However, metal oxide sensors have major issues with repeatability and selectivity. In terms of repeatability, the same material prepared under slightly different conditions will behave very differently when exposed to the same analyte. Recently, it was shown that surface defects have a major impact on selectivity [33, 34]. Materials with different defect densities or types will therefore respond differently to the same analyte. Impurities also have a major impact on response to an analyte [35]. This leads to major challenges in device uniformity. Another issue with selectivity arises from the fact that the surfaces have no intrinsic selectivity [36]; anything (including moisture in the air) that can transfer a charge will trigger these sensors. Surface modification improved selectivity, but there are a limited number of options as the modifying materials must be able to withstand

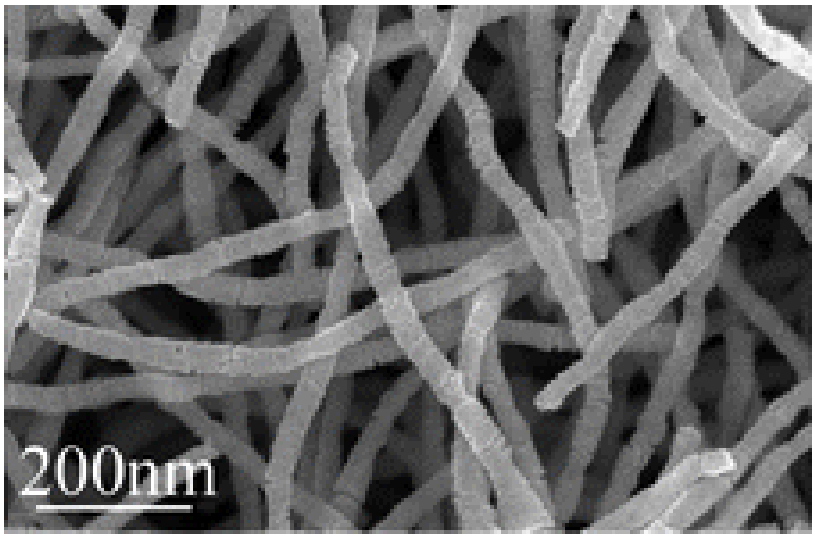

Figure 1.2. Scanning electron microscopy image of porous In_2O_3. Reprinted with permission from the Royal Society of Chemistry: J. Liu, Z. Guo, K. Zhu, W. Wang, C. Zhang, and X. Chen, "Highly porous metal oxide polycrystalline nanowire films with superior performance in gas sensors," *Journal of Materials Chemistry*, vol. 21, no. 30, pp. 11412-11417, copyright 2011.

the harsh operating conditions under which metal oxide sensors operate. Specifically, these sensor typically operate at 400 °C [36]. Such a high operating temperature also leads to a long warm-up time and high power consumption, which limit utility.

1.2.8.3 Carbon Allotropes

Carbon allotropes, specifically carbon nanotubes (CNTs) and graphene, are heavily researched because of their large surface area and chemical robustness. Carbon nanotubes are tubular structures of sp^2 bonded carbon atoms [37] (Figure 1.3). Interestingly, the direction of periodicity relative to the nanotube axis (*i.e.*, the chirality) determines the electronic properties (*i.e.*, whether the nanotube is semiconducting or metallic) [38]. For semiconducting CNTs, the band gap is determined by a combination of chirality and diameter [39]. While CNTs have acceptable sensitivity

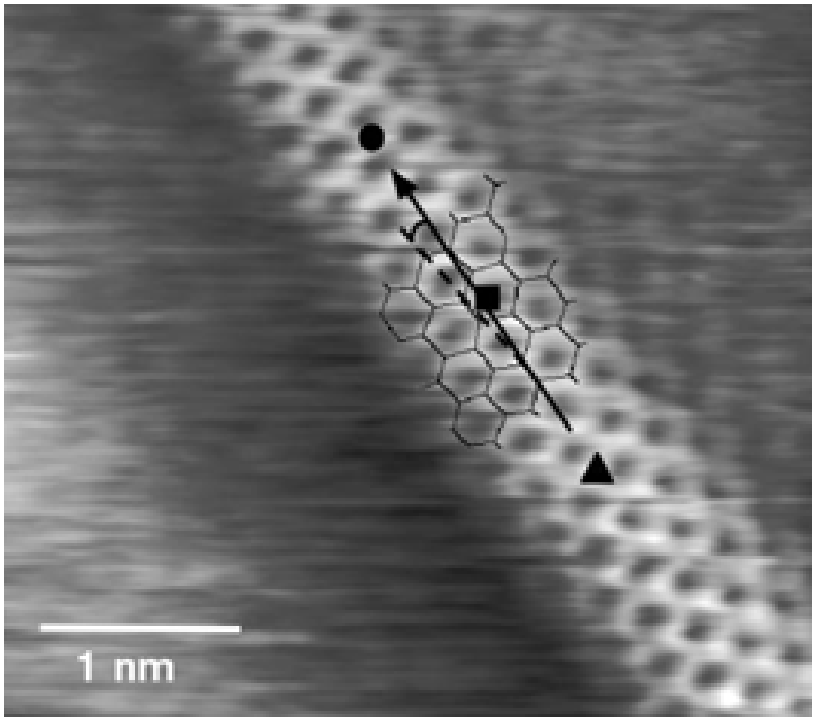

Figure 1.3. Transmission electron microscopy image of a single-walled carbon nanotube. A schematic of the chemical structure is overlaid as a guide. Reprinted with permission from Macmillan Publishing, Ltd.: T. W. Odom, J.-L. Huang, P. Kim, and C. M. Lieber, "Atomic structure and electronic properties of single-walled carbon nanotubes," *Nature*, vol. 391, vol. 6662, pp. 62-64, copyright 1998.

[40], selectivity tends to be quite poor. The poor selectivity arises from the nonspecific nature of the CNT's surface. Improvement can be achieved through covalent functionalization [41], although this destroys the electronic properties in most cases [42, 43]. This leads to an optimization problem: more functionalization improves selectivity at the cost of conductivity. To avoid the trade-off, noncovalent surface functionalization is a promising alternative [44, 45], although the nature of the interface is not clearly understood [46]. A study of this interface is presented in Chapter 3. Finally, CNTs are very expensive at this time. While they can be synthesized cheaply through arc discharge, the product includes nanotubes of all chiralities. These must be purified to create repeatable devices. The purification process is quite costly [47].

Graphene provides a similar surface as CNTs with a different morphology; instead of a tubular structure, graphene is an atomically-thick sheet of sp^2 bonded carbon atoms. While graphene boasts high charge carrier mobility (>10,000 $cm^2 \cdot V^{-1} \cdot s^{-1}$) [48] and has demonstrated the ability to detect single molecules [49] (Figure 1.4), it faces many of the same problems as CNTs. Selectivity is poor. As with CNTs,

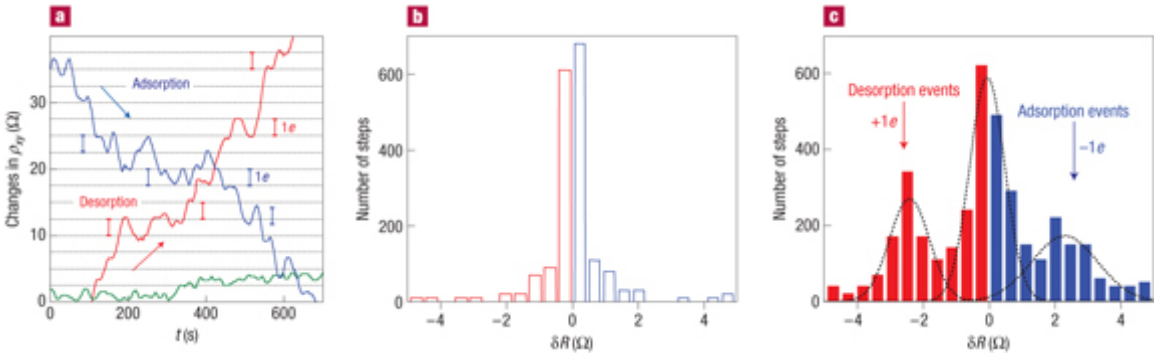

Figure 1.4. Single molecule detection by graphene. a) Adsorption and desorption profiles of NO_2 in an inert atmosphere. b) Signal deviations without the analyte present demonstrating the background noise. c) Signal deviations in the presence of the analyte. Two new peaks are observed and are attributed to adsorption and desorption events. Reprinted with permission from Macmillan Publishing, Ltd.: F. Schedin, A. K. Geim, S. V. Morozov, E. W. Hill, P. Blake, M. I. Katsnelson, and K. S. Novoselov, "Detection of individual gas molecules adsorbed on graphene," *Nature Materials*, vol. 6, no. 9, pp. 652-655, copyright 2007.

surface modification is a major research topic. A variety of surface modifications have been demonstrated, although they drastically change graphene's electronic properties [50]. The other major challenge comes from manufacturing. High quality graphene is manufactured using a mechanical exfoliation method (*i.e.*, the "scotch tape method"). This method is not suitable for high volume production. Other methods, such as chemical vapor deposition, are appropriate for commercial manufacturing, but the graphene produced by these techniques is plagued by defects. These issues are a major barrier to practical use for graphene.

1.2.8.4 Dichalcogenides

Two-dimensional dichalcogenides, such as $MoSe_2$ and WS_2, offer the same major advantage of graphene (large surface area to volume ratio). However, they also offer the additional advantage of possessing a band gap [51]. The band gap reduces thermal noise, which can improve the sensitivity in sensors by increasing the signal-to-noise ratio. Dichalcogenides also suffer many of the same drawbacks of graphene. Selectivity is poor due to their nonspecific surfaces [52]. Compared to graphene, surface modification of dichalcogenides is less understood [53]. Producing these materials is also relatively expensive. Growth is generally performed using chemical vapor deposition, which uses costly precursor materials. Alternatively, mechanical exfoliation can be used [54]. Since research in this field is relatively new, it is possible some of these issues will be overcome, but it will take many more years of work.

1.3 Deficiencies and Opportunities

The demand for chemical sensors is huge. However, very few sensing techniques have achieved commercial success. We have identified eight criteria that a sensor should fulfill to meet the needs described in Section 1.1. These criteria are:

- **Cost:** Cost is defined as how much the end user must pay to purchase and operate the sensor.

- **Production:** Production refers to how easy a sensor is to produce, including factors such as production time and the use of specialty parts. Dogs, for example, require months of training before they are effective. MS and IMS frequently use radioactive sources for ionization, which are difficult to procure and handle.
- **Sensitivity:** Sensitivity describes the sensors ability to respond to a minimal amount of target material. Sensitivity is crucial for reducing false negatives.
- **Selectivity:** The inability for undesired chemicals to trigger the sensor is the selectivity. Selectivity reduces false positives.
- **Power:** Power refers to how much energy is used to operate and maintain a sensor. Dogs take a large amount of energy because of feeding and care. Metal oxide chemiresistors consume most of their energy due to heating; these sensors generally operate at elevated temperatures.
- **Simplicity:** The ease with which a user can operate a sensor is defined as its simplicity. Dogs require significant maintenance, but provide clear signaling. MS and IMS can provide a simple user interface, but require sample preparation.
- **Speed:** Speed describes how fast a sensor responds after it begins sampling the analyte. Dogs, MEMS, AFP, electrochemical cells, and chemiresistors respond within seconds. MS and IMS are relatively slow because of sample preparation and desorption. High speed is required for real-time detection.
- **Duty Cycle:** The amount of time a sensor is able to sample is referred to as the duty cycle. Dogs have a low duty cycle because they

fatigue and are susceptible to environmental conditions that render them ineffective. Infrared spectroscopy, MEMS, AFP, electrochemical cells, and chemiresistors are all capable of sampling continuously, so their duty cycles are high.

A summary of sensor technologies and how well they meet the defined criteria is presented in Table 1.1. There is no sensor technology that meets all eight requirements. The table also identifies a trade-off: selectivity comes with increased cost. While different applications will have different selectivity requirements (in some cases, false positives might be more acceptable than others), certainly delivering high selectivity at a low cost will enable new markets. These new applications will have major implications to the defense, automotive, environmental, food, safety, aerospace, and medical industries.

Herein, strategies to deliver selectivity to low-cost sensor systems are presented. These techniques center around the use of organic semiconductors, which have yet to be described. Operationally, these sensors behave either as or similarly to chemiresistors. However, organic semiconductors provide improved selectivity over other materials, which will be discussed in the following chapter. Additionally, organic semiconductor sensors operate at room temperature, making them among the best

Table 1.1. Comparison of sensor technologies and their ability to meet the required criteria. The previously undefined acronyms used here are infrared spectroscopy (IS), electrochemical cell (EC), and chemiresistor (CR).

Criteria	Dogs	MS	IMS	IS	MEMS	AFP	EC	CR
Cost	○	○	○	◐	●	◐	●	●
Production	○	◐	◐	◐	●	◐	●	◐
Sensitivity	●	●	◐	●	●	●	◐	●
Selectivity	●	●	◐	●	○	◐	◐	○
Power	○	◐	◐	◐	◐	◐	●	◐
Simplicity	◐	○	◐	○	●	●	●	●
Speed	●	○	○	◐	●	●	●	●
Duty Cycle	○	○	○	●	●	●	●	●

in terms of power consumption. The goal of this work is to develop methods to use organic semiconductors as chemical sensors with electronic signaling. Such sensors are expected to play a significant role in the $52.9B chemical detection market.

CHAPTER 2

ORGANIC SEMICONDUCTORS AS CHEMICAL SENSORS

Chemiresistors meet nearly all criteria listed in Table 1.1, but fall short in three areas: manufacturability, selectivity, and power consumption. Manufacturability issues result in large variation from one device to the next. This arises from the random nature in which chemiresistive materials are deposited. Meanwhile, the nonspecific surfaces of chemiresistive materials results in poor selectivity. Finally, many chemiresistive materials, such as metal oxides, require elevated temperatures, which consumes a significant amount of power. However, all of these issues can be addressed by using organic semiconductors as sensing materials. The aim of the work contained herein is to address the materials issues in organic semiconductors that are preventing them from commercial success. In this chapter, the basic concepts of organic semiconductors and their use as chemical sensors will be discussed.

2.1 Overview

In order to understand the benefits of organic semiconductors for sensors, the fundamental science underlying these materials is necessary. In this section, the mechanism behind electrical conductivity, materials, fabrication techniques, and advantages for sensors will be discussed.

2.1.1 Electrical Conductivity

Conductive organic materials were first reported in 1977 by Heeger, Shirakawa, and MacDiarmid, an achievement that earned them the Nobel Prize in Chemistry

in 2000. Specifically, they found that polyacetylene can be tuned from an insulator to a semiconductor and eventually to a conductor through doping with halogen ions [55]. This discovery paved the way for a variety of organic semiconductor devices, including photovoltaic cells [56], light-emitting diodes [57], and field effect transistors [58]. Nearly 40 after their discovery, organic semiconductors are still an active research topic.

Charge motion through organic semiconductors is typically via hopping [59], although band-like behavior has been observed in highly ordered materials [60]. Molecular packing has a major impact on conductivity; the more the π-orbitals of adjacent molecules overlap, the higher the conductivity will be. Similarly, reorganization energy also has an impact. Smaller reorganization energy leads to a higher conductivity [61]. These two factors dominate charge movement between the lowest unoccupied molecular orbitals (LUMOs) of adjacent molecules. However, films of organic semiconductors contain a variety of states, including immobile states in the band tails and traps within the band gap [62]. These immobile states are detrimental to conductivity because they localize charges. This can be overcome either through the addition of thermal energy [63] or doping [64]. With these states arising from defects in the crystal structure, there is further need to improve the crystal structure.

2.1.2 Materials and Fabrication

Organic semiconductors fall into two classes. Small molecules are the top performer in terms of charge carrier mobility, with a record of 40 $cm^2 \cdot V^{-1} \cdot s^{-1}$ [65]. Crystallinity is incredibly important because charges travel through the overlapping π-orbitals of adjacent molecules. Defects and grain boundaries contribute trap states within the band gap that hinder charge transport [66]. Highly crystalline films have been fabricated through thermal evaporation. These films are subject to large charge anisotropy, which causes variation between devices due to the random orientation of the grains [67] (Figure 2.1). When modified with soluble side groups, small molecules

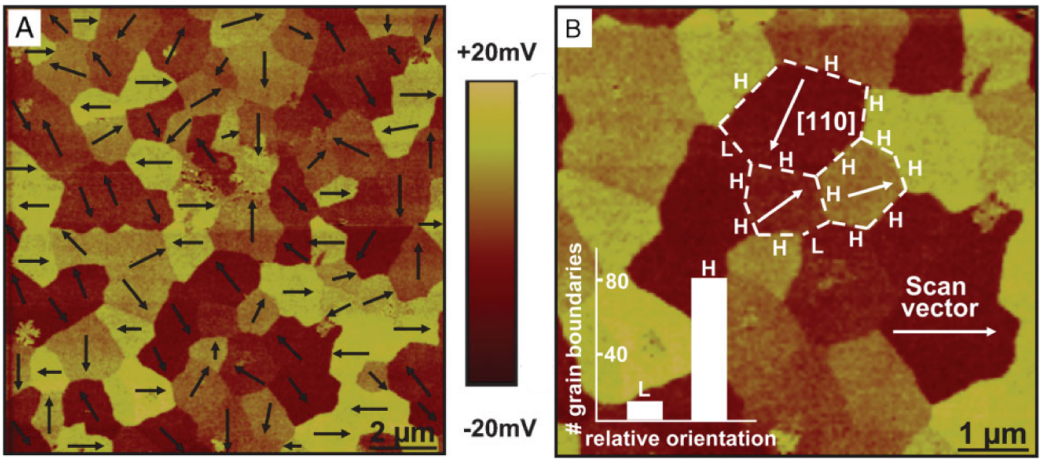

Figure 2.1. Grain boundaries and orientation of a pentacene film. A) Transverse shear microscopy (TSM) map of grain orientation. Arrows indicate the [110] direction. B) Zoomed TSM image denoting high- and low-angle grain boundaries. Reprinted with permission from John Wiley and Sons: V. Kalihari, E. Tadmor, G. Haugstad, and C. D. Frisbie, "Grain orientation mapping of polycrystalline organic semiconductor films by transverse shear microscopy," *Advanced Materials*, vol. 20, no. 21, pp. 4033-4039, copyright 2008.

can be solution processed [68, 69], although films manufactured with these processes tend to have lower mobilities.

Polymers comprise the other class of organic semiconductors. Since they have a conjugated backbone, crystallinity is not a requirement for charge transport, although order does result in a higher mobility in some materials [70]. Polymers historically have lagged behind small molecules in terms of mobility, although that gap has closed in recent years with polymers achieving 0.85 $cm^2 \cdot V^{-1} \cdot s^{-1}$ [71]. These materials boast two major advantages. First, solution processing is more suitable because of the eased order requirement (Figure 2.2). Solution processing is ideal for low-cost, rapid fabrication. Examples of techniques used for processing polymer semiconductors include spin casting [72] and inkjet printing [73]. Secondly, polymer films tend to be much smoother than films of small molecules, largely due to processing methods (spin casting polymers versus vapor-phase deposition for small molecules, which results in Stranski-Krastanov growth) [74]. This is important for applications requiring conduction along the top surface, which will be discussed further in Chapter 4.

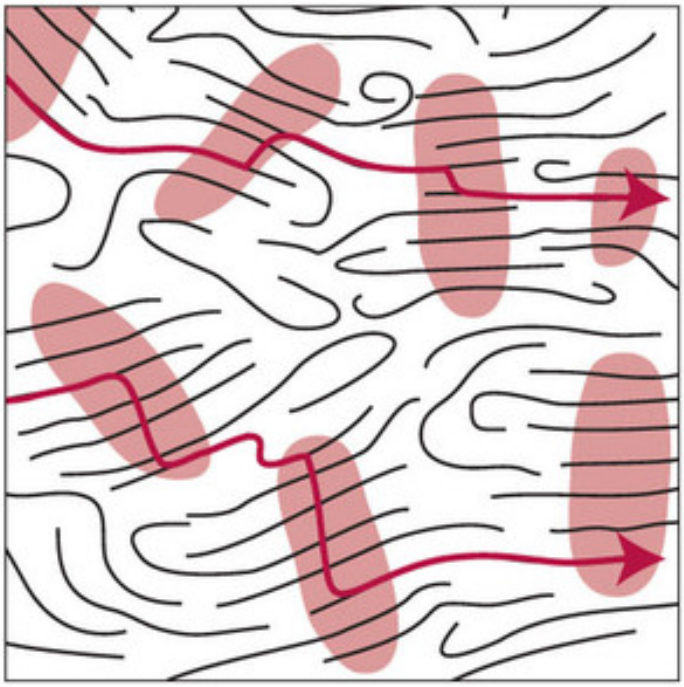

Figure 2.2. Grain orientation and connectedness in a polymer film. Grains are oriented randomly as in pentacene, but polymers can span multiple grains. The conjugated backbones of these bridging polymers facilitate charge transport through the film. Reprinted with permission from Macmillan Publishing, Ltd.: V. Podzorov, "Conjugated polymers: Long and winding polymeric roads," *Nature Materials*, vol. 12, no. 11, pp. 947-948, copyright 2013.

2.1.3 Advantages for Sensors

Organic semiconductors offer several advantages over other materials when used in sensors. Perhaps the most beneficial is the tunable surface. Organic molecules can be modified easily, so they can be tailored to interact with a specific analyte. This includes both physical and thermodynamic facets. In terms of physical (how well the sensing material grabs onto the analyte), features such as hydrogen bonding sites can be added or the hydrophobicity can be tuned. Adjusting the thermodynamics requires changing the molecular structure by adding electron-rich or electron-deficient moieties. Finally, the morphology of organic semiconductors is relatively easy to control, allowing the creation of highly porous films for enhanced interaction with the analyte and, thus, higher sensitivity.

2.2 Fluorescence Sensing

Fluorescent sensing represents a simple platform for creating sensors. Sensing can occur either in solution or on a simple substrate (*e.g.*, quartz), which eases material testing. Photoexcitation of a molecule produces an exciton. Relaxation of the exciton to the ground state produces fluorescence (radiative decay) and heat (nonradiative decay). Depending on the electronic structure of the molecule, the fluorescence yield can approach 100%. In the presence of an analyte, charge transfer occurs between the analyte and the sensor molecule, quenching the fluorescence. This process is purely thermodynamic, provided the charge transfer rate is faster than the exciton decay rate. These turn-off fluorescence sensors represent the simplest form of organic semiconductor sensors.

A method to substantially improve sensitivity was developed by Swager in 1995 [25]. By polymerizing sensor molecules, amplification was achieved (see Section 1.2.6). Rather than being localized to a single molecule, an exciton is free to diffuse along the polymer's conjugated backbone. An analyte molecule adsorbed within the exciton diffusion length will quench the fluorescence of all molecules within that range [75]. Typical exciton diffusion lengths in polymers are a few nanometers, providing a signal amplification of around a thousand [76]. The major challenge with these materials is that they create a solid film, which limits analyte diffusion [77]. Therefore, the film needs to be very thin (ideally thinner than the exciton diffusion length) to provide a sufficient change in fluorescence. Consequently, the fluorescence signals are very small. In commercial devices such as the FIDO by FLIR, an expensive photomultiplier tube is required to achieve the necessary sensitivity. While these materials are relatively inexpensive, detecting the small signals they provide necessitates an expensive system.

In 2007, the Zang Lab made a major breakthrough in chemical sensing. Nanofibers comprised of perylene tetracarbozxyllic diimide (PTCDI) molecules were grown through a self-assembly process. When photoexcited, these nanofibers demonstrated excellent

fluorescence and high sensitivity to a desired analyte [78]. The origin of the high sensitivity is attributed to two features: 1) the large surface area to volume ratio of the nanofiber structure provides a large interface for charge transfer with the analyte [79], and 2) the crystalline backbone of the nanofiber allows for long range exciton diffusion, producing amplification an order of magnitude larger than AFP [78] (Figure 2.3). In fact, the exciton diffusion length is estimated to be on the order of 100 nm [80]. These nanofibers demonstrated sensitivity down to the parts per trillion level in the lab, with the limit of detection projected to be even lower [81]. An optimized system is expected to push the detection lower still.

2.3 Electronic Sensing

For commercial products, electronic sensors are preferable to those based on fluorescence. High-performance fluorescence sensors generally feature expensive photomultiplier tubes, while electronic sensors use inexpensive integrated circuits. Creating an array, which enhances selectivity, also is greatly simplified using electronic sensors. An array of fluorescent sensors requires complicated light management, adding cost and size to the system.

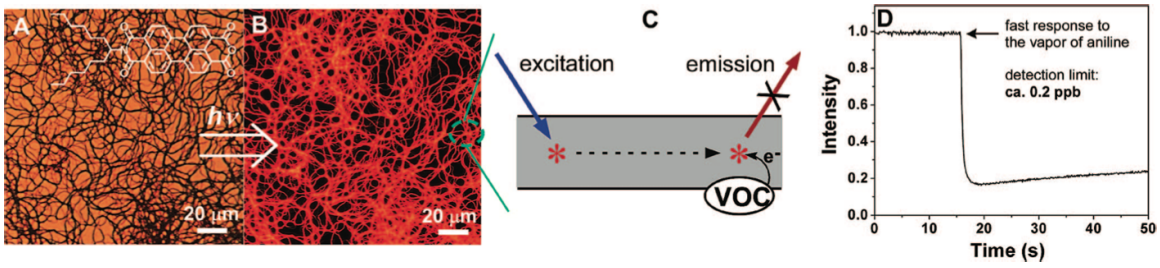

Figure 2.3. Overview of sensing with a fluorescent nanofiber. A, B) Optical and fluorescence microscopy images of organic nanofibers. C) Schematic depicting excitation, exciton diffusion, and fluorescence quenching. D) Example of a sensor response to aniline. Reprinted with permission from the American Chemical Society: L. Zang, Y. Che, and J. S. Moore, "One-dimensional self-assembly of planar π-conjugated molecules: Adaptable building blocks for organic nanodevices," *Accounts of Chemical Research*, vol. 41, no. 12, pp. 1596-1608, copyright 2008.

In addition to simplicity, chemiresistors also offer improved selectivity over their fluorescent counterparts. This is because in addition to thermodynamic and physical effects, the response of chemiresistors also depends on kinetics. Consider the drift-diffusion equation:

$$J = qn\mu E + qD\frac{dn}{dx} \tag{2.1}$$

where J is the current density, q is the unit charge, n is the charge carrier density, μ is the charge carrier mobility, E is the electric field, D is the diffusion coefficient for charges, and $\frac{dn}{dx}$ is the diffusion gradient of charge carriers in the x direction. In the presence of the analyte, n is the only factor that changes because of charge transfer. Therefore, $\Delta J \propto \Delta n$. In this case, Δn is the net change in charge carriers and the sensor signal is clearly related to charge transfer between the sensor and the analyte (Figure 2.4). The forward and back electron transfer rates must be appropriate for the current to change. Consider a chemiresistor that carries electrons and receives an electron from the analyte, causing an increase in current with appropriate kinetics.

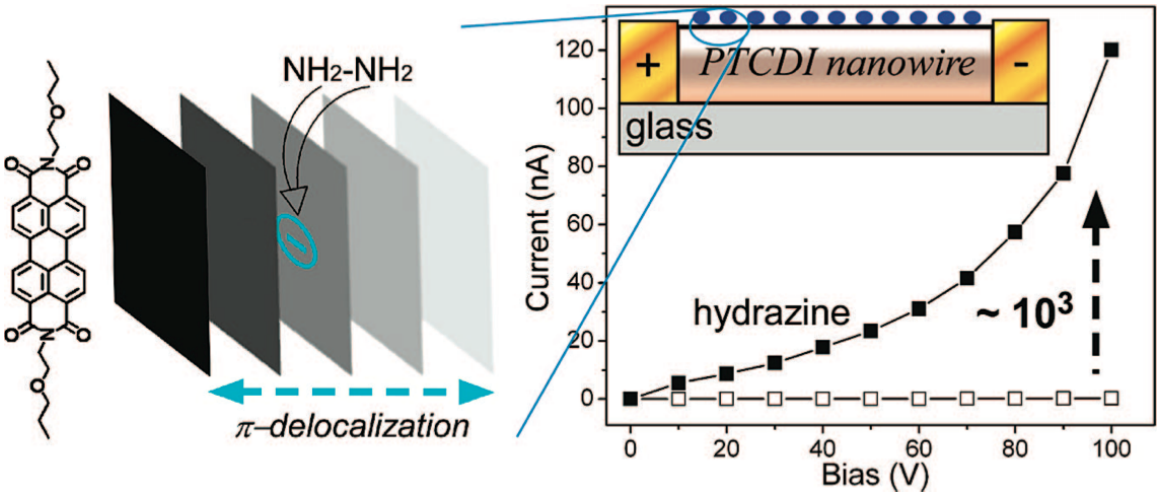

Figure 2.4. Schematic depicting charge transport along the π-conjugated backbone of the nanofiber. Example of a sensor response to hydrazine. Reprinted with permission from the American Chemical Society: L. Zang, Y. Che, and J. S. Moore, "One-dimensional self-assembly of planar π-conjugated molecules: Adaptable building blocks for organic nanodevices," *Accounts of Chemical Research*, vol. 41, no. 12, pp. 1596-1608, copyright 2008.

If the electron transfer rate from the chemiresistor to the analyte is much faster than the electron transfer rate from the analyte to the chemiresistor, $\Delta n \rightarrow 0$. Thus, if the forward electron transfer is too slow relative to the back electron transfer, no change in current is observed (Figure 2.5).

Kinetics provides a very important tool for improving selectivity. Tuning simply requires changing the spacing between the chemiresistor and the analyte (*e.g.*, by introducing longer side groups on the molecules that comprise the chemiresistor) [82]. An example of this benefit is in amine detection. Some amines are very similar chemically, but are very different otherwise. For example, the prescription medicine Adderall differs from methamphetamine by only one methyl group. However, the former is legal while the latter is not. The similar molecular structures produce similar physical interactions with the sensing material. Since both are amines, the thermodynamics of electron transfer are similar as well. Thus, distinguishing between Adderall and methamphetamine is nearly impossible for fluorescence sensors. However, the

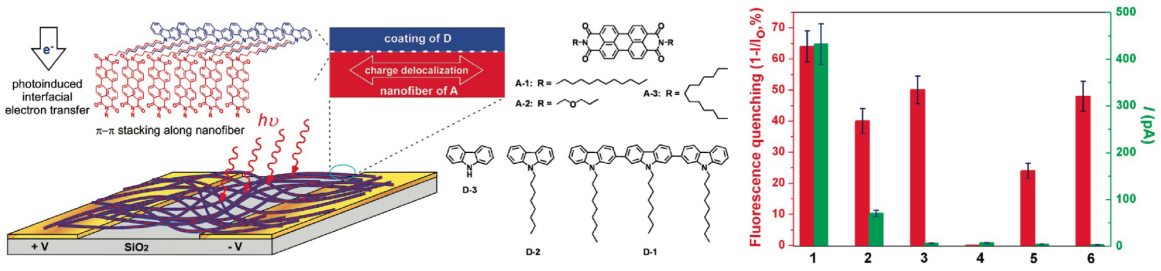

Figure 2.5. Schematics of donor-acceptor interface, the device used for photoconductivity measurements, and molecular structures. Photoresponse and fluorescence quenching were measured for: A-1 nanofibers coated with D-1 (1); A-1 nanofibers coated with D-2 (2); A-1 nanofibers coated with D-3 (3); A-2 nanofibers coated with D-1 (4); A-3 film coated with D-1 (5); and A-3 film coated with D-3 (6). Examining the A-1 nanofibers reveals that all three demonstrate a large fluorescence response to each donor molecule. However, a change in conductivity is only observed for donors with large alkyl chains, which hinder the back electron transfer process. Reprinted with permission from the American Chemical Society: Y. Che, H. Huang, M. Xu, C. Zhang, B. R. Bunes, X. Yang, and L. Zang, "Interfacial engineering of organic nanofibril heterojunctions into highly photoconductive materials," *Journal of the American Chemical Society*, vol. 133, no. 4, pp. 1087-1091, copyright 2011.

additional methyl group changes the kinetics by changing the position of the amine relative to the sensing material. Thus, the two molecules produce different current changes. Since both elicit a response, two chemiresistors are used and their relative responses distinguish between the two molecules (Figure 2.6). This demonstrates a major advantage of chemiresistors.

Another noteworthy feature of chemiresistors based on organic semiconductors is that the range of detectable analytes can be extended by using photocurrent. Molecular structures comprised of electron accepting cores connected to strong electron donating moieties have the potential for large photocurrents. When light is absorbed, it stimulates charge transfer from the side group to the core, which increases the charge carrier density and, therefore, the conductivity [83]. The presence of the strong electron donor makes it possible for these materials to detect weakly oxidizing chemicals, including most explosives (*e.g.*, 1,3,5-trinitroperhydro-1,3,5-triazine (RDX), 2,4,6-trinitrotoluene (TNT), octahydro-1,3,5,7-tetranitro-1,3,5,7-tetrazocine (HMX), pentaerythritol tetranitrate (PETN)). Electron withdrawal by the analyte leads to

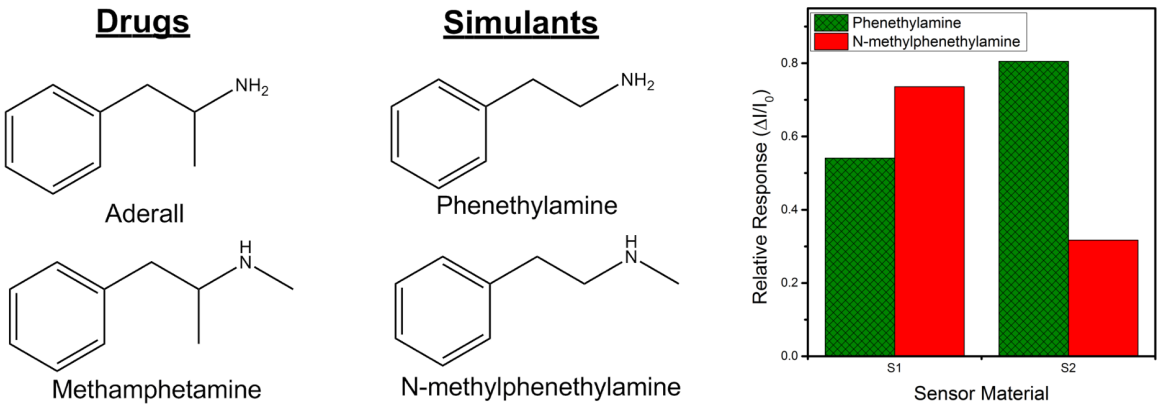

Figure 2.6. Molecular structures of Aderall and methamphetamine with their simulants and sensor responses. The simulants were used in this study. Two different nanofibers were exposed. Although both nanofibers respond to both drugs, one has a larger affinity for Aderall while the other responds more strongly to methamphetamine. By comparing the relative responses of these sensors, it is possible to distinguish between these two drugs. Thus, sensor arrays are necessary for applications requiring high sensitivity.

a reduction in current [83]. Weakly oxidizing explosives like nitromethane remain difficult to detect for most fluorescence sensors because partial charge transfer and weak donor-acceptor interaction do little to quench fluorescence. However, these weak interactions can be detected through electrical current modulation, which is sensitive even to a slight change in the charge carrier density. Using organic semiconductors as chemiresistors adds improved selectivity and enabled detection of weakly oxidizing materials.

2.4 Challenges

There are two major issues preventing organic semiconductors from use in commercial products. Perhaps the largest issue is conductivity. Organic semiconductors tend to be very nonconductive, stemming from low charge carrier densities and mobilities. While a few molecules have charge carrier mobilities exceeding 10 $cm^2 \cdot V^{-1} \cdot s^{-1}$, most tend to be much lower, with typical mobilities from 10^{-6} to 10^{-4} $cm^2 \cdot V^{-1} \cdot s^{-1}$. Sensors comprised of organic semiconductors are generally capable of carrying at most 10 nA of current when 10 V is applied. This is too low for integration with most off the shelf integrated circuits. Improving conductivity is a major challenge for organic semiconductors. In chemiresistors, the same material must provide both the interaction with the analyte and electrical conductivity. These two requirements make modification particularly difficult, as changing one property can affect the other.

The other major issue is repeatability (*i.e.*, device to device variation). Commonly, chemiresistors are one-dimensional nanomaterials deposited from a solution. These materials deposit randomly on the substrate, which leads to a wide range in device properties. Consider the resistance of a wire:

$$R = \rho \frac{L}{A} \tag{2.2}$$

where R is the resistance, ρ is the resistivity, L is the length, and A is the cross-sectional area. Now, considering a nanowire deposited randomly across an electrode

pair with a gap, g, geometry shows that $g = L\cos(\theta)$, where θ is the angle of the nanofiber relative to the gap. Substituting this into Equation 2.2 yields:

$$R = \rho\frac{g}{A\cos(\theta)} \tag{2.3}$$

Thus, a clear relationship between nanowire alignment and device resistivity is demonstrated. In many cases, multiple nanofibers are used and averaging improves repeatability to some extent. In an ideal world, θ would always be unity to improve uniformity between devices and reduce resistance as much as possible.

Our efforts to address these challenges are presented in this dissertation. Three methods to solve the conductivity issue are presented, including one that improves device to device uniformity. In Chapter 3, nonconductive organic semiconductors are incorporated into a network of carbon nanotubes. The results indicate that sensing is not based on electron transfer, but rather by a swelling mechanism that impedes current flow between carbon nanotube junctions. Chapter 4 presents a new field effect transistor structure for airborne chemical detection. This architecture separates sensing and electrical conduction so that the sensing material need not be conductive. Relaxing the conductivity requirement allows for a wide range of sensing materials to be used. Finally, in Chapter 5, alignment of organic nanofibers using dielectrophoresis is demonstrated. This technique enables repeatable nanowire devices by ensuring consistent deposition. These early results represent an encouraging step toward commercialization.

CHAPTER 3

FUNCTIONALIZING SINGLE-WALLED CARBON NANOTUBES WITH ORGANIC MATERIALS

Carbon nanotubes (CNTs) offer higher conductivity than organic semiconductors and a surface that is easy to modify with functional molecules. These features make CNTs strong candidates to improve sensors based on organic semiconductors. However, interfacial interactions between organic molecules and CNTs are poorly understood. In this chapter, the interface between CNTs and an oligomer is investigated and a novel sensor for nitroaromatic explosives is demonstrated.

3.1 Overview

To put the sensing performance of carbon nanotubes in context, it is constructive to first discuss their physical properties. Carbon nanotubes are highly desirable for sensors because of their large surface area to volume ratio. In fact, in single-walled carbon nanotubes, every atom is on the surface, which enables the entire structure to interact with the environment. Additionally, CNTs possess high charge carrier mobility, easing integration with commercial electronics. Finally, the surface can be tailored for selectivity to specific analytes.

3.1.1 Challenges

While the electronic properties are highly desirable (see Appendix B for details), carbon nanotubes have experienced limited use outside of the laboratory. There are a number of issues preventing their practical applications involving processing and

challenges arising from surface effects. Addressing each of these issues is required for real world implementation of carbon nanotube devices.

Carbon nanotubes exist in a wide range of diameters, lengths, and chiralities. Ideally, a single chirality could be selected, leading to more uniform devices. However, this is not possible [84]. Synthesis of carbon nanotubes is generally performed through arc discharge [37], laser ablation [85], or chemical vapor deposition (CVD) [86]. All generally produce carbon nanotubes with a range of chiralities and number of walls. Recently, a novel seeded chemical vapor deposition method produced CNTs of a single chirality. An end cap was synthesized and CVD was used to extend the structure into a nanotube. Changing the chirality is proposed to simply require a new seed. However, only armchair CNTs have been produced; seeds for chiral structures may involve difficult synthesis or be unstable [87].

Insolubility in nearly all solvents makes carbon nanotubes difficult to process. Introducing soluble groups has been a major research interest, with both covalent and noncovalent methods available. Covalent methods involve chemical reactions and solubility is achieved at the expense of changing the electronic properties. Covalent modification converts sp^2 bonds to sp^3, which changes the band structure [42]. Alternatively, noncovalent modification does not require a chemical reaction and does not disrupt the carbon nanotube's band structure. Instead, the functional material is physically adsorbed on the surface of the CNT through van der Waals forces (*e.g.*, $\pi - \pi$ interactions). While the band structure is not significantly affected, doping can occur through charge transfer [88]. This method is a proven means to fabricate solution processed electronic devices from carbon nanotubes.

Finally, due to the nonspecific nature of their surface, carbon nanotubes are very sensitive to changing environmental conditions. This led to confusion about charge transport. Early experiments showed that carbon nanotubes are intrinsically p-type. These studies were performed under ambient conditions [89]. However, when in

vacuum, carbon nanotubes switch from conducting holes to conducting electrons. The change is due to oxygen. Adsorbed oxygen acts as an electron acceptor and p-dopes the CNT [90]. Sensitivity to the operating environment is a major challenge, especially in applications in which the CNT cannot be encapsulated, such as sensors.

3.1.2 Interaction with Polymers

Polymers functionalization of carbon nanotubes is a proven means to introduce solubility. The repeat units of these polymers have two components: a soluble side chain and a π-conjugated group that adsorbs onto the surface of the CNT through a special van der Waals interaction: π-π stacking. These polymers have been used to suspend CNTs in chloroform [88], acetone [91], toluene [92], and water [93], depending on the side chain.

Purification of CNTs is also achievable using polymers. Enrichment of semiconducting and metallic species was demonstrated. More frequently, purification is based on the CNT's diameter. However, it is not clear what mechanism leads to a polymer preferring one carbon nanotube over another. Theories include donor-acceptor interaction [94] and diameter selectivity through steric effects [95].

Charge transfer between polymers and carbon nanotubes is complicated and unpredictable. Functionalization with a phenylene ethynylene oligomer, an electron donor, yielded the predicted electron transfer from the oligomer to the CNT [88]. However, functionalization with poly(3-hexylthiophene) (P3HT), also predicted to be an electron donor, yielded very different results. Surprisingly, the electron transferred from the CNT to the polymer, seemingly in spite of unfavorable thermodynamics. The authors propose that the Fermi level alignment between the P3HT and CNT changes the thermodynamics to favor charge transfer in the opposite direction [96]. Clearly, more work is necessary to understand the interface between CNTs and functional materials.

3.2 Results

To use carbon nanotubes as sensors, significant progress is needed to improve processing and chemical selectivity. Functionalization with organic molecules provides a potential means to address both issues. However, a lack of understanding of the polymer/CNT interface makes the design of sensing materials impossible. Here, functionalization using a novel carbazole-based oligomer is described. The oligomer is a combination of two materials our lab has previously proven to functionalize CNTs [88], or interact strongly with nitroaromatic explosives [97]. A study of the interface demonstrates the formation of a charge transfer complex and a built-in electric field that hinders charge transfer between the CNT and analyte. Sensors for nitroaromatic explosives are demonstrated; the sensing mechanism is based on swelling of the oligomer. Sensitivity is several orders of magnitude higher than traditional sensors based on polymer swelling because of the high surface area and porosity of the film. The results presented herein demonstrate a new method to design sensing materials for highly conductive chemiresistors operating at room temperature. Experimental details are presented in Appendix A.

3.2.1 Dispersion

Single-walled carbon nanotube (>93% semiconducting, primarily (7,6) and (6,5) chiralities) were functionalized with carbazolylethynylene (Tg-Car) oligomers following a procedure previously developed in our lab to fabricate the Tg-Car/CNT composite (Figure 3.1). The suspension was stable and free of precipitates. Chloroform offers a low vapor pressure, which facilitates solution processing. An energy diagram was developed from density functional theory calculations for the oligomer and values from the literature for CNTs. The oligomer features a wide band gap of 3.1 eV and is expected to behave as an electron donor to the CNT.

The solution was deposited onto a clean SiO_2 substrate. Atomic force microscopy images were obtained (Figure 3.2). The images demonstrated a film free from carbon

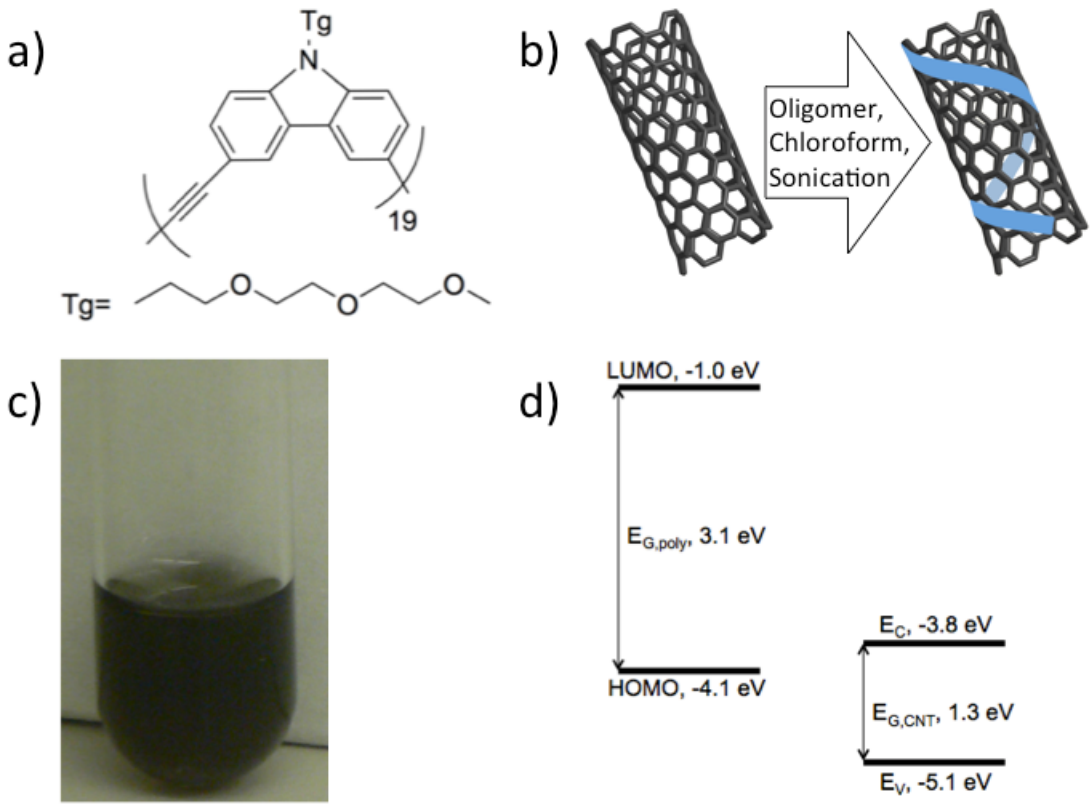

Figure 3.1. CNT dispersion with Tg-Car and band diagram. a) Molecular structure of the Tg-Car oligomer. b) Schematic of the functionalization procedure. c) Photograph of the Tg-Car/CNT dispersion in chloroform. d) Band diagram of the Tg-Car oligomer and (6,5) CNTs referenced to the vacuum level. Reprinted with permission from John Wiley and Sons: B. R. Bunes, M. Xu, Y. Zhang, D. E. Gross, A. Saha, D. L. Jacobs, X. Yang, J. S. Moore, and L. Zang, "Photodoping and enhanced visible light absorption in single-walled carbon nanotubes functionalized with a wide band gap oligomer," *Advanced Materials*, vol. 27, no. 1, pp. 162-167, copyright 2015.

nanotube bundles, indicating excellent dispersion by the oligomer. Height measurements were taken for both the Tg-Car/CNT and bare CNT films to determine the diameters. The functionalized CNTs had a diameter of 1.2 ± 0.2 nm. This is significantly larger than the diameter of the pristine CNTs, which had a diameter of 0.8 ± 0.1 nm, which agrees with the manufacturer's specifications. These measurements confirm the presence of the oligomer on the surface of the CNTs.

Further confirmation of the presence of the oligomer was obtained by adhesion

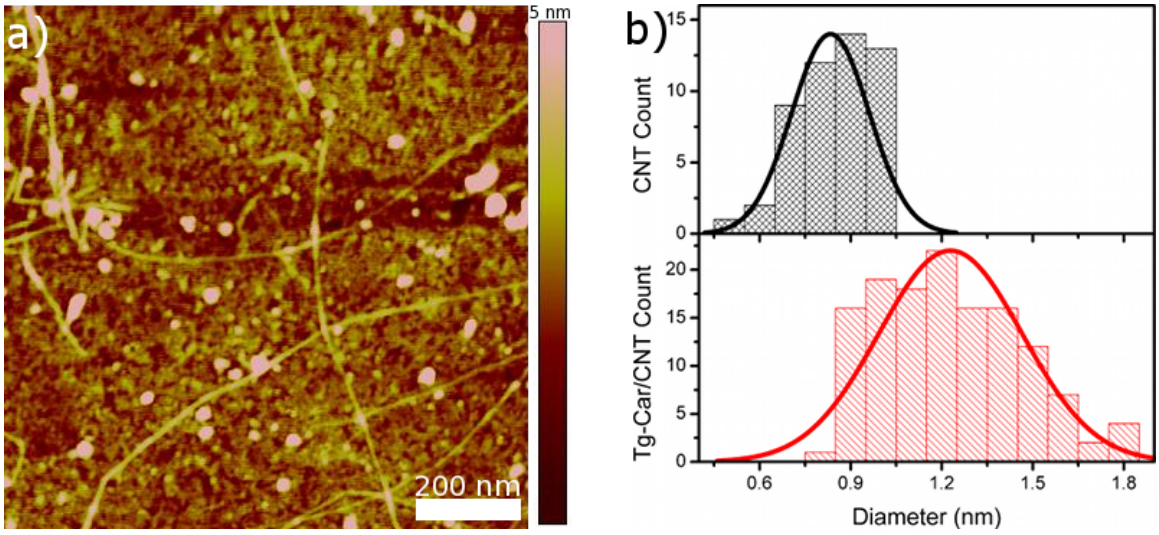

Figure 3.2. Image and measurements of the Tg-Car/CNT film. a) Atomic force microscopy image of the Tg-Car/CNT film. b) Histogram of the diameter measurements for the bare CNTs (top) and Tg-Car/CNTs (bottom). Reprinted with permission from John Wiley and Sons: B. R. Bunes, M. Xu, Y. Zhang, D. E. Gross, A. Saha, D. L. Jacobs, X. Yang, J. S. Moore, and L. Zang, "Photodoping and enhanced visible light absorption in single-walled carbon nanotubes functionalized with a wide band gap oligomer," *Advanced Materials*, vol. 27, no. 1, pp. 162-167, copyright 2015.

force microscopy. Using the SiO_2 substrate as a common reference, large differences in the adhesion forces of the CNT and Tg-Car/CNT materials are clearly visible (Figure 3.3). Line scans show an adhesion force approximately seven times smaller in the Tg-Car film. Aggregates of Tg-Car oligomer are visible on the substrate, which give similar values for adhesion force. Furthermore, the entire surface of the Tg-Car/CNT has a uniform adhesion force, demonstrating full coverage of the CNT by the oligomer. These adhesion force microscopy measurements prove the Tg-Car oilgomer is present on the surface of the CNTs.

Raman spectra of bare CNTs and Tg-Car/CNT were used to examine potential chirality selectivity (Figure 3.4). Functionalization caused a slight increase in the radial breathing mode (RBM). For example, the RBM of (7,5) CNTs shifted from 283.2 cm^{-1} to 285.8 cm^{-1}. This further demonstrates surface functionalization. Chiralities were assigned to RBMs based on values from the literature. The relative

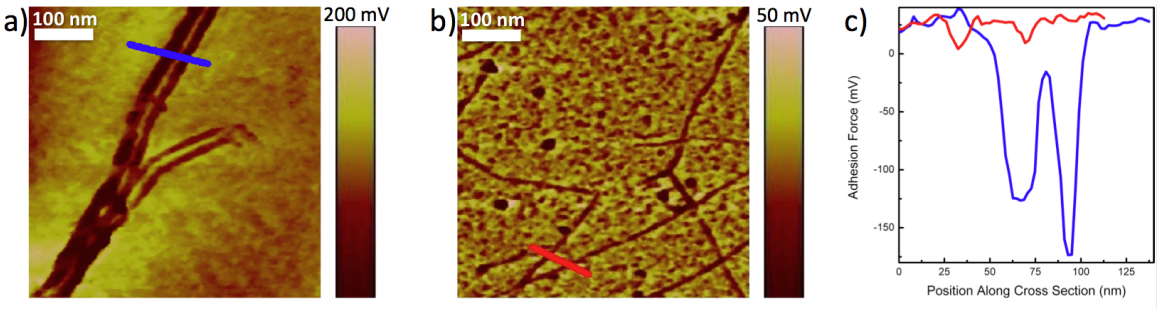

Figure 3.3. Adhesion force microscopy measurements of a) CNT and b) Tg–Car/CNT films. c) Line scans of the image corresponding to the annotations in a) and b). Reprinted with permission from John Wiley and Sons: B. R. Bunes, M. Xu, Y. Zhang, D. E. Gross, A. Saha, D. L. Jacobs, X. Yang, J. S. Moore, and L. Zang, "Photodoping and enhanced visible light absorption in single-walled carbon nanotubes functionalized with a wide band gap oligomer," *Advanced Materials*, vol. 27, no. 1, pp. 162-167, copyright 2015.

fraction of (6,5) and (7,6) nanotubes decreased, whereas (8,3) CNTs remained at the same concentration.

3.2.2 Optical Properties

Solid-state absorption spectra were measured for Tg-Car, Tg-Car/CNT, and bare CNTs (Figure 3.5). No absorption was observed for the oligomer in the visible region. The bare CNTs showed little absorption overall. The oligomer dominates the absorption of the Tg-Car/CNT composite, but an increase is observed in the visible region. Normalizing the spectra to the absorption measured at 900 nm (CNT-only absorption) more clearly demonstrates the enhanced absorption. This enhancement begins at 847 ± 27 nm. The formation of a charge transfer complex between the CNT and oligomer is proposed as the origin of the enhanced absorption.

3.2.3 Field Effect Transistors and Photoresponse

To investigate the charge transfer between the oligomer and CNT, field effect transistors (FETs) were fabricated and compared to FETs using bare CNTs as the channel material. These transistors were tested in the dark and under illumination from a tungsten lamp. The FET comprised of the bare CNTs showed no response

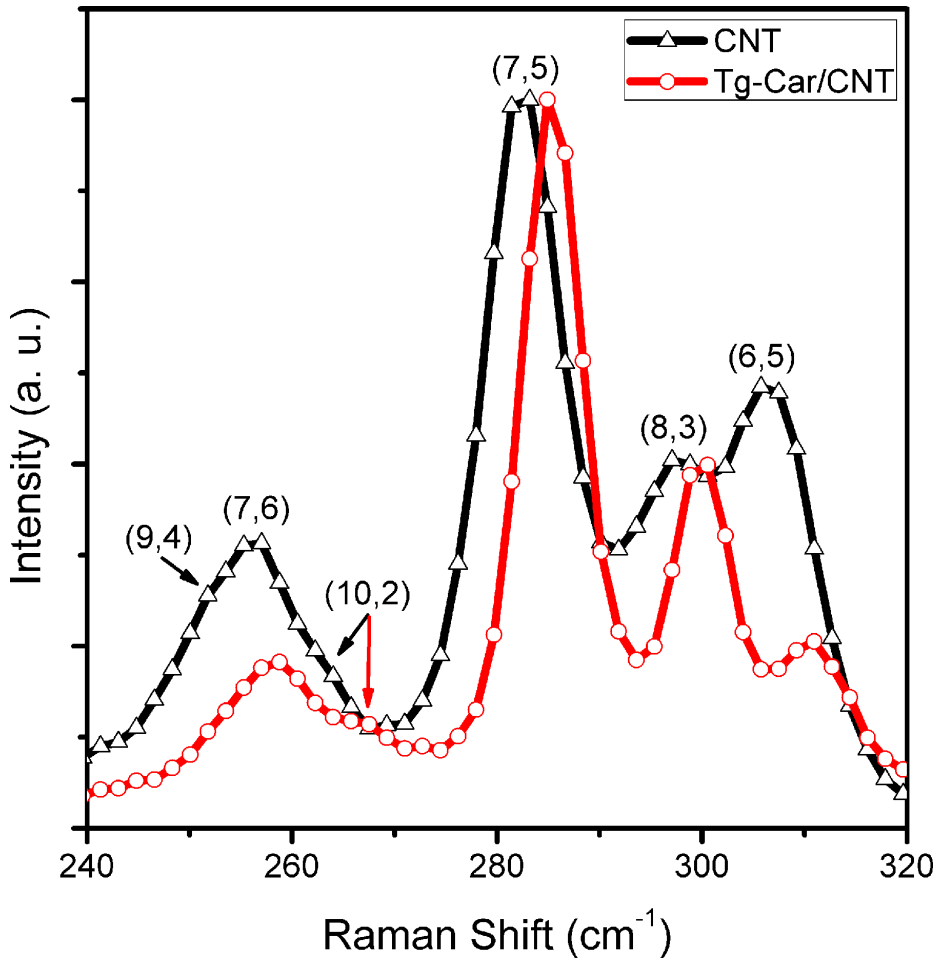

Figure 3.4. Raman spectra of the CNT and Tg-Car/CNT materials. Reprinted with permission from John Wiley and Sons: B. R. Bunes, M. Xu, Y. Zhang, D. E. Gross, A. Saha, D. L. Jacobs, X. Yang, J. S. Moore, and L. Zang, "Photodoping and enhanced visible light absorption in single-walled carbon nanotubes functionalized with a wide band gap oligomer," *Advanced Materials*, vol. 27, no. 1, pp. 162-167, copyright 2015.

to light. However, the FET featuring the Tg-Car/CNT material demonstrated a large, positive shift in threshold voltage of 4.2 ± 0.4 V (Figure 3.6). Such a shift is indicative of p-type doping in the CNT. Restated, electrons transfer from the CNT to the oligomer, contrary to the prediction that the oligomer would be the electron donor. Further complicating the situation is the fact that tungsten lamps emit few photons capable of exciting the oligomer (those with wavelengths below 400 nm); the existence of a photoresponse is unexpected.

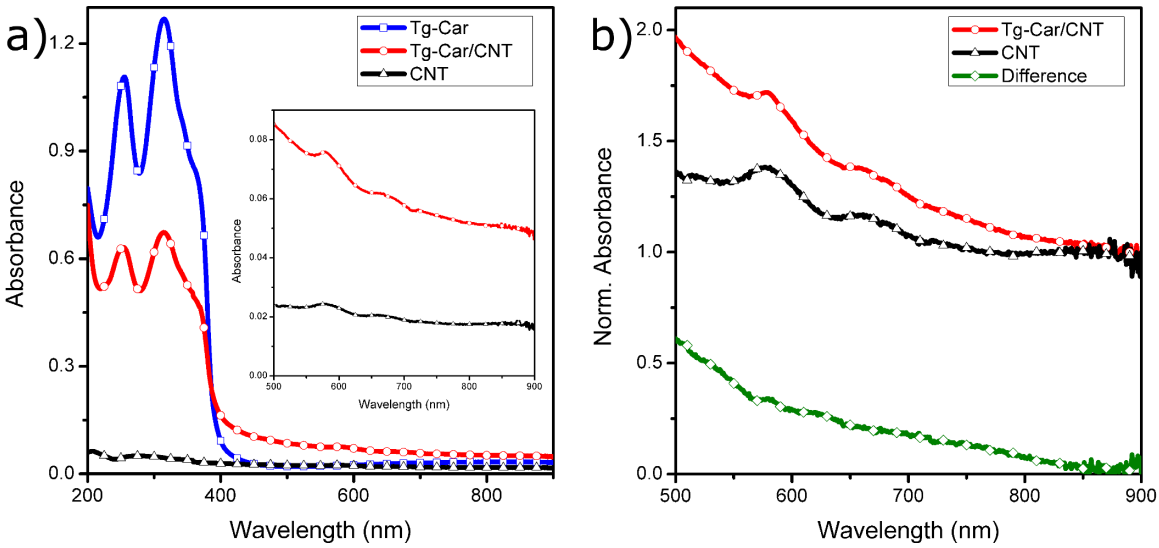

Figure 3.5. Optical absorbance of the Tg-Car, CNT, and Tg-Car/CNT films. a) Absorption spectra for Tg-Car, Tg-Car/CNT, and bare CNT films. b) Absorption spectra for CNT and Tg-Car/CNT films normalized to the absorption at 900 nm to eliminate artifacts due to concentration differences. The difference between the two spectra is included for reference, which demonstrates the improved absorption in the visible region in spite of the wide band gap of the oligomer. Reprinted with permission from John Wiley and Sons: B. R. Bunes, M. Xu, Y. Zhang, D. E. Gross, A. Saha, D. L. Jacobs, X. Yang, J. S. Moore, and L. Zang, "Photodoping and enhanced visible light absorption in single-walled carbon nanotubes functionalized with a wide band gap oligomer," *Advanced Materials*, vol. 27, no. 1, pp. 162-167, copyright 2015.

To investigate the response and recovery kinetics, the photoresponse was measured as a function of time. Both the response and recovery followed exponential curves (Figure 3.7). The time constant of the response is 8.9 s, while the recovery time constant an even larger 41.1 s. It is unclear why the response is so slow, but an explanation of the slow recovery will be presented in Section 3.2.5.

Further probing the photoresponse, the illumination spectrum was modified. The flux of photons with energies exceeding the band gap of the CNT (1.3 eV) was kept constant while the cut-on wavelength varied. The threshold voltage remained constant until the photons with wavelengths less than 495 nm were removed and decreased thereafter. Projecting the data to zero shift in threshold voltage shows that no photoresponse occurs to light with a wavelength greater than 833 $\pm$ 37 nm

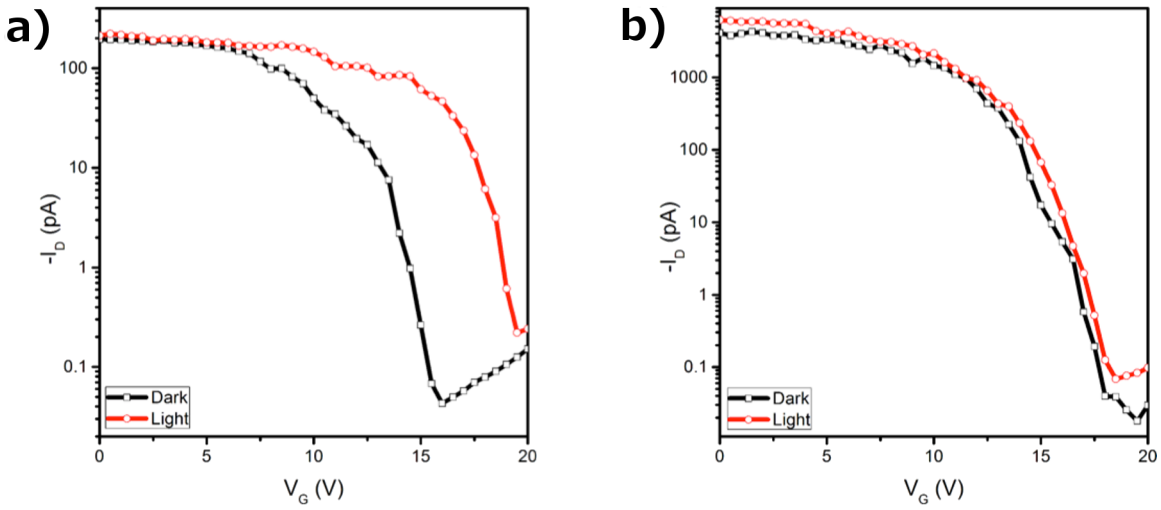

Figure 3.6. Photoresponse of FETs made with a) Tg-Car/CNT and b) bare CNTs as the channel material. Reprinted with permission from John Wiley and Sons: B. R. Bunes, M. Xu, Y. Zhang, D. E. Gross, A. Saha, D. L. Jacobs, X. Yang, J. S. Moore, and L. Zang, "Photodoping and enhanced visible light absorption in single-walled carbon nanotubes functionalized with a wide band gap oligomer," *Advanced Materials*, vol. 27, no. 1, pp. 162-167, copyright 2015.

(or less than 1.5 eV) (Figure 3.8). While this energy does not correspond to the band gap of either material, it does correlate with the absorption data. Excitation in the CNT alone can be ruled out by this experiment. Since the flux of photons whose energies exceed the band gap of the CNTs is constant, the threshold voltage would not have changed if excitation of the CNT alone were responsible. Using the spectra from the tungsten lamp and the absorption spectra, the number of absorbable photons in the enhanced region were calculated for each cut-on wavelength and plotted against the threshold voltage shift. Including a fourth data point at the origin, a clear linear relationship is observed, with a R^2 greater than 0.99. This provides further evidence that the enhanced absorption reported in the previous section is responsible for the shift in threshold voltage.

Other potential factors can also be eliminated from consideration. For example, it would be possible to create electrons energetic enough to transfer to the oligomer through S_{22} absorption in the CNT. The majority species used in this study, (6,5) and

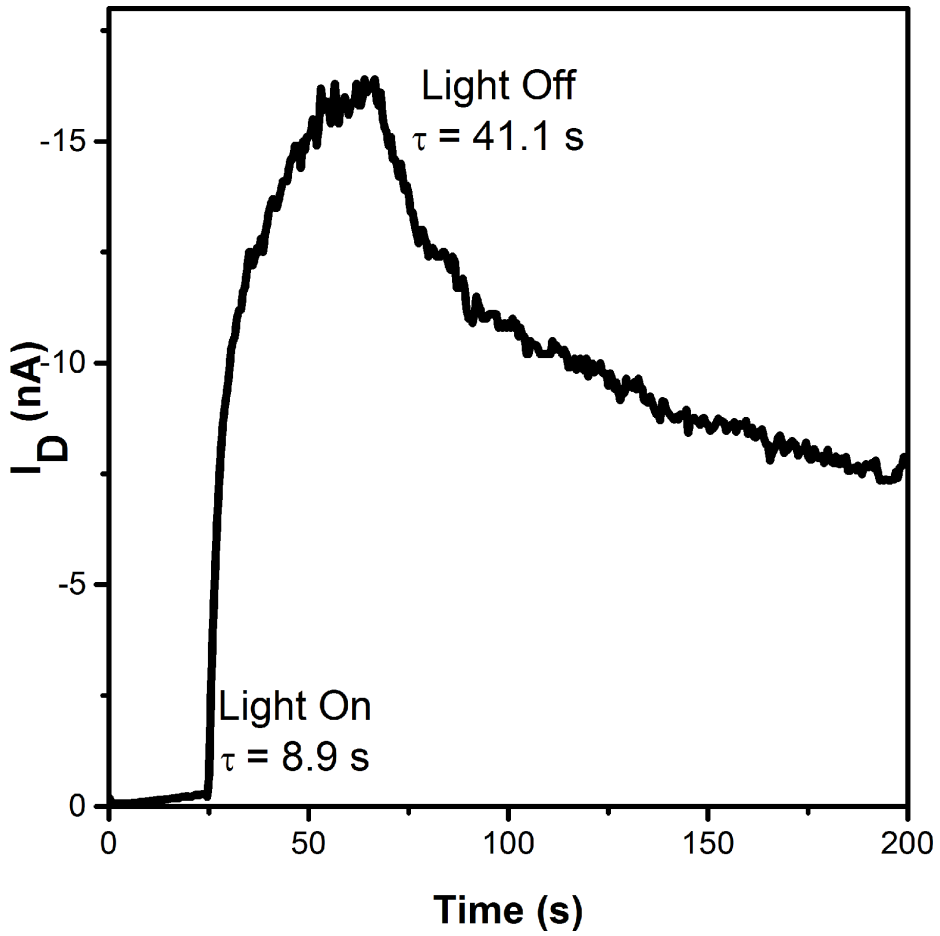

Figure 3.7. Photoresponse and recovery of Tg-Car/CNT.

(7,6), have S_{22} absorption peaks at 579 nm (2.2 eV) and 652 nm (1.9 eV), respectively. However, the broadband enhancement cannot be explained by S_{22} absorption because it yields well-defined peaks, which are clearly visible. Additionally, the energetics are not favorable because the S_{22} level of the conduction band is very close to the LUMO of the oligomer. While charge transfer is possible, the dominant process is most likely thermalization to the S_{11} band. Finally, this process can be ruled out because a threshold voltage shift is observed at 700 nm, which is too low in energy for S_{22} absorption. Alternatively, threshold voltage shifts have been observed by photoinduced desorption of oxygen, which serves as an accepter to the CNT. However, desorption of adsorbed oxygen only occurs under ultraviolet light, which is

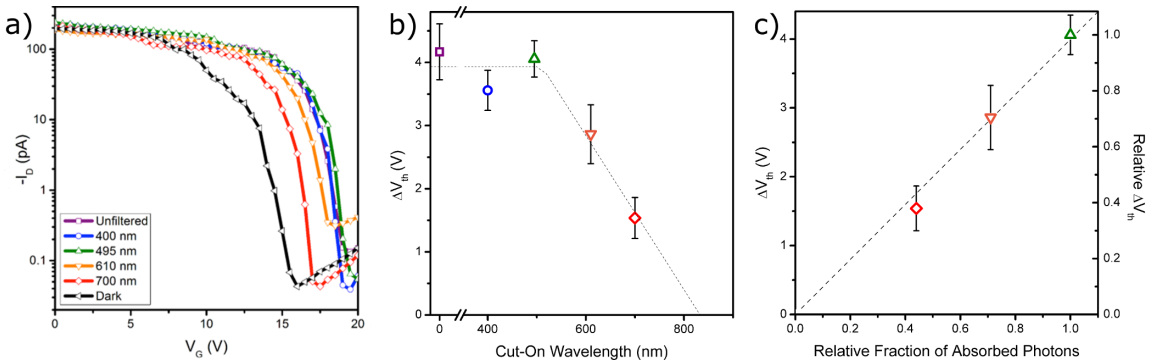

Figure 3.8. Transfer characteristics of Tg-Car/CNT FETs under different illumination conditions. a) Transfer characteristics of the Tg-Car/CNT transistors under different excitation spectra. b) Shift in threshold voltage as a function of cut-on wavelength. c) Shift in threshold voltage as a function of the number of absorbable photons in the enhanced region observed in the absorption spectrum. Reprinted with permission from John Wiley and Sons: B. R. Bunes, M. Xu, Y. Zhang, D. E. Gross, A. Saha, D. L. Jacobs, X. Yang, J. S. Moore, and L. Zang, "Photodoping and enhanced visible light absorption in single-walled carbon nanotubes functionalized with a wide band gap oligomer," *Advanced Materials*, vol. 27, no. 1, pp. 162-167, copyright 2015.

not present here. Repeating photoresponse experiment in an argon environment did not significantly change the shift in threshold voltage.

3.2.4 Sensors

Building on previous success detecting nitroaromatic explosives with materials based on carbazole, chemiresistors were fabricated from Tg-Car/CNT. These sensors were exposed to 4-nitrotoluene (NT). Exposures were performed through dilution of a saturated vapor of the desired analyte. Sensors were operated at a constant 1 V bias and the current was monitored. Responses to NT at concentrations of 1.5, 2.0, and 3.0 ppm are shown in Figure 3.9.

There are two curious features of the sensor response. First, the sign of the current change is the opposite of what was expected. Because carbon nanotubes conduct holes and nitrotoluene withdraws electrons, the conductivity should increase when exposed to the analyte [98]. However, it decreases. Secondly, the recovery time constants are significantly faster than the optical test. The recovery time constants for the 1.5 ppm,

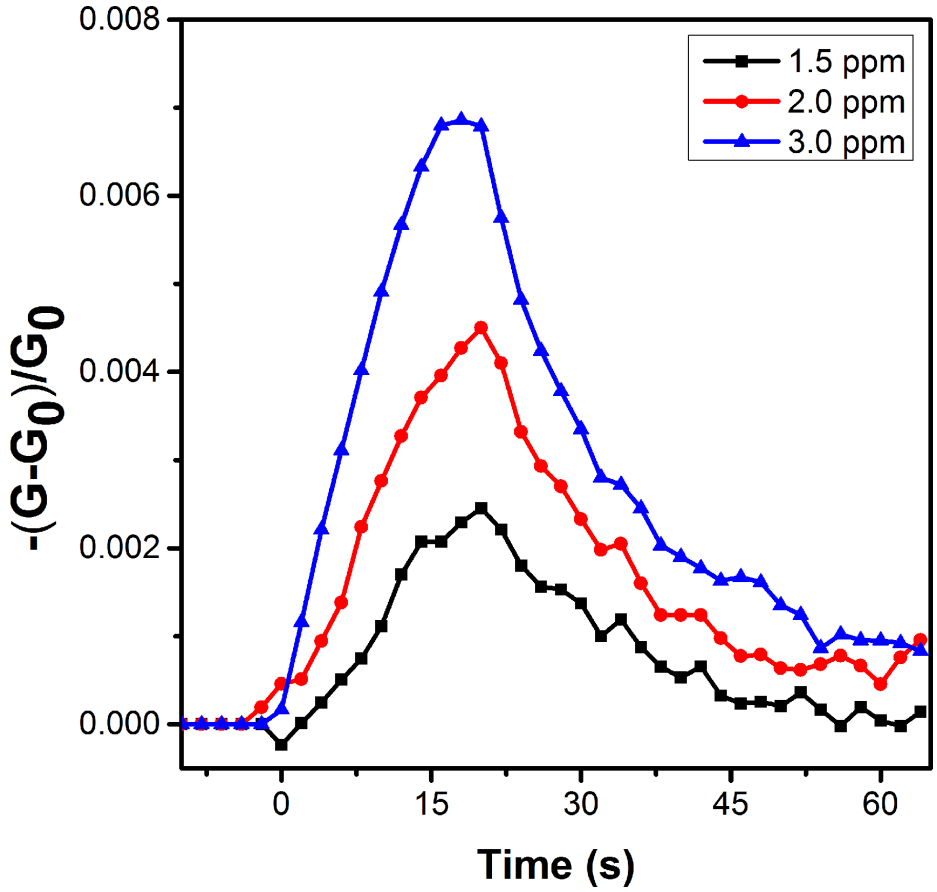

Figure 3.9. Sensor response to nitrotoluene at different concentrations.

2.0 ppm, and 3.0 ppm exposures are 16.6 s, 12.0 s, and 12.2 s, respectively. This is notably faster than the recombination observed in the photoresponse test. These two factors indicate that charge transfer is not the mechanism responsible for the sensor response.

3.2.5 Discussion

There are two major questions raised by the data presented in this chapter: 1) what is the origin of the enhanced visible light absorption?, and 2) why does the conductivity of the Tg-Car/CNT sensor decrease under exposure to nitrotoluene when it is expected to increase? An explanation of these behaviors will be presented here.

The unusual absorption is attributed to the formation of a charge transfer complex between the carbon nanotube and the oligomer. The Fermi level of the oligomer lies

in the middle of the oligomer's band gap since it is not intentionally doped and the Fermi level of the CNT sits at the edge of the valance band due to oxygen doping. Aligning the two Fermi level reveals that an electron transferring from the CNT to the oligomer requires 1.6 ± 0.1 eV of energy, corresponding to a wavelength of 792 ± 89 nm. This correlates well with the experimental data. Another feature of this band alignment is the formation of a 2.5 eV energy barrier at the interface (Figure 3.10). This energy barrier prevents the back transfer process, which produces a net increase of holes in the CNT. The increased hole concentration increases the threshold voltage of the field effect transistors because it requires a stronger electric field to turn the transistor off.

The oligomer also has a major impact on the sensing capabilities of CNTs. Whereas charge transfer dominates the sensor response in bare CNTs, another effect must dictate the response in Tg-Car/CNTs because of the opposite polarity of the change in current. In the bare CNTs, electrons transfer from the CNT to the analyte to increase conductivity. However, the field effect transistor data show that the Tg-Car/CNT films already show increased conductivity due to charge transfer. The major difference in charge carrier pathway is the presence of the oligomer between CNTs at intertube junctions, effectively creating tunnel barriers. With a proven affinity for nitroaromatic chemicals, the oligomer adsorbs explosive molecules. The extremely thin films (a few angstroms) enable diffusion into the oligomer, causing swelling. Swelling increases the tunneling distance charges must overcome, leading to a decrease in current. This effect is similar to early chemiresistors that use conductive materials (*e.g.*, carbon nanotubes, carbon black) in an insulating polymer matrix (*e.g.*, polystyrene, polyethylene). The polymer creates a thick film through which the analyte must diffuse. By contrast, the processing method of the Tg-Car/CNT film eliminates excess insulating material, with oligomer only present on the surface of the carbon nanotubes. This creates a porous film with a large surface area. The advantage

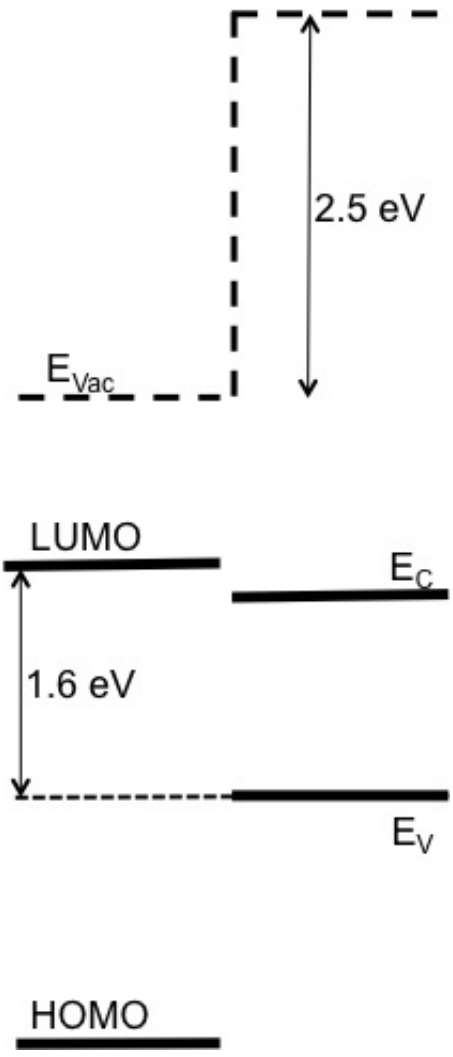

Figure 3.10. Proposed band alignment of the Tg-Car oligomer and CNT. Reprinted with permission from John Wiley and Sons: B. R. Bunes, M. Xu, Y. Zhang, D. E. Gross, A. Saha, D. L. Jacobs, X. Yang, J. S. Moore, and L. Zang, "Photodoping and enhanced visible light absorption in single-walled carbon nanotubes functionalized with a wide band gap oligomer," *Advanced Materials*, vol. 27, no. 1, pp. 162-167, copyright 2015.

of this morphology is improved sensitivity, achieving detection in the sub-ppb range, whereas traditional chemiresistors based on polymer swelling are sensitive only in the ppm range. The oligomer essentially negates the conductivity change due to charge transfer and replaces it with swelling. This may also be useful in detecting charge transfer inactive chemical species, such as fuels (*e.g.*, octane), which is difficult for room temperature chemiresistors.

3.3 Summary

Semiconducting, single-walled carbon nanotubes were functionalized with a designer oligomer. The oligomer added solubility to the carbon nanotubes in chloroform, which enabled solution processing. When deposited on an SiO_2 substrate, the film was free of carbon nanotube bundles and quite uniform. The oligomer greatly eases the processing of carbon nanotubes and produces higher quality films. The improved uniformity of films is vital to the repeatability of devices.

The Tg-Car/CNT material showed an unusual absorption spectra, demonstrating absorption in the visible range despite the oligomer's wide band gap. Excitation of this new absorption band produced strange effects in field effect transistors. While the oligomer was originally expected to donate electrons to the carbon nanotube, it accepts electrons instead. The reason for this is proposed to be the formation of a charge transfer complex between the carbon nanotube and the oligomer. Excitation of this complex causes electron transfer from the carbon nanotube to the oligomer. Furthermore, an electric field forms at the interface of the two materials, which prevents electrons from transferring back to the carbon nanotube.

Chemiresistors were fabricated from the Tg-Car/CNT material and produced a peculiar response to nitrotoluene. Whereas bare CNTs increase conductivity in the presence of a nitroaromatic chemical, the Tg-Car/CNT chemiresistors became less conductive. The oligomer prevents direct interaction between the carbon nanotube and analyte. Instead, the oligomer acts as a tunnel barrier between carbon nanotubes, which changes its thickness in the presence of an analyte. The sensing mechanism is polymer swelling, instead of the charge transfer seen in bare CNTs.

This work is expected to impact two fields: sensing and solar energy. For sensors, this morphology is unique to chemiresistors based on polymer swelling. The ultra-thin layer of oligomer allows pores to remain in the film, which facilitates diffusion for the analyte. This leads to a high sensitivity, which is several orders of magnitude better

than in tradition chemiresistors based on polymer swelling. The fact that sensing does not involve charge transfer also suggests this strategy could be used to detect charge transfer inactive species, such as saturated hydrocarbons. Switching to solar energy, two major issues in using CNTs for photovoltaic cells are insolubility and narrow absorption bands. The oligomer addresses both of these problems. Solubility is provided through noncovalent functionalization without disruption to the CNT's electronic properties. Meanwhile, the formation of the charge transfer complex provides broadband absorption across the visible spectrum. Furthermore, the formation of the electric field at the CNT/oligomer interface may enhance charge separation while hindering recombination. This work may provide a new technique to improve the performance of photovoltaic cells based on carbon nanotubes.

CHAPTER 4

DUAL-GATE ORGANIC FIELD EFFECT TRANSISTORS FOR CHEMICAL SENSORS

While organic semiconductors make excellent chemical sensors because of their ability to be tailored to a specific analyte, low conductivity prevents them from being used in a practical application. Splitting the sensing and charge carrying duties between different materials is a potential means to approach commercial devices. In this chapter, we explore using a field effect transistor to carry current with a gate electrode functionalized with organic sensing materials. Charge transfer between the analyte and sensing material changes the bias of the gate, modulating the current. The novelty of this work involves the addition of a second gate, which increases sensitivity.

4.1 Overview

Field effect transistors have been explored for chemical sensing applications for over 40 years. In spite of the long development time, these sensors have not yet become commercially applicable. Here, we review the history and progress of these sensors. Specifically, we will focus on their limitations and how our work addresses these problems.

4.1.1 Organic Field Effect Transistors as Chemical Sensors

Because of the large gabin of transistors (see Appendix B for more information), they seemed to be promising candidates for high-sensitivity chemical sensors. These sensors are called "chemical-sensing field effect transistors (chemFETs)." The original work was performed in 1970s by Prof. Jiří Janata, in the Department of Materials Science and Engineering at the University of Utah [99]. Janata's gas sensing chemFETs are a form of potientiometric sensors. Molecules adsorbed on the surface of the electrode change the work function. This changes the bias of the transistor, resulting in a change in current [100]. To provide selectivity, his team coated the gate electrode in organic materials, typically conducting polymers [101]. Alternatively, the conducting polymer can be used as the channel material and left exposed to the environment. These two generations of chemFETs (Figure 4.1) have yet to see commercial success, although lab results are promising. In this chapter, a third generation of chemFETs – the dual-gate chemFET – is presented, developed in Prof. Janata's former department.

Early chemFETs used the "sensing-semiconductor" configuration. A voltage is applied to the gate electrode to drive the transistor into saturation, increasing conductivity and sensitivity [102]. In this configuration, the semiconducting channel material is exposed to the environment, covering the dielectric layer and gate electrode. This type of sensor achieved high sensitivity, with detection limits in the parts per billion range [103, 104]. However, selectivity was very poor. There are two main reasons for this. First, there are a number of ways to affect the conductivity of an organic semiconductor in addition to charge transfer. The introduction of trap states at the dielectric/semiconductor interface occurs when molecules diffuse, either through the semiconductor crystal or at grain boundaries. If there is a chemical present that is soluble in the organic semiconductor, it can cause swelling, which decreases conductivity [105]. Secondly, the semiconductors used in these devices are generally

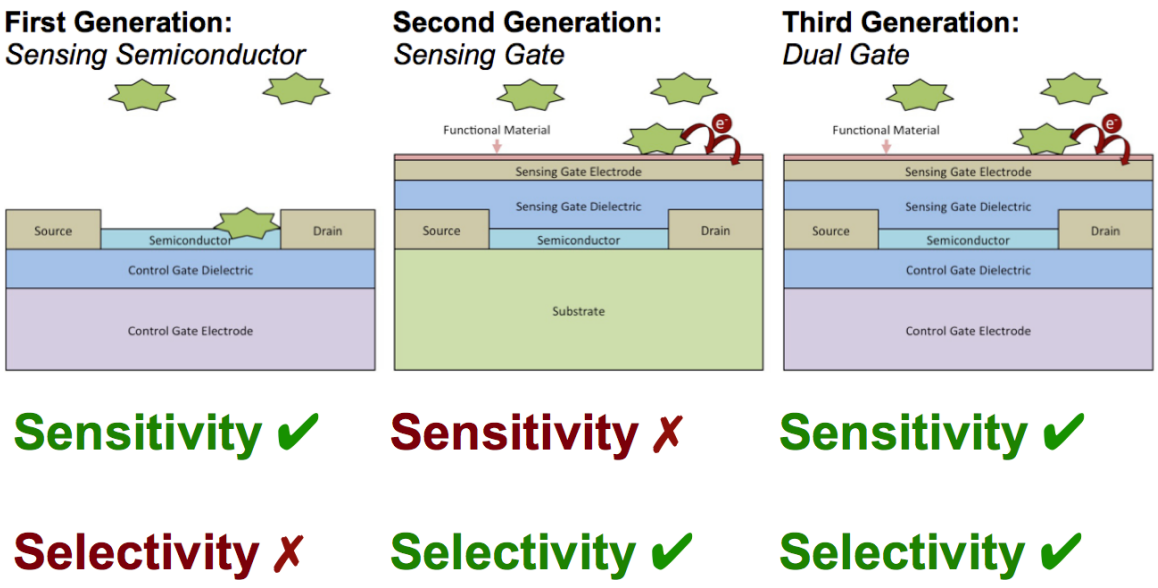

Figure 4.1. Schematic drawings of a sensing-semiconductor, sensing-gate, and dual-gate chemFETs.

nonspecific [106]. In order to achieve high sensitivity, high charge carrier mobility is required. This feature is rare among organic semiconductors, limiting the materials that can be used. Since the semiconductor responds directly to the analyte, this is a problem. To add selectivity, the organic semiconductor molecules need to be tailored to the target analyte, but this frequently is detrimental to the charge carrier mobility. Selectivity could be improved by decoupling selectivity and charge conduction.

To separate selectivity and charge conduction, "sensing-gate" chemFETs were developed. The structure of these sensors is essentially an inverted sensing-semiconductor chemFET. The organic semiconductor is buried under the dielectric layer and gate electrode. The gate electrode is functionalized for selectivity to a specific molecule [107]. The gate is floating and is biased through charge transfer events from the analyte [108, 100]. Using this configuration did improve selectivity. Decoupling the charge transport and sensing responsibilities allows a much broader range of sensor materials to be used [101]. However, sensitivity is poor. The main reason for poor sensitivity is trap states in the organic semiconductor. These traps cause threshold

voltages to be large [109]. For sensors, the consequence is that a large amount of analyte must be accumulated before the sensor can give a response (Figure 4.2). The first charges transferred to the gate electrode only serve to fill trap states in the organic semiconductor; no charge channel is created. Reducing the threshold voltage is a potential means to improve sensitivity while maintaining the high selectivity of this configuration.

4.1.2 Modifying Threshold Voltage

Filling trap states (*i.e.*, reducing the threshold voltage) is of critical importance to improving the sensitivity of sensing-gate chemFETs. A number of methods exist to control the threshold voltage, although the applications generally target electronics (see Appendix B for an overview). In this context, the dual-gate architecture has proven to be a powerful tool. This threshold voltage shift can be understood by exam-

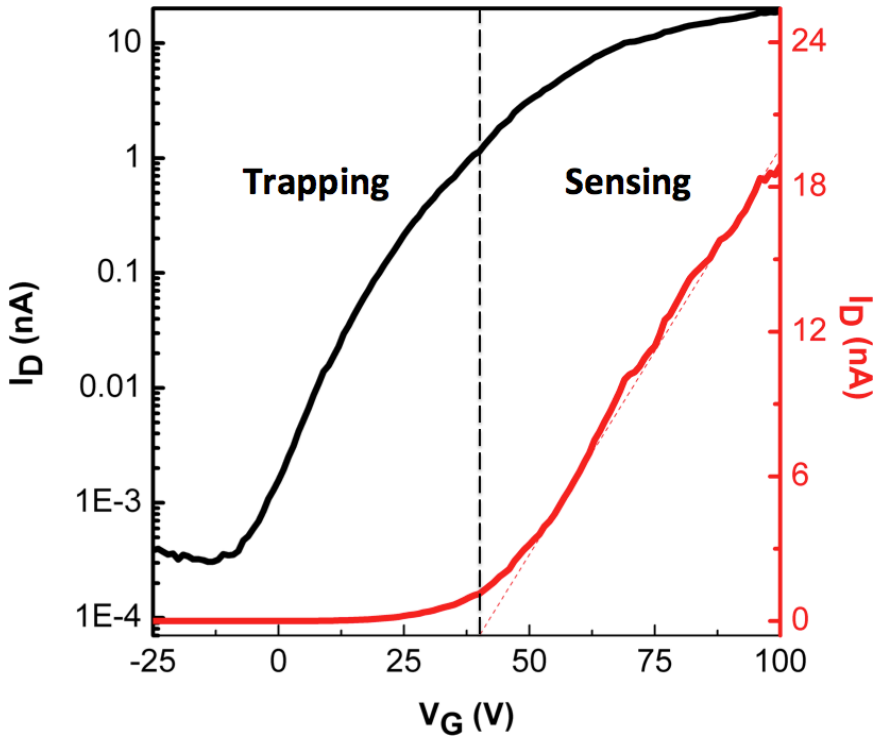

Figure 4.2. Trap states cause large threshold voltages in organic field effect transistors. These trap states must be overcome before an appreciable signal can be generated through sensing.

ining the charge accumulation at a metal-insulator-semiconductor interface. Charge carrier density decays exponentially from the interface [110]. Increasing the voltage applied to the metal increases the charge (electron) carrier density. The point at which the accumulated charge carrier density meets the intrinsic level denotes the accumulation width (Figure 4.3). If we consider the metal-insulator-semiconductor shown to be the bottom gate-bottom gate dielectric-semiconductor, an interesting effect occurs if we place the top dielectric within the accumulation width. Changing the voltage on the bottom gate changes the charge carrier density at the semiconductor-top dielectric interface. As discussed earlier, changing the charge carrier density changes the threshold voltage.

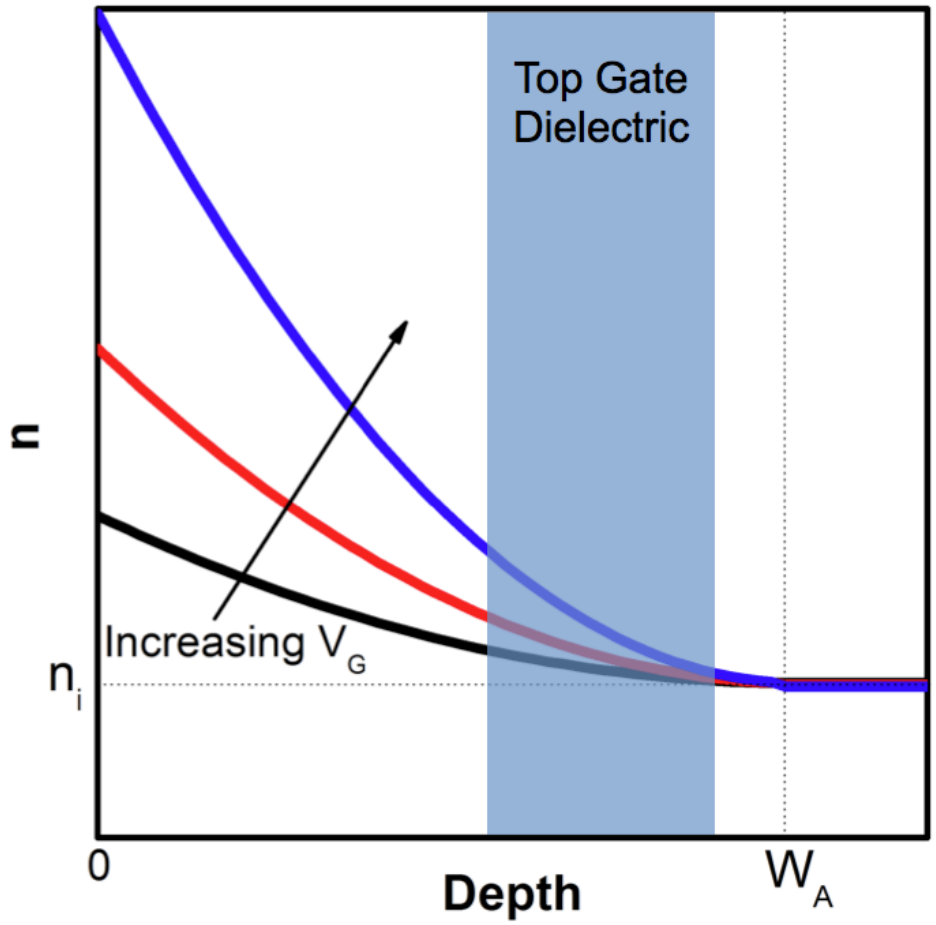

Figure 4.3. A voltage applied to one gate changes the charge density on the opposite interface, changing the threshold voltage of that gate.

To achieve high sensitivity, the conductive pathway should be along the semiconductor/top gate dielectric interface. In practice, this is difficult. Small molecule organics are generally employed as the semiconductor layer because of their high charge carrier mobility. However, charges are typically immobile at the semiconductor/top gate dielectric interface due to surface roughness. In spite of this, DG-FETs have been used as chemical sensors for analytes in solution. However, a significant improvement in sensitivity has been elusive. Because of the lack of conductivity along the top dielectric/semiconductor interface, the signal is typically a shift in threshold voltage along the bottom gate instead of a change in current. The signal is typically small because of losses through the semiconductor layer (demonstrated in Figure 4.3). Additionally, threshold voltage shift is relatively time consuming to measure and calculate compared to a change in current. There is significant room for improvement in sensors based on DG-FETs, with aspirations of detecting vapor-phase chemicals.

4.2 Results

The true potential of DG-FETs as chemical sensors has not yet been realized. Sensitivity is the main challenge. The low sensitivity arises from losses across the semiconductor layer. As seen in Figure 4.3, a large change at one interface yields only a small change at the other. With charge transport only possible along the bottom interface, the sensor response is limited to the smaller change. A clear path to improving sensitivity would be to move the charge transport channel to the top channel so it can be directly affected by the sensing gate. This would require an improved interface at the semiconductor/top dielectric interface.

In this work, a dual-gate field effect transistor with conductivity at the top interface is demonstrated. In fact, the two gates behave symmetrically, with either able to modulate the threshold voltage of the other. When used as a sensor, the DG-FET demonstrated a signal four orders of magnitude larger than the equivalent

sensing-gate chemFET to ammonia in the vapor phase. This work represents a major improvement to chemFETs with the first demonstration to vapor-phase chemicals.

The device described in this chapter is shown in Figure 4.4. Heavily doped silicon is used as the substrate and bottom gate electrode. A thermal oxide layer (300 nm) serves as the bottom gate dielectric. Source and drain electrodes (70 nm Au/5 nm Ti) are patterned on the dielectric layer. The semiconductor is Polyera ActivInk N2200 (10 nm), which possesses among the highest charge carrier mobilities in a polymer.

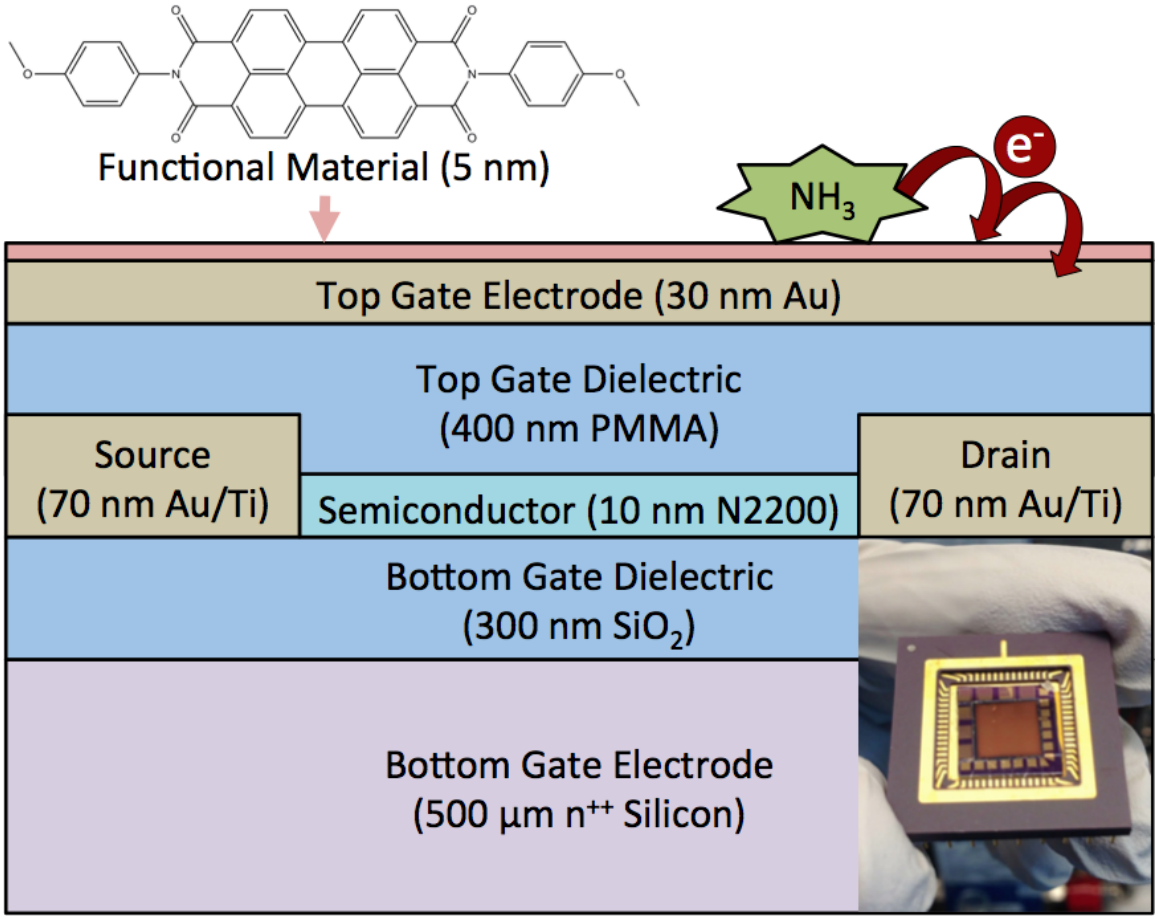

Figure 4.4. Cross-sectional schematic of the DG-FET. The inset shows a photograph of the dual-gate device. Reprinted with permission from the Institute of Electrical and Electronics Engineers: B. R. Bunes, T. Knowlton, D. L. Jacobs, P. Slattum, and L. Zang, "Dual gate architecture for high sensitivity, high selectivity chemical-sensing field effect transistors." Valencia, ES: IEEE Sensors 2014, November 2014, copyright 2014.

Polymethylmethacrylate (400 nm) serves as the top dielectric. Gold (30 nm) and a perylene tetracarboxyllic diimide derivative (5 nm) serve as the top gate electrode and functional material, respectively. The methods and materials are described in Appendix A.

4.2.1 Conductivity along the Top Interface

To achieve high sensitivity in a dual-gate chemFET, a prerequisite is conductivity along the semiconductor/top dielectric interface. The main cause for a lack of conductivity at this interface in previous devices is high surface roughness. Organic semiconductors based on small molecules were used in these studies because of their high charge carrier mobilities. To achieve high conductivity, these materials are deposited through thermal sublimation and film formation is through Stranski-Krastanov growth, leaving a rough texture. Recently, a polymer with a high electron mobility was developed. When this polymer is spin coated, the resulting film has a low surface roughness, equivalent to the SiO_2 surface used as the bottom dielectric (Figure 4.5).

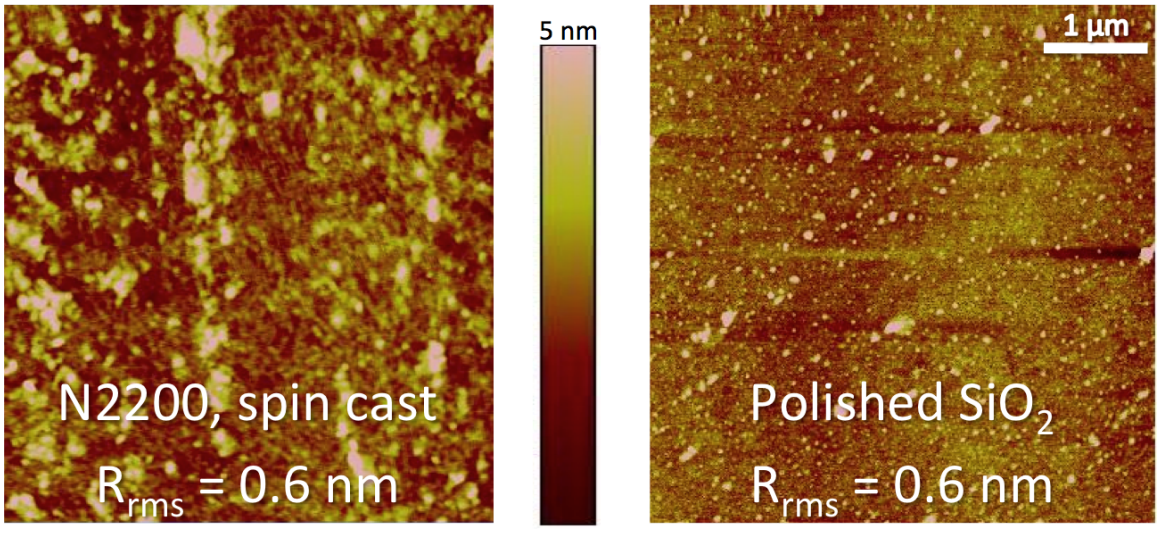

Figure 4.5. Atomic force microscopy image of the silicon oxide and semiconductor layers demonstrating an equivalent roughness.

To evaluate conductivity, transfer characteristics were taken for both the bottom gate and top gate portions of the DG-FET (Figure 4.6). The curves matched closely, indicating nearly equivalent conductivity along the top and bottom interfaces. This corresponds well with the surface roughness data. A slight difference in the capacitance of the two dielectric layers might explain the minor deviations.

4.2.2 Threshold Voltage Shift

With the formation of a conductive pathway at the top interface demonstrated, the next step is to show control over the threshold voltage using the bottom gate.

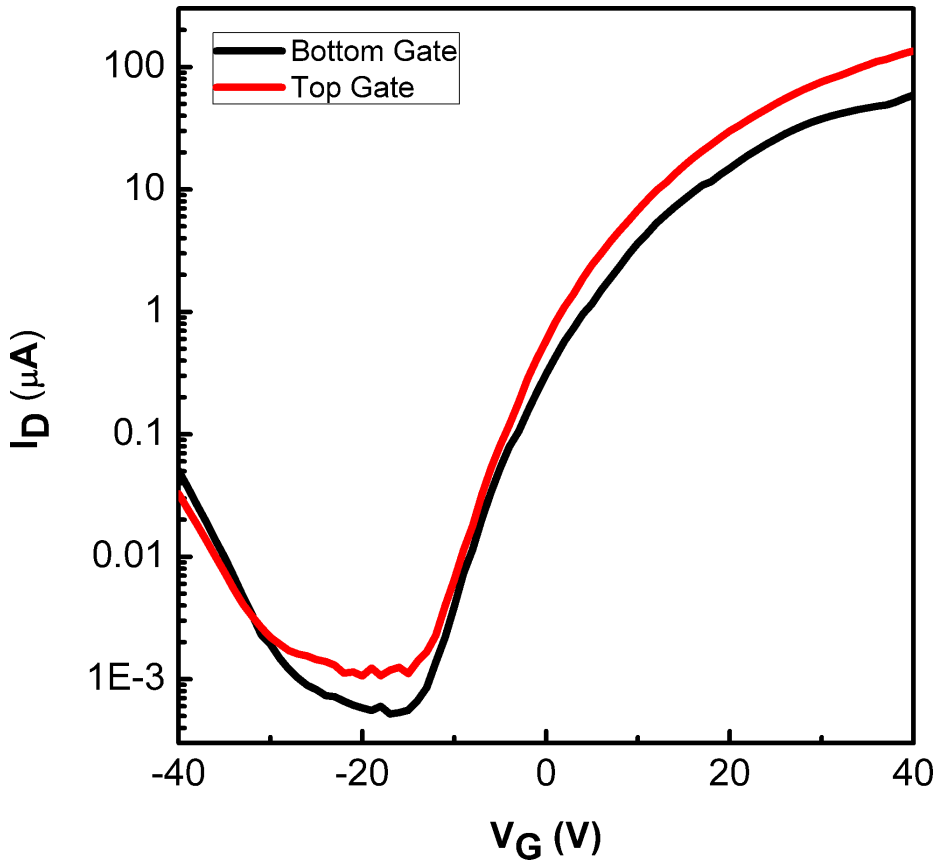

Figure 4.6. Demonstration of charge conduction along the semiconductor/top dielectric interface. The current is equivalent to the bottom gate device. Reprinted with permission from the Institute of Electrical and Electronics Engineers: B. R. Bunes, T. Knowlton, D. L. Jacobs, P. Slattum, and L. Zang, "Dual gate architecture for high sensitivity, high selectivity chemical-sensing field effect transistors." Valencia, ES: IEEE Sensors 2014, November 2014, copyright 2014.

Transfer characteristics were measured by sweeping the top gate while holding the bottom gate at a constant bias (Figure 4.7). Stepping the bias from -40 V to 40 V changed the thereshold voltage from 21 V to -10 V. With negative and zero biases on the bottom gate, the on/off ratio was 10^4-10^5. With positive threshold voltages, the on/off ratio decreases to 10^3. Formation of a channel at the bottom interface causes an increase in off current, which decreases the on/off ratio. This issue could

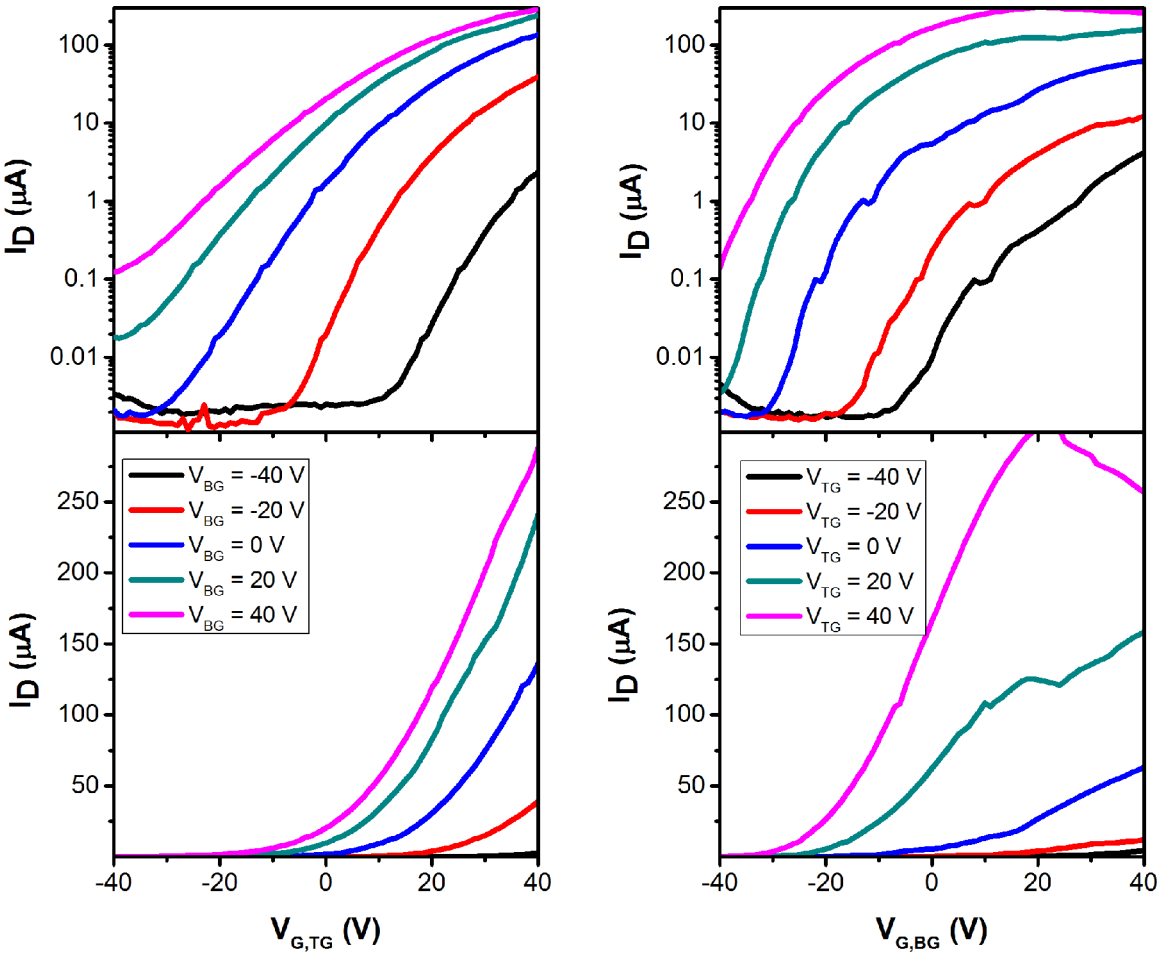

Figure 4.7. Semilogrithmic (top) and linear (bottom) transfer characteristics in which the top gate is swept and the bottom gate has a constant bias (left), and the bottom gate is swept while the top gate is held at a constant bias (right). A shift in threshold voltage is apparent. Reprinted with permission from the Institute of Electrical and Electronics Engineers: B. R. Bunes, T. Knowlton, D. L. Jacobs, P. Slattum, and L. Zang, "Dual gate architecture for high sensitivity, high selectivity chemical-sensing field effect transistors." Valencia, ES: IEEE Sensors 2014, November 2014, copyright 2014.

potentially be resolved by introducing traps at the bottom interface, for example, through texturing or the use of a monolayer with electron traps.

To further explore the device, the transfer characteristics were measured sweeping the bottom gate while holding the top gate constant (Figure 4.7). Similar to the other case, the threshold voltage shifts with a changing top gate bias. Plotting the threshold voltages against the bias (Figure 4.8). The inverse linear relationship suggests biasing one gate fills trap states near the opposite semiconductor/dielectric interface, exhibited by the decreasing threshold voltages. Filling these trap states is a proposed route to improved sensitivity in chemical sensors.

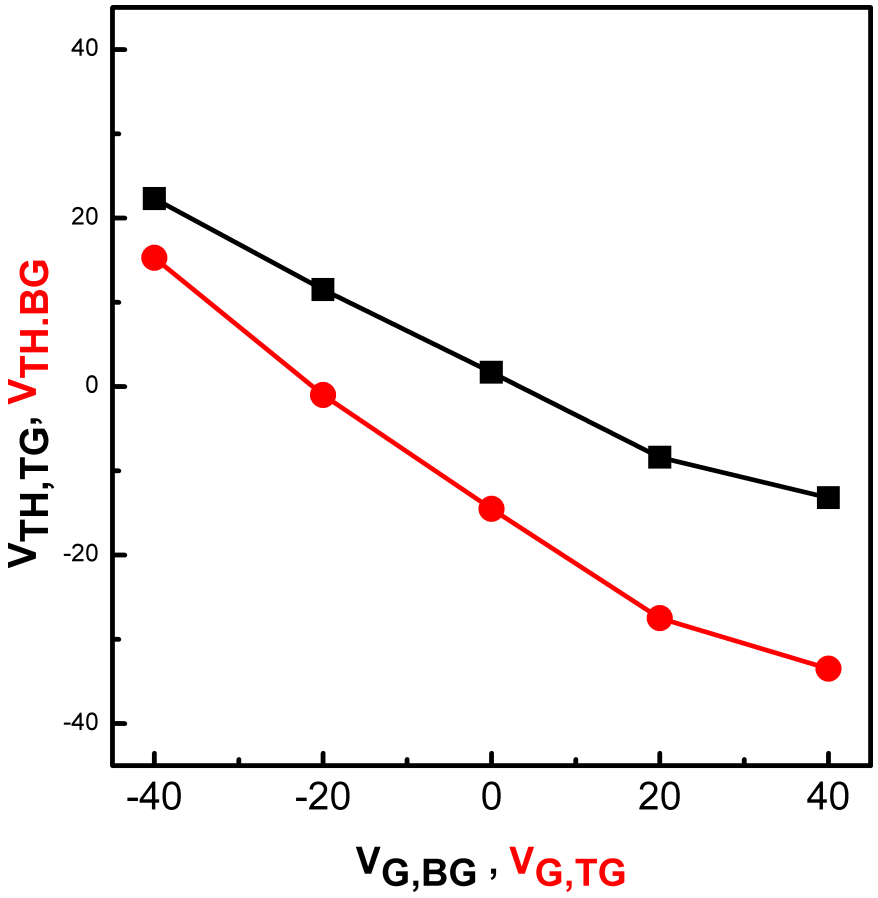

Figure 4.8. Comparison of one gate's ability to change the threshold voltage of the other.

4.2.3 Chemical Sensing

The device characterization experiments proved that the two criteria we identified (conductivity along the semiconductor/top dielectric interface and control of the threshold voltage) for improved sensitivity were met. Next, we explore the sensing capabilities to ammonia gas, representing the first DG-FET sensors to detect gas-phase chemicals.

To demonstrate the DG-FETs ability to detect airborne chemicals, a brief exposure to a saturated ammonia vapor was performed. A 10 mL syringe was filled from the head space of a bottle containing an ammonia-water solution (35 wt. % ammonia). The syringe was emptied onto the sensor. The same device was used for the DG-FET ($V_{G,BG} = 40V$) and SG-FET ($V_{G,BG} = 0V$). Both sensors demonstrated a rapid response, within seconds, and both showed a hundred-fold decrease in current (Figure 4.9). However, the current carried by the DG-FET was approximately four orders of magnitude larger. Since the noise margin did not change significantly, the DG-FET has a signal to noise ration (SNR) that is 10^4 larger than the SG-FET. Because the limit of detection is governed by the SNR, the DG-FET sensor is expected to be 10^4 times as sensitive as the SG-FET.

4.3 Summary

A lack of conductivity prevents many potential sensor materials from practical use. Arrays of sensors are required to achieve adequate selectivity in most applications; electronic sensors are the most straight-forward, cost effective means to create an array. Thus, a generalizable approach to produce an electronic signal from any sensor material is desirable. Such a method would enable a vast range of materials to be used, increasing selectivity to essentially any level desired.

To this end, we designed a novel generation of chemFET. In this version, a second gate electrode is attached to the bottom of a sensing gate chemFET. The major challenge was finding an appropriate material for the semiconducting layer. Small

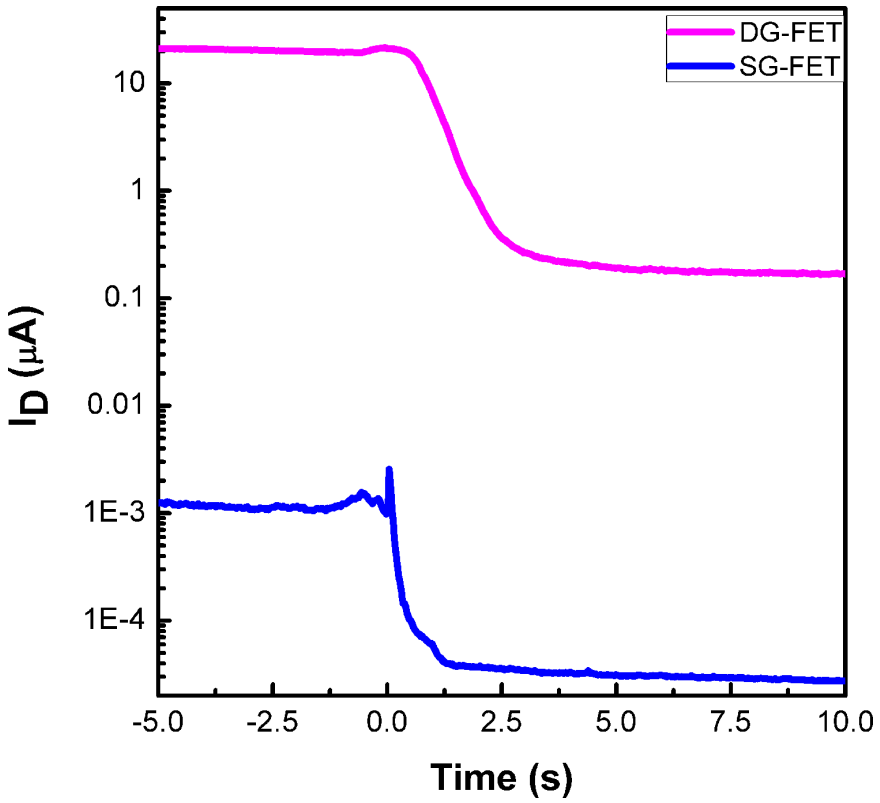

Figure 4.9. Comparison of sensor responses of a DG-FET and a SG-FET. The bottom gate voltage is set at 40 V for the DG-FET. The DG-FET provides a signal four orders of magnitude larger than the SG-FET. Reprinted with permission from the Institute of Electrical and Electronics Engineers: B. R. Bunes, T. Knowlton, D. L. Jacobs, P. Slattum, and L. Zang, "Dual gate architecture for high sensitivity, high selectivity chemical-sensing field effect transistors." Valencia, ES: IEEE Sensors 2014, November 2014, copyright 2014.

molecules can have sufficiently high charge carrier mobility, but form very rough films incapable of forming a conduction pathway along the top interface. Polymers form smooth films, but traditionally have suffered from low charge carrier mobility. A new material, Polyera ActivInk N2200, is a semiconducting polymer with a high electron mobility. Using this material, we fabricated a DG-FET capable of forming a charge channel along both the top and bottom semiconductor/dielectric interfaces with nearly identical transfer characteristics.

This DG-FET demonstrated the ability of one gate to modulate the threshold voltage of the other. In previous devices, the top gate could only be used to change

the threshold of the bottom gate because of the aforementioned surface roughness of the semiconductor. This led to poor sensitivity in sensors because of losses incurred across the semiconductor. By switching to the polymer, our device showed high sensitivity by using the bottom gate to modulate the threshold voltage of the top gate. In fact, the DG-FET sensor was sensitive enough to detect chemicals in the vapor phase, a first for this class of device.

When exposed to a saturated vapor of ammonia, the DG-FET's current dropped by two orders of magnitude. The sensing-gate chemFET produced a similar response, but the absolute current was four orders of magnitude lower from the beginning. Because of the higher current in the DG-FET, the requirements for the associated analog-to-digital converter (ADC) are less strenuous. This may enable adequate sensitivity using lower cost components. Another way of looking at this is the signal to noise ratio, which dictates the limit of detection. Since the noise is not significantly different between the two devices, the DG-FET's SNR is four orders of magnitude higher, which is expected to translate to four orders of magnitude more sensitive. Further work is required to evaluate the sensitivity improvement.

CHAPTER 5

NANOFIBER ALIGNMENT VIA DIELECTROPHORESIS

Organic semiconductors show a broad range of conductivity. Some are nearly conductive enough for practical purposes. For these materials, only a small improvement is necessary. In this chapter, we explore the impact of nanofiber alignment on conductivity. A process for aligning nanofibers using dielectrophoresis was developed. Aligned nanofibers yielded devices with a tenfold increase in conductivity compared to their randomly deposited counterparts.

5.1 Overview

When a nanofiber is deposited on electrodes, three variables can be used to describe its relative position. The location is defined as x and y, while its orientation (*i.e.*, the angle of the nanofiber relative to the shortest path between the electrodes) is defined as θ. All variables are important to control to fabricate uniform devices. The location must be well-defined to ensure nanofibers are present on the electrodes and in the necessary quantities. Meanwhile, θ has a major impact on the resistivity of the resulting device. A method to control all three variables is necessary to achieve uniform devices.

Of course, this represents a simplified case in which the nanofiber completely bridges the electrode gap. In many cases, charges move through a network of nanofibers. In addition to the resistance from the increased path length caused by misalignment, charges are further impeded by nanofiber-nanofiber junctions (Figure 5.1). Nanofiber

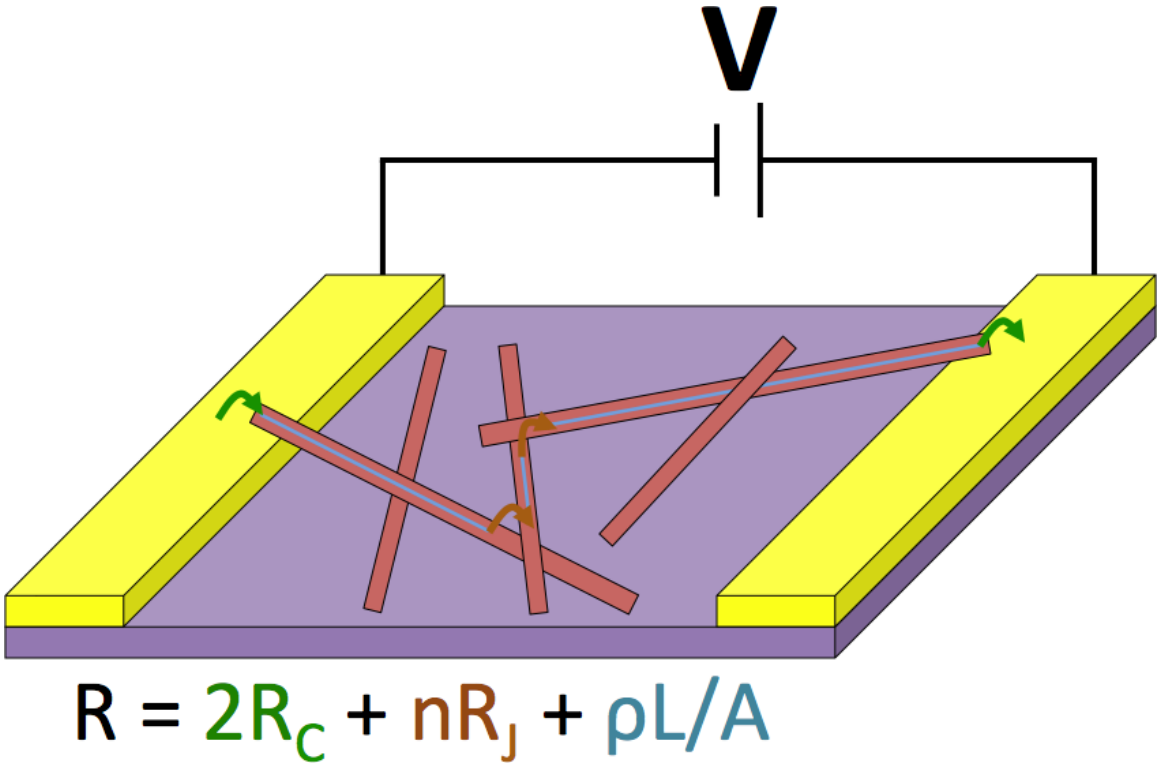

Figure 5.1. Schematic of the sources of resistance in a nanofiber network. The arrows and lines trace an electron's path between electrodes. Their colors correspond to the resistance terms in the equation.

networks are quite complicated. Too little alignment adds too much resistance by introducing many junctions. On the other hand, perfect alignment yields high resistance by reducing the total number of percolation pathways; nanowires are less likely to overlap if they are all oriented in the same direction [111]. Thus, we can write the total resistance as:

$$R = 2R_C + nR_J + \frac{\rho}{A}\ell \tag{5.1}$$

where R is the total resistance, R_C is the contact resistance, R_J is the resistance at a nanofiber-nanofiber junction, n is the number of nanofiber-nanofiber junctions a charge must cross between electrodes, ρ is the resistivity of the nanofiber, A is the nanofiber's cross-sectional area, and ℓ is the length of the charge's path between electrodes. While there has been a substantial amount of research on reducing R_C

and ρ, reducing n and ℓ would also reduce the overall resistance. Furthermore, n and ℓ are random variables, which lead to large variation between devices. Both of these variables can be controlled through alignment. Various alignment techniques have been explored (see Appendix B for a summary). In this chapter, we explore aligning organic nanofibers using dielectrophoresis (see Appendix B for details) to improve conductivity and uniformity in chemical sensors.

5.2 Results

Copper phthalocyanine (CuPc) was selected as the nanofiber material because of its unusually large dielectric constant [112]. The major challenge was producing the nanofibers because no example of nanofiber formation using solution processing could be found in the literature. A new technique, inspired by [113], was developed (see Appendix A for details). The resultant nanofibers were, on average, 6.2 $\pm$ 2.8 μm in length (Figure 5.2). This is crucial for nanofiber alignment because the optimal length for dielectrophoresis is around the size of the electrode gap [114].

5.2.1 Alignment

Alignment was first performed using sawtooth electrodes to determine the ideal alignment conditions. Sawtooth electrodes are ideal for this stage because they concentrate the electric field at specific locations, which is helpful in determining successful alignment. After much trial and error, it was determined that an electric field of 4 MV_{pp} m^{-1} alternating at a frequency of 14 kHz was optimal. These conditions produced repeatable alignment at a relatively high yield (Figure 5.3).

Sawtooth electrodes do not allow for a control experiment (*i.e.*, devices using randomly deposited nanofibers). For this purpose, interdigitated electrodes were employed. Some devices utilized aligned nanofibers using the process conditions optimized using the sawtooth electrodes. Others were deposited with randomly oriented nanofibers. The aligned nanofibers had an average misalignment of 17 $\pm$

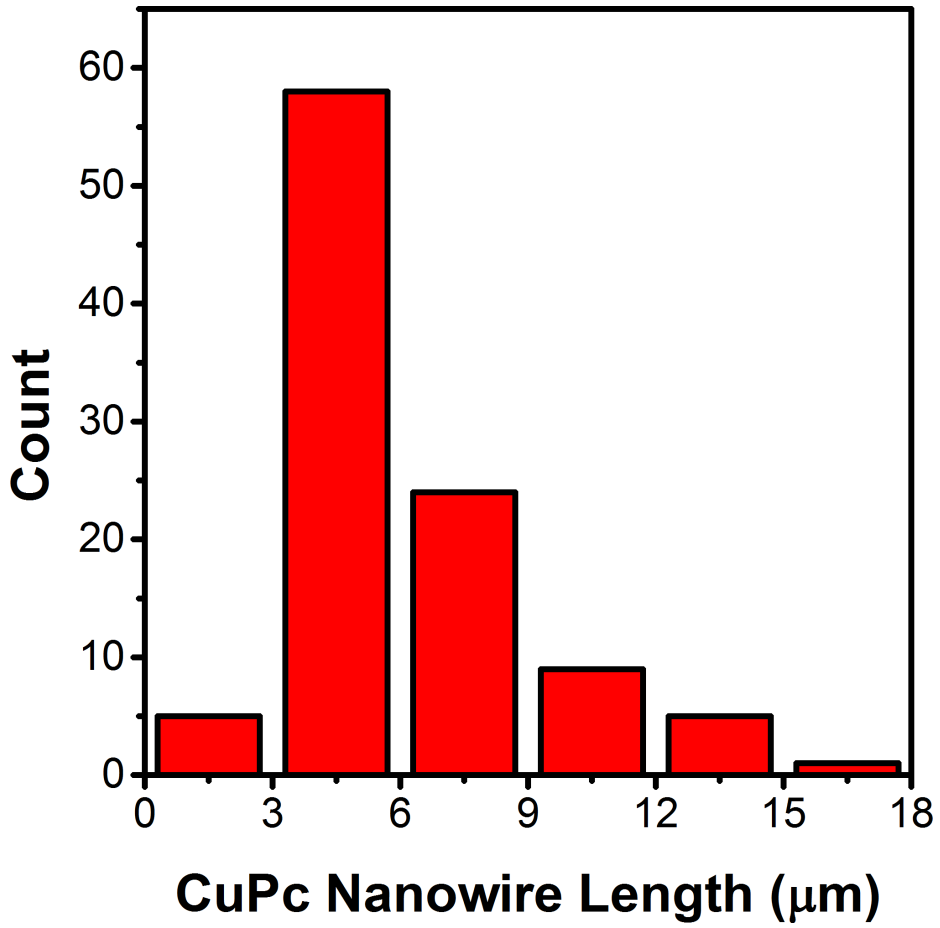

Figure 5.2. Histogram of CuPc nanofiber length.

15.5°. On the whole 72.5% (74 out of 102 measured) had a misalignment of at most 20°. The nanofibers also preferentially deposited across the electrode gap, which further improves device yield and conductivity (Figure 5.4).

5.2.2 Electrical Characterization

Current-voltage curves were measured for unaligned and aligned nanofiber devices. Five of both types were measured (Figure 5.5). The aligned nanofiber devices achieved currents that were an order of magnitude higher than their random counterparts. The I-V curves display significant concavity, which may arise from energy barriers at the contacts or the field-dependence of the charge carrier mobility. Transimpedance was calculated for all devices at 5 V. Devices using aligned nanofibers showed a

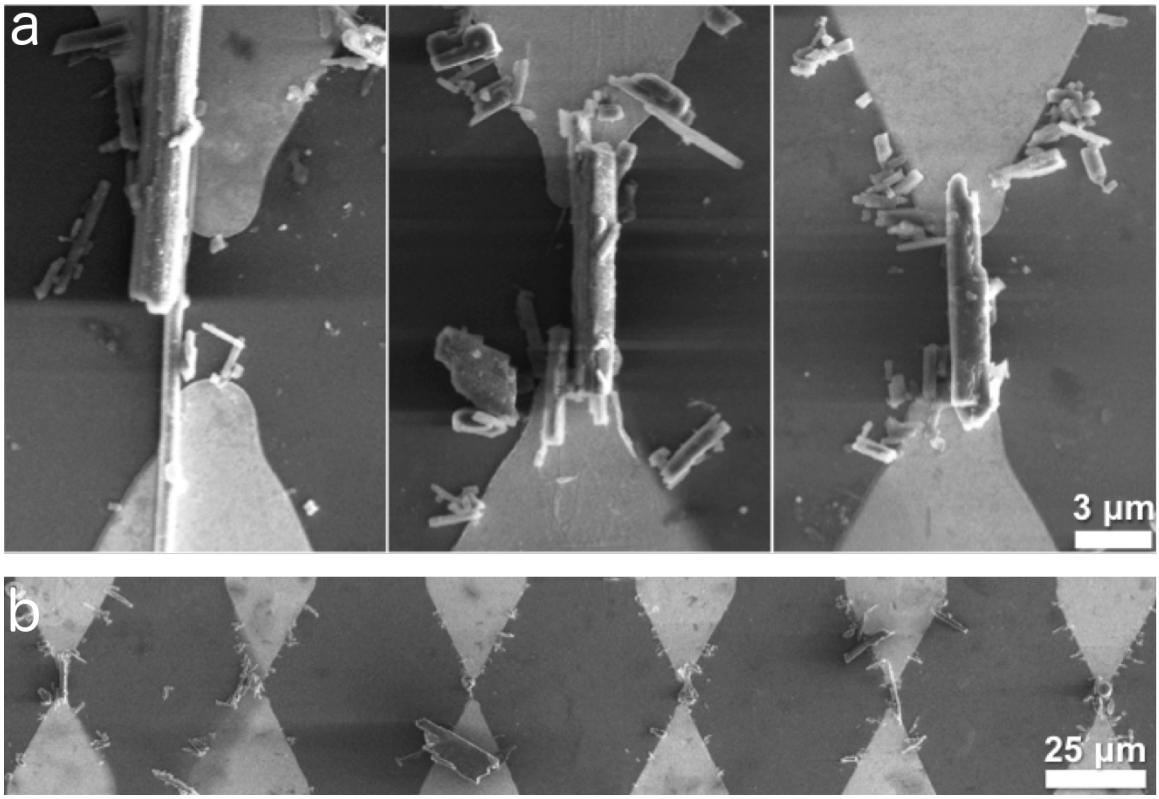

Figure 5.3. Scanning electron microscopy images of CuPc nanofibers aligned using sawtooth electrodes. a) Zoomed images showing the nanofibers on the sawtooth electrodes. b) Image of six adjacent sawtooth electrodes each containing a CuPc nanofiber.

transconductance of 7.4 ± 2.0 nS while the random nanofiber devices had a lower transconductance of 0.68 ± 0.40 nS. Importantly, the variation between devices was reduced from 59.0% to 27.6%, although the sample size is not sufficiently large to be definitive. While further work is needed to understand the improvement in device-to-device uniformity, this work demonstrates the potential of dielectrophoresis to improve both the uniformity and conductivity of nanofiber devices.

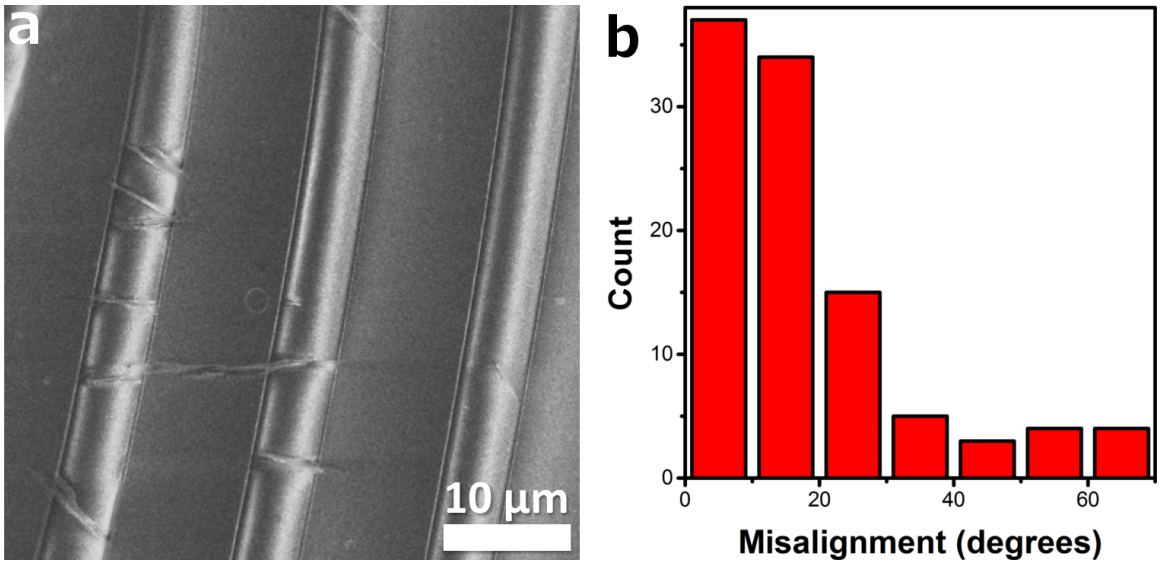

Figure 5.4. Alignment of CuPc nanofibers on interdigitated electrodes. a) Scanning electron microscope image of CuPc nanofibers on interdigitated electrodes. b) Histogram of misalignment angles of the aligned nanofibers.

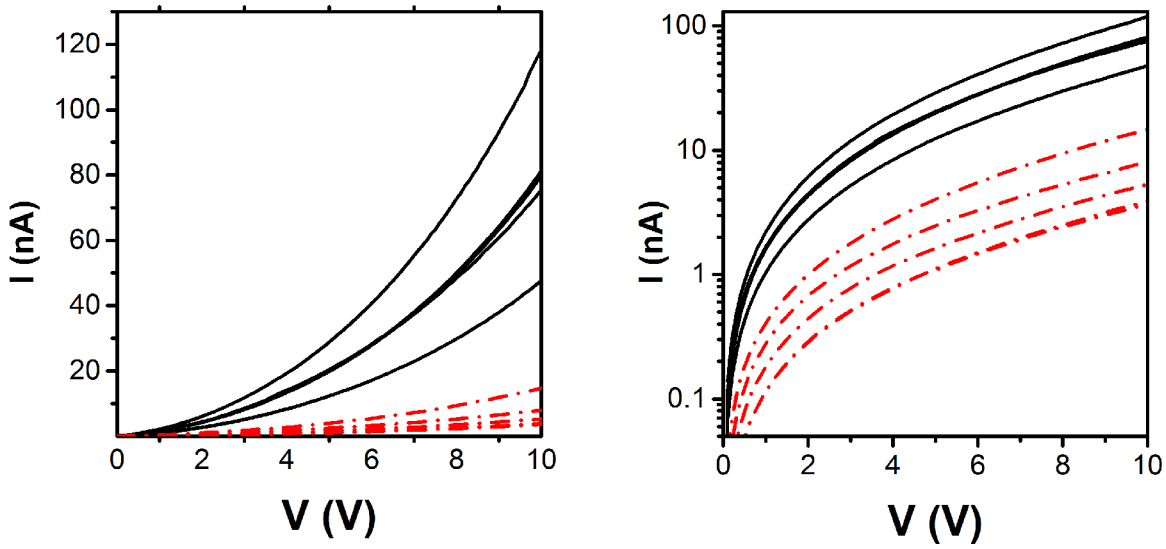

Figure 5.5. I-V curves for the devices with aligned (solid black lines) and random nanofibers (dashed red lines) on linear (left) and semilogarithmic (right) axes.

5.3 Summary

The randomness of the orientation of nanofibers contributes to low conductivity and device-to-device variation. Overcoming randomness is necessary to achieve an adequate device yield for real-world applications. Furthermore, increasing conductivity is a requirement for many devices based on organic semiconductors. To this end, we explored aligning nanofibers using dielectrophoresis.

After fabricating CuPc nanofibers and developing the dielectrophoresis process using sawtooth electrodes, interdigitated electrodes were employed to determine the effect of orientation on the device properties. We achieved a relatively high degree of orientation, with 72.5% of nanofibers within 20° of perfect alignment. Alignment increased the transconductance by an order of magnitude and may have improved device-to-device uniformity as well.

This work brings potential impact to a number of fields. A variety of devices use organic nanofibers, including transistors, sensors, light emitters, photodetectors, and waveguides. Fine control of the orientation of these materials can improve the uniformity of devices, which eases product design. Additionally, the increased conductivity eases the requirements on associated hardware, leading to decreased costs. Dielectrophoresis may prove to be an enabling technology for organic semiconductors to achieve commercial success.

CHAPTER 6

CONCLUSION AND OUTLOOK

Detecting airborne chemicals has wide-reaching implications in industries ranging from defense to healthcare. The two major barriers to addressing market needs are cost and selectivity. Selective techniques, such as mass spectrometry, tend to be very expensive. Conversely, low-cost techniques like chemiresistors generally lack selectivity. Organic semiconductors offer improved selectivity over other chemiresistive materials at a low cost, although a single material is insufficient on its own. An array of sensors is required to achieve sufficient selectivity. In this case, the responses of each sensor are used to create a fingerprint for each chemical species.

Electronic sensors are ideal for creating an array because of their simplicity and the availability of low cost supporting hardware (*e.g.*, analog-to-digital converters). However, organic semiconductors tend to have poor conductivity, if any. To derive any benefit from the superior chemical selectivity of these materials, the conductivity must be improved. In this dissertation, we described three proof of concept experiments to demonstrate new sensing techniques. First, nonconductive sensor materials were placed onto conducting materials. A carbazole-based oligomer was used as a surface functionalization for carbon nanotubes. The composite material showed a strong response to charge transfer inactive analytes through a swelling mechanism. Secondly, nonconductive sensor materials were placed on the gate of a field effect transistor. The novelty of this work was the inclusion of a second gate electrode, which changed the turn-on voltage of the sensing gate. This led to

improved sensitivity. Finally, nanofibers comprised of organic semiconductors were aligned across electrodes using dielectrophoresis. Alignment is expected to increase conductivity slightly, but moreover will improve uniformity between devices.

In order to add conductivity, we formed a composite material by functionalizing carbon nanotubes with sensor materials. While we demonstrated a sensor response to nitroaromatic explosives and have proposed a sensing mechanism, there is still more work to do. A major undertaking is to fully understand the formation of the enigmatic energy barrier and how it impacts charge transfer. Changing the Fermi level of the functional material would be a potential method to explore this phenomenon, but changing the Fermi level without changing the morphology is difficult for most materials. An exception is polyaniline, which shifts its Fermi level in the presence of sodium or iodine ions. A more chemistry-intensive approach is through halogenation of other functional materials, such as poly(3-alkylthiophene)s. Absorption spectra can be used, as in this study, to measure the size of the energy barrier. Kelvin probe microscopy might be a useful tool for measuring charge transfer. Finally, a photoluminescence study would demonstrate the impact of the built in electric field on charge transfer. A larger energy barrier is expected to produce faster fluorescence quenching. Further exploration of the nature of the oligomer-CNT interface can be performed using calculations. Density functional theory would be incredibly valuable examining the energy level alignment and charge transfer. These studies would further the understanding of the interface between carbon nanotubes and noncovalent functional materials.

Another research focus should be the soluble portion of the functional material. Because this part of the functional material resides on the surface, it is responsible for interacting with the analyte. A simple study would be using alkyl chains of varying lengths to study sensing alkane molecules. In theory, smaller alkyls should be selective to smaller alkanes due to steric hindrance. Thus, varying the alkyl length is a potential

means to obtain selectivity. It is important to note that the swelling mechanism of these sensors operates at room temperature and without charge transfer. Room temperature detection of charge transfer inactive species is a major challenge for most techniques, so this represents a step toward a desirable technology.

Finally, the enhanced absorption and charge separation observed in this study might be useful for solar cells. Carbon nanotubes generally have narrow absorption bands due to van Hove singularities. As a result, few solar cells with CNTs in the active layer have reached a power conversion efficiency above 1%. The addition of the oligomer produced broadband absorption in the visible range. Furthermore, the proposed electric field formation at the oligomer-CNT interface seems to assist charge separation, which would reduce recombination losses. To build practical devices, the morphology must be optimized by changing the concentrations of the donors and accepts in solution, changing the soluble portions of the oligomer, and developing the optimal process steps. The lengths of the CNTs is also a major issue. CNTs that are too long will short the solar cell; CNTs that are too short become soluble, which impedes their ability to be functionalized. Finally, the optimized active layer can be incorporated onto a flexible substrate, leading to a solar cell with a high power to weight ratio, which is of interest for space and defense applications.

Moving to chemical sensing with a dual-gate field effect transistor, we demonstrated the ability to generate an electrical signal from nonconducting sensing media. While the concept is now proven, significant work is required before these devices can impact the real world. For example, the device described in this dissertation is far from optimal. Changing the semiconductor to a two-dimensional material would increase the communication between the gates. Materials such as graphene or dichalcogenides (*e.g.*, MoS_2, WSe_2) are roughly an order of magnitude thinner than the film used in this study, which would enhance gate coupling. Increasing the capacitance of the dielectric layers is also worth exploring. Increasing the capacitance

would reduce the losses between the gate electrode and the semiconductor, leading to a stronger sensor signal. Rather than using easily-obtained, low cost thermal oxide and PMMA, a thinner dielectric layer with a higher dielectric constant could be used instead. Materials such as Al_2O_3 and HfO have significantly higher dielectric constants, which would lead to dielectric layers with a higher capacitance. Furthermore, these films can be grown using atomic layer deposition for extremely thin films, increasing capacitance even more. The major challenge with thinning these films will be the source and drain electrodes, which are generally at least 30 nm thick. If the electrodes are thicker than the semiconductor and the top dielectric, then the top gate can come into contact with them, causing shorting. On the other hand, electrodes that are too thin may add significant resistance.

Nanostructures also may play a significant role in DG-FET sensors. Sensitivity can be enhanced by increasing the interaction area between the sensor material and the environment. Depositing nanofibers instead of molecules, for example, would add surface area. Alternatively, the top gate electrode can be textured to increase its surface area. Because the sensor molecules are deposited at room temperature, they are immobilized on the surface; the resulting film of sensor molecules should have the same texture as the electrode materials. Nanostructures might also be useful within the semiconductor channel. In this work, we demonstrated symmetric conductivity along the two semiconductor/dielectric interfaces. However, this is not necessarily desirable. As seen in Figures 4.7 and 4.9, the on/off ratio suffers when applying a high bottom gate voltage. This is attributed to the formation of a conduction pathway along the semiconductor/bottom dielectric interface. The higher off current also limits the dynamic range of the sensor. It is unclear how significant this issue will be. In the current device, the on/off ratio of 10^2 yields a 99% change in current. Expanding this to 10^4 would make for a 99.99% change in current, so the return might not be significant. If it is deemed necessary, nanostructures can be formed on the bottom

dielectric to disrupt the conduction pathway, as in the case of the semiconductor/top dielectric interface in the DG-FETs based on small molecules. Alternatively, a self assembled monolayer comprised of molecules that offer charge traps could be used.

Further development of the sensor material is also needed. The perylene di-imide molecule used in this study is good for electron donating species, such as amines. Examining a variety of substituents for PTCDI might lead to selectivity between similar amines, which is required for distinguishing legal Aderall from illegal methamphetamine, for example. Other functional materials might enable detecting other species. Phthalocyanines are of particular interest because their central metal can bind to different species through specific coordination. For example, transition metals like Cu or Fe coordination metals bind strongly to cyanide, whereas titanyl reacts with peroxides. The sensor material need not be organic. Inorganic materials, such as SnO_2 demonstrate charge transfer between many analytes, although they require elevated temperatures and lack selectivity. Further development of sensor materials can improve the selectivity of DG-FET sensors.

Finally, perhaps the most intriguing opportunity for DG-FET sensors is extending the dynamic range. As we discussed earlier, adding the bottom gate allows us to reduce the amount of analyte that must be accumulated before a signal is observed. However, it does not address the challenge of a relatively small dynamic range (defined as the concentration range that produces a nonsaturated signal) in sensors based on field effect transistors. If the bottom gate voltage can be changed on the fly, it could move the sensing window to a different concentration. This would greatly expand the dynamic range. A simple control circuit could be used to this end, or a microcontroller with an analog output. These future research directions have the potential to make the DG-FET sensor a powerful tool for applications involving chemical sensing.

Along with the two methods to enable use of nonconductive sensor materials, we also demonstrated an improvement to the uniformity of sensors comprised of

organic semiconductors with a small increase in conductivity. A major source of device-to-device variation arises from random deposition. Our alignment of nanofibers utilizes dielectrophoresis on organic materials. While the alignment was demonstrated with a high yield, further work is necessary. Due to time constraints, we were unable to do a full evaluation of the sensors. Using these aligned nanofibers as field effect transistors would be particularly useful in examining the device-to-device variation in the electrical context. The sensor responses also need to be evaluated. We expect the aligned nanofibers will have significantly less deviation than the unaligned fibers. This is important for applications such as breath analysis, where the sensors must be able to detect a difference of a few parts per million.

Further improvement of variation may be achievable by following the work of Dr. Gary Hunter's team at the NASA Glenn Research Center. For inorganic materials, such as SnO_2 and carbon nanotubes, they realized that variations at the electrode/semiconductor interface were contributing to nonuniformity. They developed a process to deposit their sensor materials in photoresist. After deposition, the photoresist was patterned and developed, and metal was deposited, encasing the contact to the semiconductor. The remaining resist was stripped, exposing the portion of the semiconductor within the electrode gap to the environment. A similar process could be used for organic semiconductors. The CuPc nanofibers used in this study were in dichlorobenzene, which is a good solvent for many polymers. The major challenge would lie in stripping the polymer without disturbing the nanofibers. This will be a major challenge because in order for codeposition to work, the nanofibers and polymer need to have similar solubilities, but similar solubilities will result in them being stripped by the same solvents. This may or may not be an insurmountable challenge. Futhermore, the polymer will increase the viscosity of the solvent, which will make it more difficult for the nanofibers to align themselves with the electric field. An alternative application is one-step deposition and encapsulation of organic semi-

conductors for electronic applications. Because organic semiconductors are sensitive to their environments, encapsulation is often necessary to create reliable circuits.

Finally, dielectrophoretic alignment of materials other than CuPc should be explored. Because dielectrophoresis requires the material to be aligned to have a high dielectric constant, CuPc was selected for this proof of concept study. While CuPc might be useful for detecting cyanide, it would be ideal to demonstrate alignment of other materials. Since significant sensor research into PTCDI has already been performed, it is a strong candidate material. However, its relatively low dielectric constant (on par with most organic solvents) poses a major challenge. It might be possible to introduce side chains that have a larger dielectric constant, but it is unclear whether or not that will be sufficient. An extreme example would be to introduce coordination sites so that metals can be incorporated, which is what gives CuPc its exceptionally large dielectric constant. The PTCDI molecules could be asymmetric, with the coordination group on one side and the sensing portion on the other. Soluble groups can be attached at the bay position. This strategy may enable a variety of organic semiconductors to be aligned by dielectrophoresis.

The overall theme of this dissertation is new methods for producing electrical signals from organic sensor materials. Of course, generating signals only fills part of the need. A system with which to read these signals is also necessary. Fortunately, Vaporsens, a University of Utah spin-off company, has been developing such a system. Soon, they will release hardware that supports a sensor array with a low-noise data acquisition tool. Additionally, they are working on algorithms and software to operate the sensors, read the signals, and analyze the data autonomously. The software will look at chemical signatures – the relative responses of each sensors – and index them to signatures stored in a database. The overall product will be small, lightweight, portable, simple to use, and available for a relatively low cost.

The new sensing techniques developed for this dissertation are compatible with the

technology being developed by Vaporsens. Through collaboration, these technologies can be combined, allowing Vaporsens to use a wider variety of sensor materials. Using more sensor materials improves selectivity, reducing false negatives that arise from the operating environment. This work has the potential to impact the defense, automotive, environmental, food, safety, aerospace, and medical industries. With more refinement and translational research, the techniques discussed herein could potentially address a market worth several billion dollars.

APPENDIX A

METHODS AND MATERIALS

Experimental details for all work presented in this dissertation are presented in this appendix. The reader is referred to Appendix A.1 for functionalized carbon nanotubes, Appendix A.2 for the dual gate, and Appendix A.3 for nanofiber alignment.

A.1 Functionalizing Single-Walled Carbon Nanotubes with Organic Materials

In this section, the methods and materials used in Chapter 3 are presented. The carbon nanotubes are described in Section A.1.1 and the oligomer synthesis is discussed in Section A.1.2. The procedure to functionalize the CNTs with the oligomer is presented in Section A.1.3. Materials characterization, including scanning probe microscopy (Section A.1.4), Raman spectroscopy (Section A.1.5), and absorption (Section A.1.6), are also included. Details of the field effect transistor fabrication and measurement can be found in Section A.1.7, with information regarding the light exposure in Section A.1.8 and correlating light absorption to threshold voltage shift in Section A.1.9. The calculation process used to calculate the HOMO and LUMO levels of the oligomer is presented in Section A.1.10. The final experimental details included are sensor fabrication (Section A.1.11) and a description of the analyte delivery system (Section A.1.12).

A.1.1 Carbon Nanotubes

Carbon nanotubes were obtained from Southwest Nano Technologies (SWeNT SG 65) and used without further purification. These nanotubes are 93% semiconducting.

Over 40% of the CNTs are of the (6,5) chirality. The diameters of the carbon nanotubes are 0.8 ± 0.1 nm by manufacturer's specifications, which we confirmed using atomic force microscopy.

A.1.2 Oligomer Synthesis

The oligomer was synthesized via Sonogashia coupling from 3,6-diiodocarbazole and 3,6-diethynylcarbazole. The synthetic details can be found in [115]. The average polymer contains 19 repeat units.

A.1.3 Functionalization

To disperse the CNTs, 1.0 mg of CNTs were placed into 9 mL of chloroform (reagent grade, Sigma-Adrich or Fisher Scientific) with 6.0 mg of Tg-Car. The mixture was sonicated (Fisher Scientific FS40H Untrasonic Cleaner) for 90 min., followed by centrifugation (4200 rpm, IEC Centra CL2) for 20 min. The supernatant was removed and placed into a new tube. Centrifugation was repeated two more times. Lastly, the dispersion was centrifuged at a higher speed (14,000 rpm, Beckman Coulter Microfuge 18) for 15 min. No residue was observed, which indicates nearly complete dispersion of the CNTs.

A.1.4 Scanning Probe Microscopy

Atomic force microscopy images were obtained with a Veeco NanoScope V microscope with a high-resolution "E" stage and a Digital Instruments MultiMode V controller. Adhesion force microscopy was performed with a Bruker Dimension Icon microscope with a MultiMode 8 controller. Samples were prepared by drop casting onto a SiO_2 substrate. The Tg-Car/CNT samples were cast from a 5x dilution of the stock solution and rinsed by sonication in chloroform for 5 min. to rinse away excess oligomer.

A.1.5 Raman Spectroscopy

Raman spectra were measured using a Renishaw Raman microscope with a 633 nm laser for excitation. The laser spot size was several microns. All measurements were taken under ambient conditions.

A.1.6 Absorption

Absorption spectra were measured by an Agilent Cary 100 UV-Vis spectrometer. Materials were measured in the solid state on quartz substrates. Bare CNTs and Tg-Car were measured as deposited. Tg-Car/CNT was drop cast and the excess oligomer was rinsed away by dropping chloroform and wicking the solvent away with a wipe. This process was repeated until no further change to the absorption spectrum occurred.

A.1.7 Field Effect Transistors

Field effect transistors were fabricated using a standard procedure. Electrodes were patterned as follows: wafers were cleaned with 30 s sonication in acetone, methanol, and propanol, followed by 30 min. in piranha (2:1 H_2SO_4:H_2O_2) solution; dried with blowing nitrogen and baked at 120 °C for 2 min.; spin coated with Shipley 1813 photoresist (2000 rpm, 45 s); patterned with EVG-420 aligner; developed in AZ-352 for 1 min.; sputtered 5 nm Ti for adhesion followed by 70 nm Au (Denton Discovery 18); finally, lift off was performed by soaking in acetone overnight, followed by sonication. The electrode pairs feature a 5 μm gap and a 100 μm width. Prior to use, chips were cleaned by 30 s sonication in acetone, methanol, and propanol. Tg-Car/CNT was deposited by spin casting (500 rpm, 9 s prespin, 2000 rpm 30 s spin) from solution (5x diluted from stock). Bare CNTs were similarly deposited from a DMF suspension, which had been sonicated for several hours to reduce aggregation. All electrical characterization was performed with an Agilent 4156C Semiconductor Parameter Analyzer. The source-drain voltage was -1 V in all cases. The threshold voltage was calculated by fitting the linear part of the transfer curve.

As an example of repeatability, the transfer characteristics of four devices are shown in Figure A.1. The average threshold voltage in the dark is 16.4 ± 0.9 V and shifts to 19.3 ± 0.7 V under illumination. On average, the shift is 2.8 ± 0.2 V, which is a comparably small error margin. Device mobility (as opposed to the mobility intrinsic to the material) is low. In the dark, the mobility is $3.12 \times 10^{-5} \pm 2.35 \times 10^{-5}$ $cm^2 \cdot V^{-1} \cdot s^{-1}$ and does not change significantly under illumination ($3.50 \times 10^{-5} \pm 2.96 \times 10^{-5}$ $cm^2 \cdot V^{-1} \cdot s^{-1}$). The mobility is low for two reasons. First, a small amount of Tg-Car/CNT material is used to avoid shorting by metallic CNT impurities. Such impurities would decrease the on/off ratio and eliminate the photoresponse. Secondly,

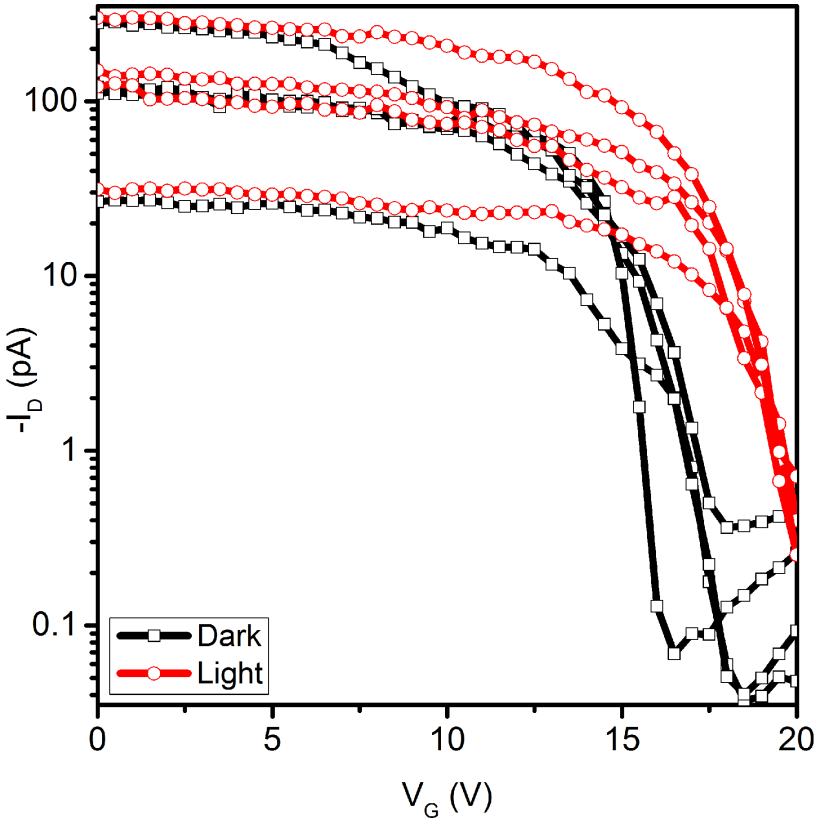

Figure A.1. Transfer characteristics of four Tg-Car/CNT field effect transistors. Reprinted with permission from John Wiley and Sons: B. R. Bunes, M. Xu, Y. Zhang, D. E. Gross, A. Saha, D. L. Jacobs, X. Yang, J. S. Moore, and L. Zang, "Photodoping and enhanced visible light absorption in single-walled carbon nanotubes functionalized with a wide band gap oligomer," *Advanced Materials*, vol. 27, no. 1, pp. 162-167, copyright 2015.

with a 5 μm gap and an average CNT length of 800 nm, the channel clearly contains a network of carbon nanotubes. Since the CNTs are coated in oligomer, charge transfer between CNTs is hindered. This is not a problem because higher mobility would not contribute to the study of the interface between the CNT and oligomer.

The effect of oxygen on the threshold voltage of FETs based on CNTs is well-known. Typically, when exposed to light, the threshold voltage is reduced because adsorbed oxygen molecules are released, which de-dopes the CNT. However, this effect only occurs with exposure to ultraviolet light. There is essentially no ultraviolet light emitted from a tungsten source. For completeness, the photoresponse was also tested in an argon atmosphere. The photoresponse was measured in air, in argon, and in air after removal of the argon (Figure A.2). In general, the threshold voltage decreased in argon, consistent with the removal of oxygen. However, the photoinduced shift in threshold voltage did not change significantly (Figure A.3). Thus, oxygen desorption can be eliminated as a potential cause of the photoresponse.

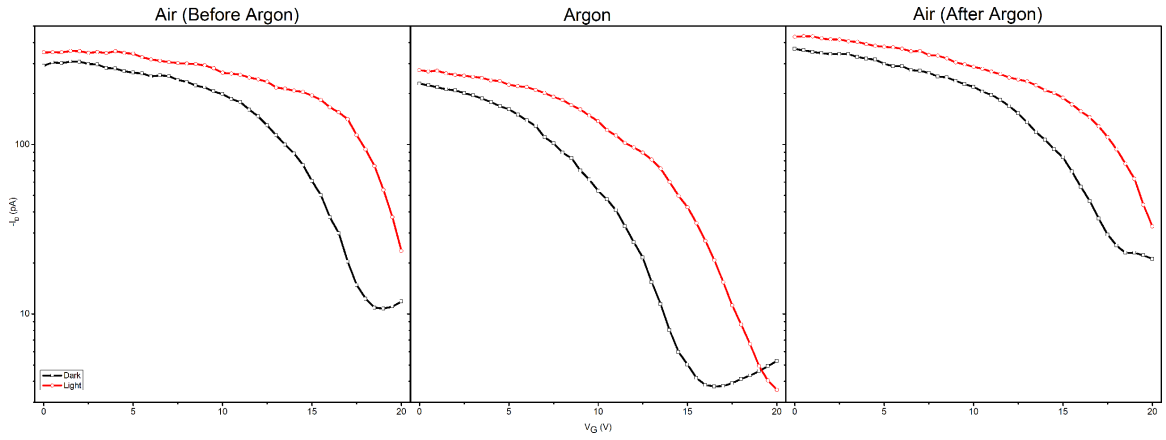

Figure A.2. Transfer characteristics of a device in air, in argon, and in air after removal of the argon. Reprinted with permission from John Wiley and Sons: B. R. Bunes, M. Xu, Y. Zhang, D. E. Gross, A. Saha, D. L. Jacobs, X. Yang, J. S. Moore, and L. Zang, "Photodoping and enhanced visible light absorption in single-walled carbon nanotubes functionalized with a wide band gap oligomer," *Advanced Materials*, vol. 27, no. 1, pp. 162-167, copyright 2015.

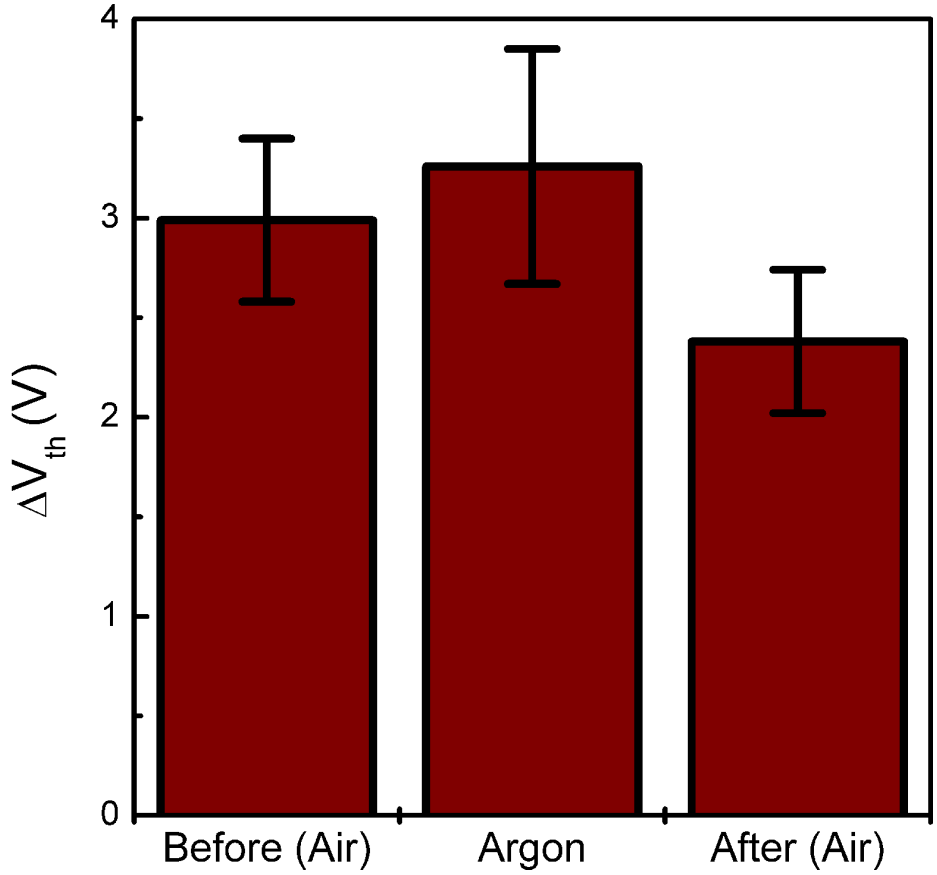

Figure A.3. Photoinduced shift in threshold voltage in argon and air (before and after argon exposure). Reprinted with permission from John Wiley and Sons: B. R. Bunes, M. Xu, Y. Zhang, D. E. Gross, A. Saha, D. L. Jacobs, X. Yang, J. S. Moore, and L. Zang, "Photodoping and enhanced visible light absorption in single-walled carbon nanotubes functionalized with a wide band gap oligomer," *Advanced Materials*, vol. 27, no. 1, pp. 162-167, copyright 2015.

A.1.8 Tungsten Lamp Spectra

With a manufacturer's specification of 3250 K, the spectra of the tungsten lamp using different filters was calculated using Planck's Law:

$$B(T) = \frac{2hc^2}{\lambda^5} \cdot \frac{1}{\exp\left(\frac{hc}{\lambda kT}\right) - 1} \tag{A.1}$$

where B is the spectral radiance ($W \cdot cm^{-2} \cdot nm^{-1}$), h is Planck's constant, c is the speed of light, λ is the wavelength, k is Boltzmann's constant, and T is temperature. Surface power density, P, is then calculated by integrating this equation over the spectrum using the Trapezoid Rule. Then, the surface power density is converted to

photon flux:

$$\Phi(\lambda) = P(\lambda) \cdot \frac{\lambda}{hc} \cdot 6.24 \times 10^{18} \tag{A.2}$$

where Φ is the photon flux ($photons \cdot cm^{-2} \cdot s^{-1}$) and P is the surface power density. Step functions were used to approximate the response of each filter, with the step occurring at the cut-on wavelength and a transmission coefficient of 0.9. This is in close agreement with the manufacturer's specifications. The spectra were adjusted to maintain a constant flux of photons whose energies exceeded 1.3 eV (the CNT's band gap) by multiplying by a constant (Figure A.4). The flux was then converted back to surface power density, which was used to set the light intensity for sample

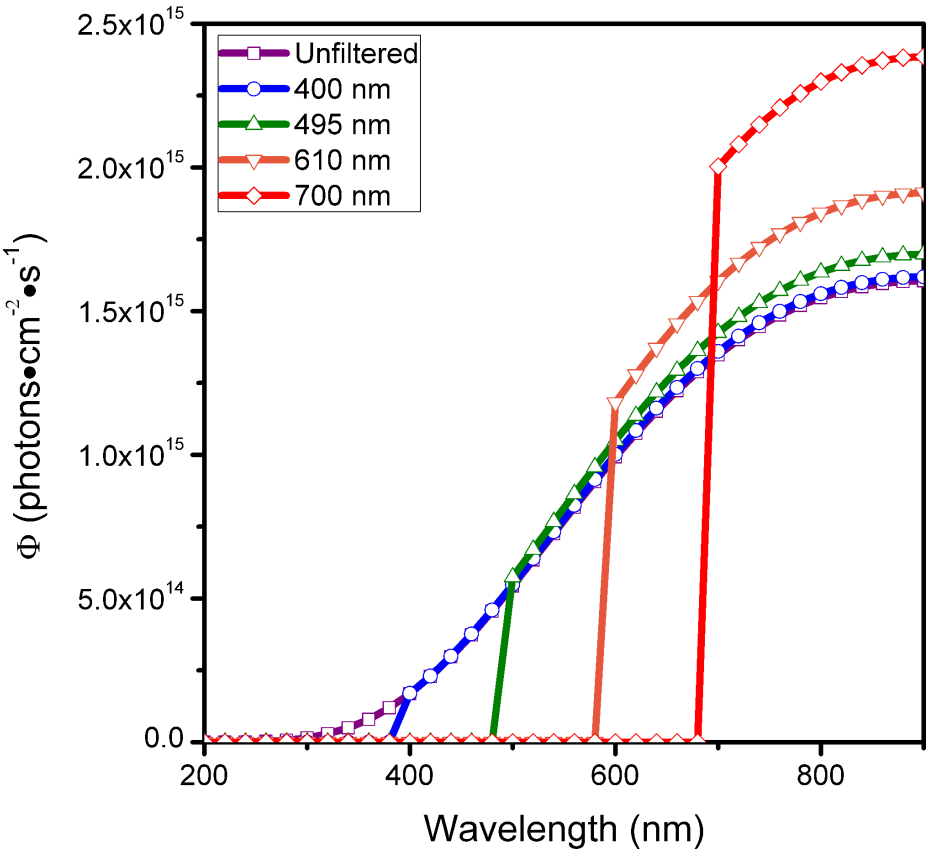

Figure A.4. Calculated spectra of the tungsten lamp using different long-pass filters. Reprinted with permission from John Wiley and Sons: B. R. Bunes, M. Xu, Y. Zhang, D. E. Gross, A. Saha, D. L. Jacobs, X. Yang, J. S. Moore, and L. Zang, "Photodoping and enhanced visible light absorption in single-walled carbon nanotubes functionalized with a wide band gap oligomer," *Advanced Materials*, vol. 27, no. 1, pp. 162-167, copyright 2015.

illumination. A Melles-Griot Broadband Power/Energy Meter 13PEM001 was used to measure surface power.

A.1.9 Calculating Absorbable Photons

The incident photon flux was multiplied by the absorption spectrum of the Tg-Car/CNT complex to approximate the number of photons absorbed (Figure A.5). This allows us to correlate absorption with the threshold voltage shift observed from FET measurements. Because thickness of the films for absorbance measurements and

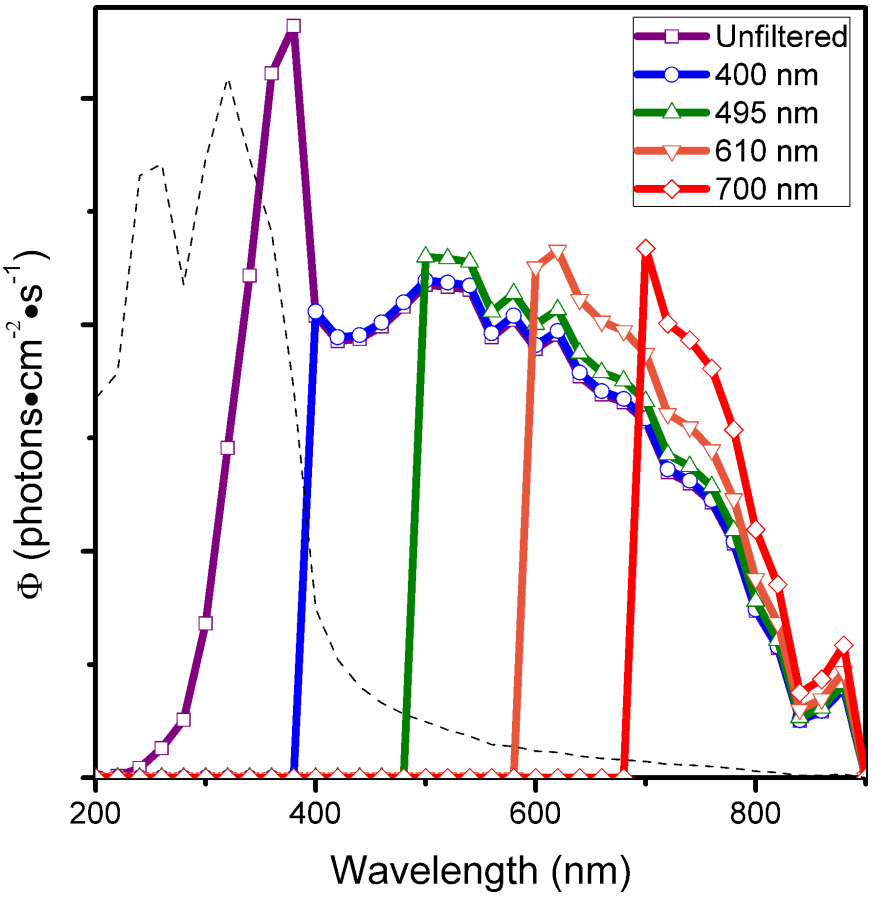

Figure A.5. Spectra of photons absorbed by the Tg-Car/CNT complex. The absorption spectrum of Tg-Car/CNT is included for reference (dashed line). Reprinted with permission from John Wiley and Sons: B. R. Bunes, M. Xu, Y. Zhang, D. E. Gross, A. Saha, D. L. Jacobs, X. Yang, J. S. Moore, and L. Zang, "Photodoping and enhanced visible light absorption in single-walled carbon nanotubes functionalized with a wide band gap oligomer," *Advanced Materials*, vol. 27, no. 1, pp. 162-167, copyright 2015.

FETs are different, the values must be compared to a reference rather than used as absolutes. Since the onset of saturation occurs using the filter with the 495 nm cut-on wavelength, this spectrum was selected as the common reference. All spectra were integrated to sum the total number of photons absorbed. Plotting these data with the shift in threshold voltage demonstrates a one to one correlation (Figure 3.8). The data are summarized in Table A.1.

A.1.10 Density Functional Theory Calculations

Two configurations of the oligomer were used to perform calculations based on density functional theory (DFT). A compressed, tubular configuration gave a band gap of 3.1 eV (LUMO: -1.0 eV, HOMO: -4.1 eV. This is in good agreement with the optical data. This is also the configuration that makes the most sense in regard to carbon nanotube functionalization. The other configuration was a stretched, zig-zag structure, which gave a larger band gap of 4.0 eV (LUMO: -1.3 eV, HOMO: -5.3 eV) (Figure A.6). This configuration can be ruled out because of the lack of experimental evidence.

Due to the large size of the oligomer and its flexible side groups, a smaller basis set, 3-21g, was used for the calculation. A tetramer was used for validation. The energy levels for the tetramer were calculated using both 3-21g and 6-31g. The two

Table A.1. Summary of the data correlating absorbed photons and threshold voltage shift. Reprinted with permission from John Wiley and Sons: B. R. Bunes, M. Xu, Y. Zhang, D. E. Gross, A. Saha, D. L. Jacobs, X. Yang, J. S. Moore, and L. Zang, "Photodoping and enhanced visible light absorption in single-walled carbon nanotubes functionalized with a wide band gap oligomer," *Advanced Materials*, vol. 27, no. 1, pp. 162-167, copyright 2015.

Cut-on Wavelength (nm)	ΔV_{th} **(V)**	**Relative Number of Absorbed Photons**	**Relative** ΔV_{th}
495	4.06 ± 0.29	1.00	1.00
610	2.86 ± 0.47	0.71	0.71
700	1.54 ± 0.32	0.44	0.38

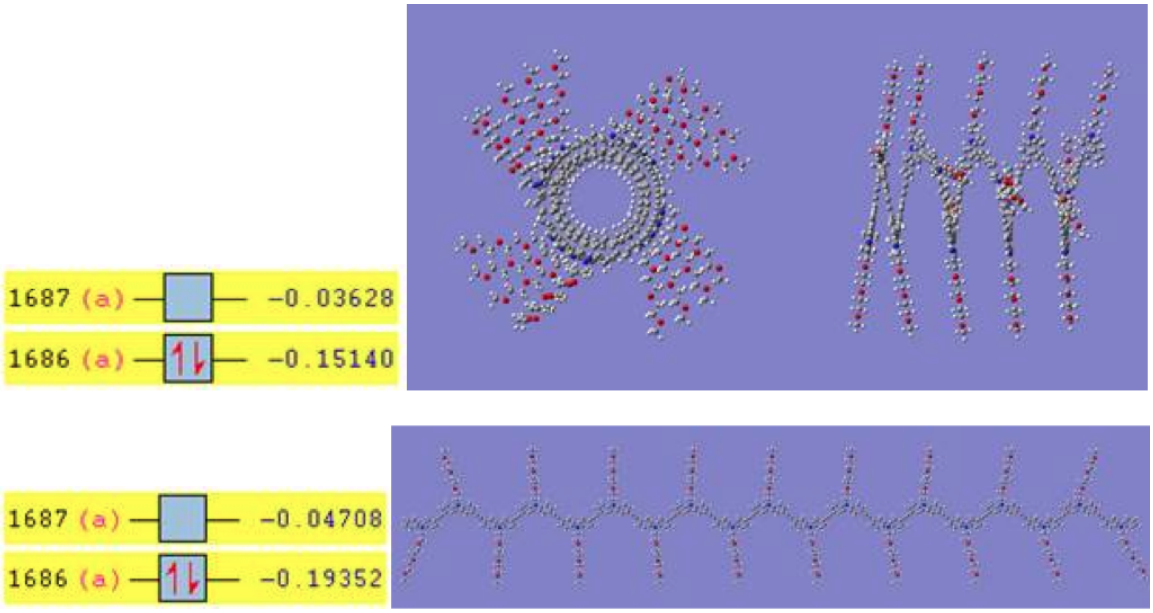

Figure A.6. DFT calculations for the oligomer in the tubular (top) and zig-zag (bottom) configurations. Reprinted with permission from John Wiley and Sons: B. R. Bunes, M. Xu, Y. Zhang, D. E. Gross, A. Saha, D. L. Jacobs, X. Yang, J. S. Moore, and L. Zang, "Photodoping and enhanced visible light absorption in single-walled carbon nanotubes functionalized with a wide band gap oligomer," *Advanced Materials*, vol. 27, no. 1, pp. 162-167, copyright 2015.

calculations gave similar results, within 0.1 eV. An error value of 0.1 eV is therefore assigned to all energy levels obtained via DFT calculation.

A.1.11 Sensor Fabrication

Sensors were fabricated by depositing Tg-Car/CNT onto interdigitated electrodes with an 80 μm gap and 2.1 mm width. The electrodes consist of a 20 nm Ti adhesion layer and a 50 nm gold layer. The chips were cleaned by successive sonication in acetone, methanol, and propanol. Tg-Car/CNT was deposited from a dilute (40×) solution in 2 μL drops until the resistance of the sensor fell in the 50-200 kΩ range. The devices were heated at 80 °C for 5 min. to remove any remaining solvent.

A.1.12 Gas Flow System

The gas flow system comprised of a clean air flow with a syringe pump (NE-4000, New Era Pump Systems) to introduce the analyte (Figure A.7). The clean air flow rate was fixed at 100 sccm. Analyte (250 mg solid or 0.5 mL liquid) was placed in the syringe, where it was allowed to equilibrate for 2 hr. Injecting the saturated vapor into the clean air stream at different rates delivered different concentrations to the sensor (Table A.2). The concentration was calculated by multiplying the saturated

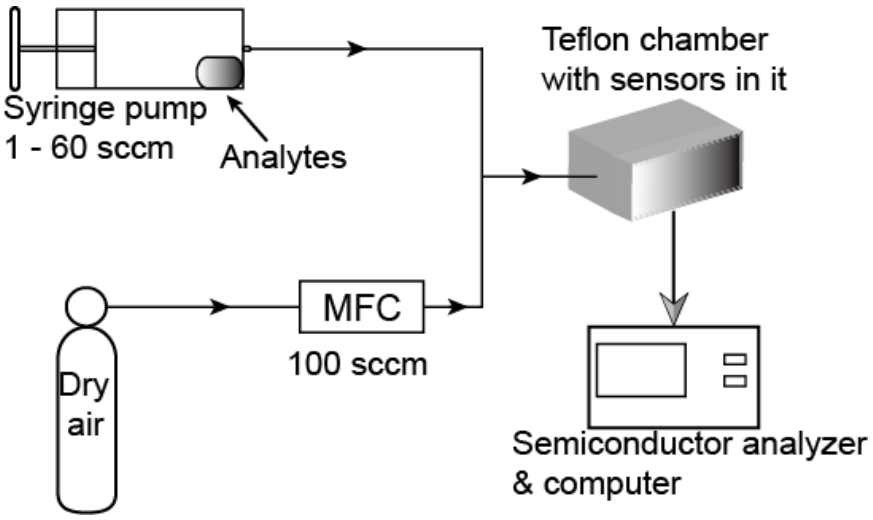

Figure A.7. Schematic of the gas flow system used for sensor testing. Reprinted with permission from the American Chemical Society: Y. Zhang, M. Xu, B. R. Bunes, N. Wu, D. E. Gross, J. S. Moore, and L. Zang, "Oligomer-coated carbon nanotube chemiresistive sensors for selective detection of nitroaromatic explosives," *ACS Applied Materials & Interfaces*, vol. 7, no. 14, pp. 7471-7475, copyright 2015.

Table A.2. Nitrotoluene delivered at various concentrations by dilution. These flows were used to generate the data presented in Figure 3.9. Reprinted with permission from the American Chemical Society: Y. Zhang, M. Xu, B. R. Bunes, N. Wu, D. E. Gross, J. S. Moore, and L. Zang, "Oligomer-coated carbon nanotube chemiresistive sensors for selective detection of nitroaromatic explosives," *ACS Applied Materials & Interfaces*, vol. 7, no. 14, pp. 7471-7475, copyright 2015.

Vapor Press. 23 °C (torr)	**Sat. Vapor Conc.**	**3 sccm**	**4 sccm**	**6 sccm**
4.02×10^{-2}	52.9 ppm	1.5 ppm	2.0 ppm	3.0 ppm

vapor concentration by the ratio of analyte flow rate to total flow rate. The sensors were housed in ceramic dual-inline packages. A teflon enclosure encased the sensor chips and the analyte flow was plumbed into it.

A.2 Dual-Gate Field Effect Transistors as Highly Sensitive, Highly Selective Chemical Sensors

In this section, the methods and materials used for the experiments presented in Chapter 4 are described. The materials are listed in Section A.2.1 and the fabrication process is outlined in Section A.2.2. The electronic characterization equipment and measurement setup are described in Section A.2.3. Finally, the gas flow system and analyte concentrations are presented in Section A.2.4.

A.2.1 Materials

ActivInk N2200 was purchased from Polyera. Polymethylmethacrylate (MW=75,000) was obtained from Polymer Sciences. Octadecyltrichlorosilane was purchased from Sigma Aldrich. The solvents used were purchased from Sigma Aldrich at the reagent grade. All materials were used as received.

A.2.2 Fabrication

Electrodes were fabricated using the same procedure described in Appendix A.1.7. In this case, the gaps were 20 μm and the width was 75 mm. After cleaning, the chips were treated with OTS by soaking in solution (100 mM in toluene) for 4 hr. The chips were then cleaned by 30 s of sonication in toluene, acetone, methanol, and propanol and dried at 120 °C for 2 min. The edges of the chip were protected with Kapton tape to prevent shorting. The ActivInk N2200 was spin cast (5 mg/mL in dichlorobenzene) using a 9 s prespin at 500 rpm and a 30 s spin at 2000 rpm. The chip was then dried in a vacuum oven at 110 °C and 0.1 atm. for 1 hr. Then, the tape was removed. The PMMA was applied via spin casting (75 mg/mL in ethyl acetate) using the same spin conditions as before. A final drying step in the vacuum oven (60 °C, 0.1 atm.) was

performed for 30 min. The top gate electrode and functional material were thermally evaporated through a shadow mask at 1.0 Å/s and 0.1 Å/s, respectively.

A.2.3 Electronic Characterization

Electronic characterization was performed using an Agilent 4156C Semiconductor Parameter Analyzer. Field effect transistor testing was performed using a Signatone probe station in a dark, shielded box. Sensors were packaged at connected to the analyzer through alligator clips and a breadboard.

A.2.4 Sensor Testing

The ammonia vapor was generated from an ammonia/water solution (35% w/w). The exposure was carried out using a 10 mL syringe. The syringe was filled from the headspace of the solution's container and emptied onto the sensor.

A.3 Nanofiber Alignment via Dielectrophoresis

The methods and materials used in the dielectrophoresis experiments (discussed in Chapter 5) are described in this section. The materials are described in Section A.3.1 and the fabrication of the nanofibers is presented in Section A.3.2. Characterization by scanning electrode microscopy is discussed in Section A.3.3. Electrode fabrication is outlined in Section A.3.4. A description of the nanofiber alignment process is in Section A.3.5. Finally, the setup for electrical testing and the method used to calculate the transconductance are presented in Section A.3.6.

A.3.1 Materials

CuPc ($>$ 99.99% pure) and o-dichlorobenzene (reagent grade) were purchased from Sigma Aldrich and used as received. Dichlorobenzene was selected as the solvent because its high boiling point enables dissolution of the CuPc and its low vapor pressure prolongs the alignment time during drop casting.

A.3.2 Nanofiber Fabrication

To fabricate the nanofibers, CuPc was placed in 20 mL o-dichlorobenzene at a concentration of 1 μM. The suspension was heated and refluxed at a temperature of 200 °C for 4 hr. while being stirred at 500 rpm. At the elevated temperature, the CuPc dissolved and the suspension became a solution. No remaining aggregates of CuPc were observed. The solution was cooled to room temperature at a rate of 50 °C/hr. with continued stirring. Cooling caused the CuPc to precipitate, forming nanofibers through $\pi - \pi$ stacking. The resulting nanofiber concentration was too low for a good yield, so the nanofiber suspension was concentrated through centrifugation (40 min. at 2000 rpm, 20 min. at 3000 rpm). This process increased the concentration by about a factor of 15, although the exact increase was not determined because some nanofibers could not be resuspended.

A.3.3 Microscopy

Scanning electron microscope images were taken using an FEI NovaNano 630 field emission microscope operating in immersion mode. The samples did not receive any coating.

A.3.4 Electrode Fabrication

Sawtooth electrodes were fabricated on silicon chips with 300 nm of polished thermal oxide. Photoresist was applied via spin casting and patterned through positive photolithography. Gold (70 nm with a 5 nm Ti adhesion layer) electrodes were sputtered onto the chips. Lift-off was performed by soaking the chips in acetone and sonicating. All chips were cleaned prior to nanofiber deposition by sonication in acetone (30 s), methanol (30 s), and propanol (30 s). The gaps between the electrodes were approximately 5 μm.

Interdigitated electrodes were fabricated by the staff at the State University of New York at Albany. The electrodes occupy a circular region with a 2 mm diameter. The gap spacing was 5 μm and the finger width was 10 μm. A positive photoresist

was coated onto a fused silica wafer. After patterning, approximately 300 nm of gold with a titanium adhesion layer was deposited by electroplating. The wafers were diced and each chip was cleaned by sonication in acetone (30 s), methanol (30 s), and propanol (30 s) prior to deposition.

A.3.5 Alignment

Nanofiber alignment was performed by applying an ac voltage to the electrodes while drop casting the nanofiber solution. The voltage supplied was 20 V_{pp} at a frequency of 14 kHz and supplied by a Rigol DG4162 function generator. Thus, the amplitude of the electric field between the electrodes was 4 MV/m. The function generator was attached to the electrodes using a homemade probe station. Heavy (18 gauge) copper wires were attached to a ring stand. The ends were looped to limit scratches on the electrodes, which can cause shorts. Alligator clips were used to attach the function generator to the probes (Figure A.8). The nanofiber solution was deposited in controlled amounts using a micropipette (2 μL for the sawtooth electrodes, 0.9 μL for the interdigitated electrodes). The control devices on the interdigitated electrodes were fabricated in the same fashion but without the use of the function generator.

A.3.6 Electrical Testing

Current-voltage curves were measured using an Agilent 4156C Semiconductor Parameter Analyzer with a Signatone probe station in an electromagnetically shielded cage. The voltage was swept from 0 V to 10 V in a step size of 0.1 V. Each data point represents the average of 10 measurements taken at each step.

Transconductance was calculated using a differential form of Ohm's Law:

$$g = \frac{dI}{dV} \tag{A.3}$$

where g is the transconductance, I is the current, and V is the voltage. Calculating a derivative on a discrete function introduces error. To minimize this error, the

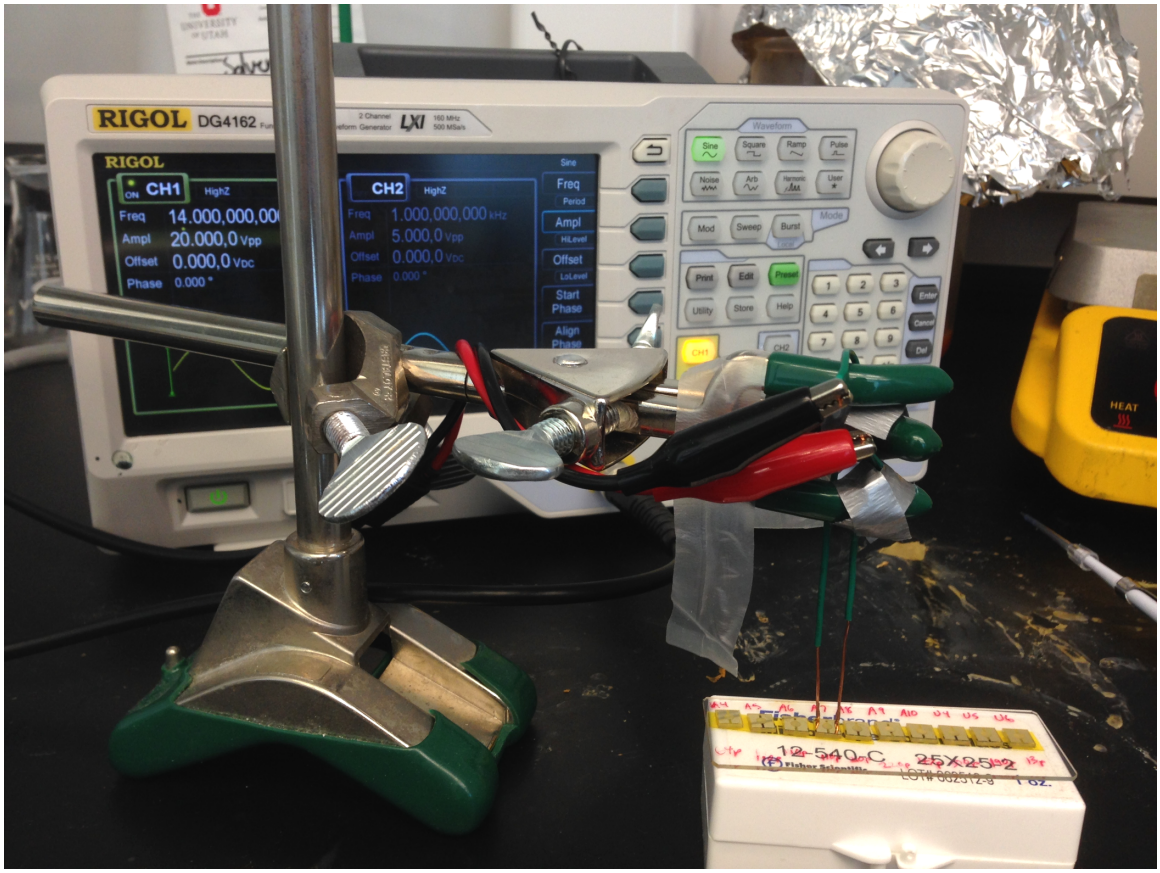

Figure A.8. Picture of the experimental setup for nanofiber alignment.

transconductance was calculated over three intervals (4.9-5.0 V, 5.0-5.1 V, and 4.9-5.1 V) and averaged. In an ideal case (purely Ohmic), the three calculations would yield the same value. However, the I-V curve is noticeably concave up, which causes these values to differ slightly.

APPENDIX B

LITERATURE REVIEWS

Additional literature reviews are presented in this appendix. An overview of the electronic properties of carbon nanotubes is presented in Section B.1. The operation of organic field effect transistors is discussed in Section B.2. Methods to modify the threshold voltage of organic field effect transistors are summarized in Section B.3. Section B.4 surveys techniques to align organic nanofibers. An overview of dielectrophoresis is provided in Section B.5.

B.1 Electronic Properties of Carbon Nanotubes

The electronic properties of carbon nanotubes are responsible for attracting much of the research interest in these materials. Carbon nanotubes come in a variety of configurations. Single-walled carbon nanotubes follow very specific rules that have been confirmed experimentally [38]. Conversely multiwalled CNTs are considerably more complicated. They can be either semiconducting or metallic, but the coupling between the nanotubes makes it difficult to make any rules regarding the conductivity [116]. For example, a double-walled CNT consisting of two semiconducting nanotubes becomes metallic with adequately small spacing [117]. The number of walls can be selected prior to growth through the choice of catalyst [118] or through separation after growth, for example, through density gradient ultracentrifugation [119].

Single-walled carbon nanotubes (SWCNTs) are the focus of the work presented in this appendix. To understand the electronic properties, it is constructive to consider a

SWCNT as a rolled sheet of graphene. The chiral vector, $\vec{C_h}$, wraps around the carbon nanotube in a plane normal to the nanotube's axis with its head and tail at the same location. It can be decomposed into unit vectors such that $\vec{C_h} = n\vec{a_1} + m\vec{a_2}$ (Figure B.1). Using this method, SWCNTs can be divided into three classes. Armchair nanotubes ($n = m$) are always metallic. Zig-zag nanotubes ($m = 0$) are metallic when n is a multiple of three and semiconducting otherwise. All other nanotubes are

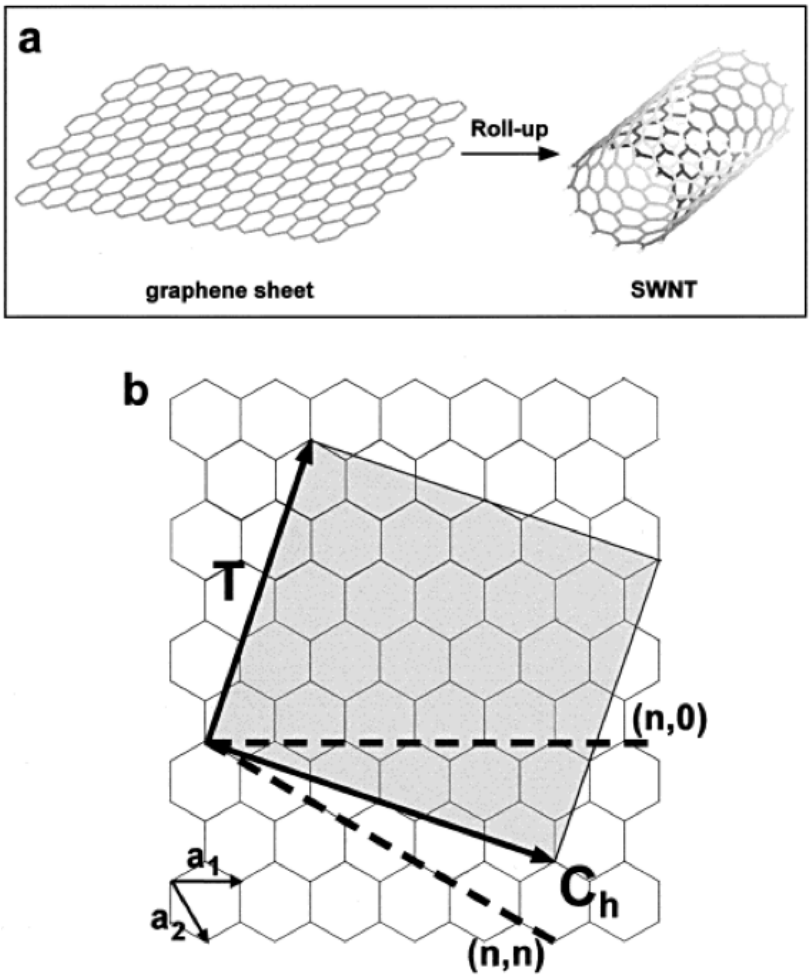

Figure B.1. Rolling graphene to form a carbon nanotube. a) Schematic of graphene rolling to form a carbon nanotube. b) Diagram describing various atomic configurations of carbon nanotubes: armchair (n,n), zig-zag (n,0) and chiral ($\vec{C_h}$). The example vector is for a (4,2) SWCNT. Reprinted with permission from the American Chemical Society: T. W. Odom, J.-L. Huang, P. Kim, and C. M. Lieber, "Structure and electronic properties of carbon nanotubes," *The Journal of Physical Chemistry B*, vol. 104, no. 13, pp. 2794-2809, copyright 2000.

designated chiral. Chiral nanotubes can be either semiconducting or metallic. They are metallic when there exists an integer, q, such that $2n+m = 3q$ and semiconducting otherwise [39].

B.2 Organic Field Effect Transistors

Since their first demonstration in 1986 [58], organic field effect transistors (OFETs) have been pursued as a potential enabling technology for flexible electronics. Indeed, OFETs have been employed in the laboratory setting to make bendable displays [120], microprocessors [121], integrated circuits [122, 123], tactile sensors [124], and RFID tags [125]. These novel applications move closer to reality with every advance in OFET performance.

Organic field effect transistors generally consist of an organic semiconductor spanning two electrodes (source and drain) separated from a third electrode (the gate) by a dielectric material. Unlike silicon transistors, the semiconductor is not typically doped. Doping organic semiconductors is a relatively new concept and undeveloped. Organic field effect transistors operate through charge accumulation, rather than inversion. When a voltage is applied to the gate electrode, charges accumulate at the semiconductor/dielectric interface. When the charges reach a sufficient density, current can travel between the source and drain electrodes (Figure B.2) [126].

B.3 Threshold Voltage Modification

Modifying the threshold voltage of organic field effect transistors receives significant attention. In addition to impacting sensors, reducing the threshold voltage is critical for applications in electronics because it would reduce operating voltages and power consumption. Using two p-type transistors with different threshold voltages is also a way to mitigate the generally poor performance of n-type organic semiconductors in digital logic applications; this enabled the first microprocessor that used only organic field effect transistors [121], along with other integrated circuits

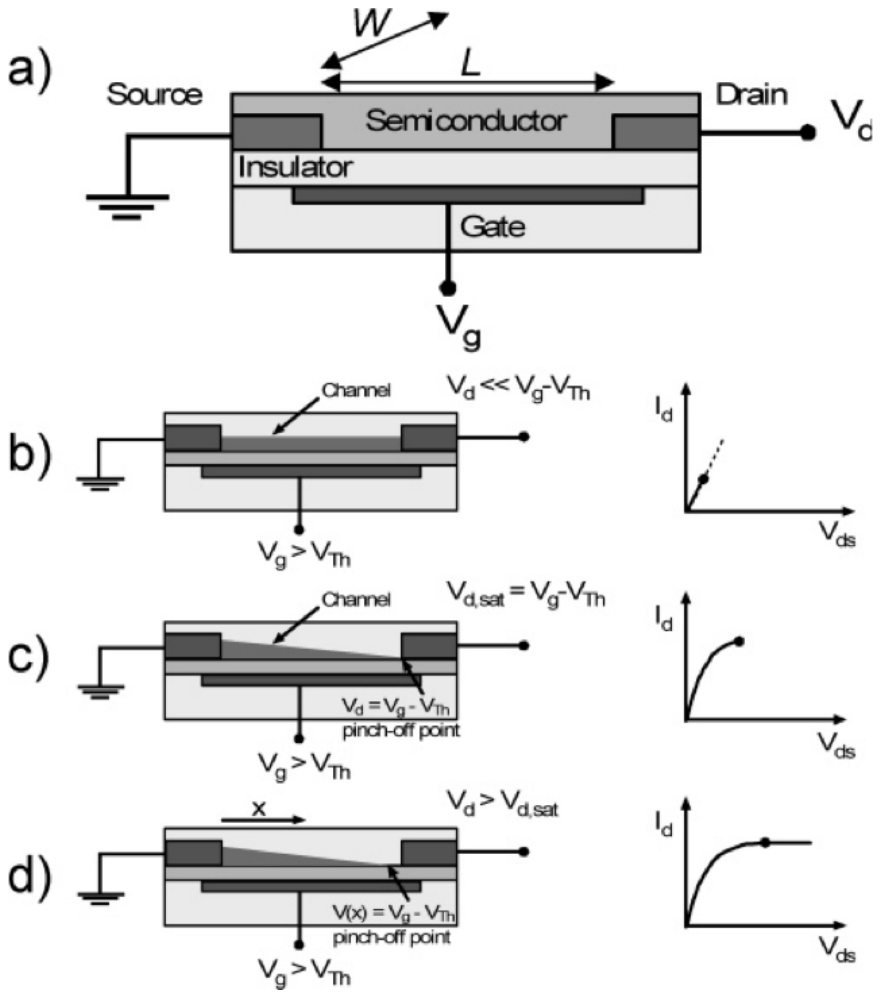

Figure B.2. Organic field effect transistors and operating modes. a) Schematic of an organic field effect transistor. b-d) Charge accumulation with a constant gate voltage and increasing drain voltage. b) The transistor operates in the linear mode with the corresponding I-V curve. c) The transistor transitions from linear to saturation. d) Pinch-off occurs and the transistor is fully saturated. Reprinted with permission from the American Chemical Society: J. Zaumseil and H. Sirringhaus, "Electron and ambipolar transport in organic field-effect transistors," *Chemical Reviews*, vol. 107, no. 4, pp. 1296-1323, copyright 2007.

[122, 123]. Generally, modifying the threshold voltage is performed by modifying the dielectric layer. Modifying the dielectric surface through ozone treatment [127] or self-assembled monolayer [128, 129] modifies the threshold voltage by changing the density of trap states. Using a thin, high-k oxide layer (such as HfO or Al_2O_3) is also effective, although it adds an expensive atomic layer deposition process [130]. Recently, doping was shown to modulate the threshold voltage of FETs based on C_{60}

[131]. While this is a promising approach, in many materials including impurities decreases charge carrier mobility (Figure B.3).

An alternative approach to modifying the threshold voltage is to use an electric field. The electric field is generated by a second gate, opposite the first. If the semiconductor layer is adequately thin (less than the accumulation width), the two gates can communicate. One gate can accumulate charges that stretch across the channel to the opposite gate's semiconductor/dielectric interface. Accumulation of charges at this interface fills trap states, which enables the transistor to turn on at

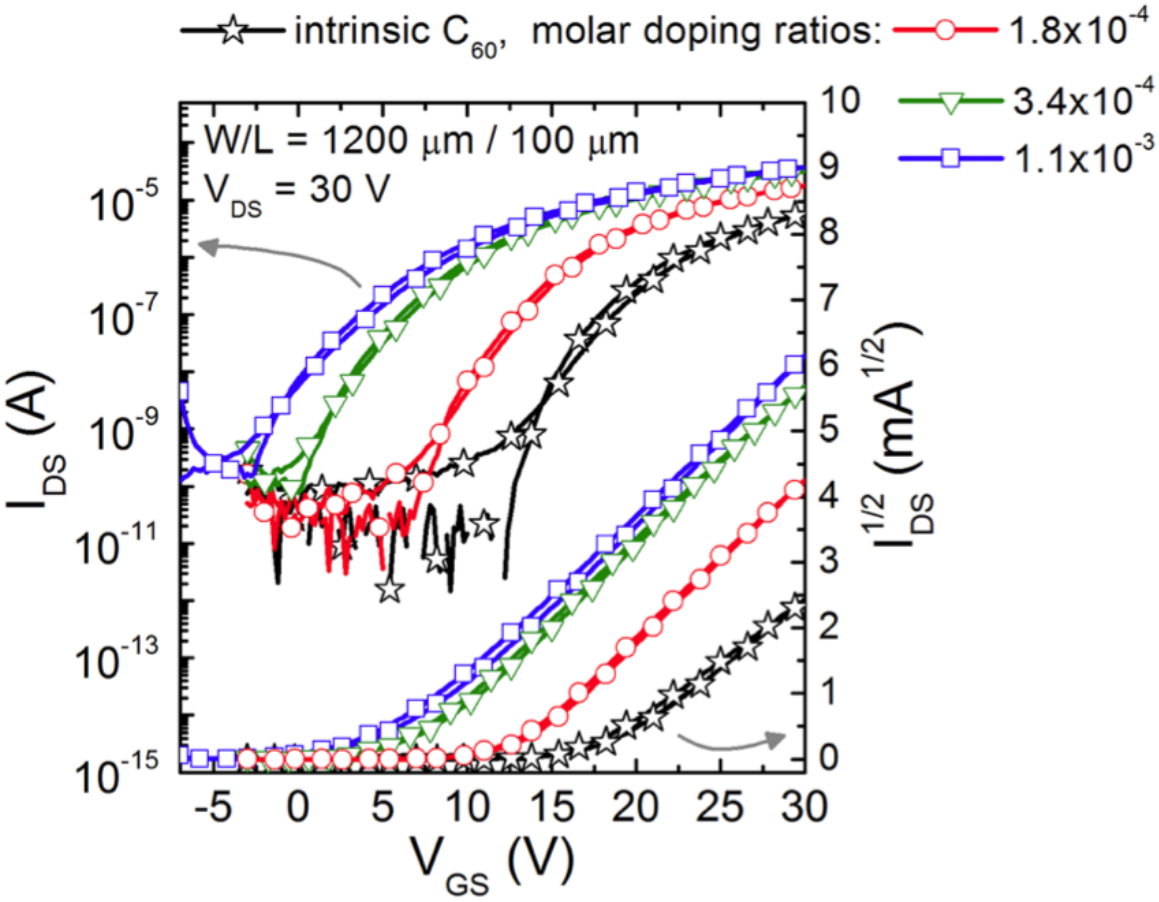

Figure B.3. Effect of doping on threshold voltage. Reprinted with permission from the American Institute of Physics Publishing, LLC.: S. Olthof, S. Singh, S. K. Mohapatra, S. Barlow, S. R. Marder, B. Kippelen, and A. Kahn, "Passivation of trap states in unpurified and purified C_{60} and the influence on organic field-effect transistor performance," *Applied Physics Letters*, vol. 101, no. 25, p. 253303, copyright 2012.

a lower applied bias. Generally, only the top gate is used to modulate the threshold voltage of the bottom gate, and rarely the other way around [132] (Figure B.4). Small molecule organic semiconductors are typically used because of their superior charge carrier mobility, but they tend to have a high surface roughness. Charge transport is only possible along the bottom of the semiconductor [133]. The dual-gate architecture is challenging, but remains a viable means to improve the performance of organic field effect transistors.

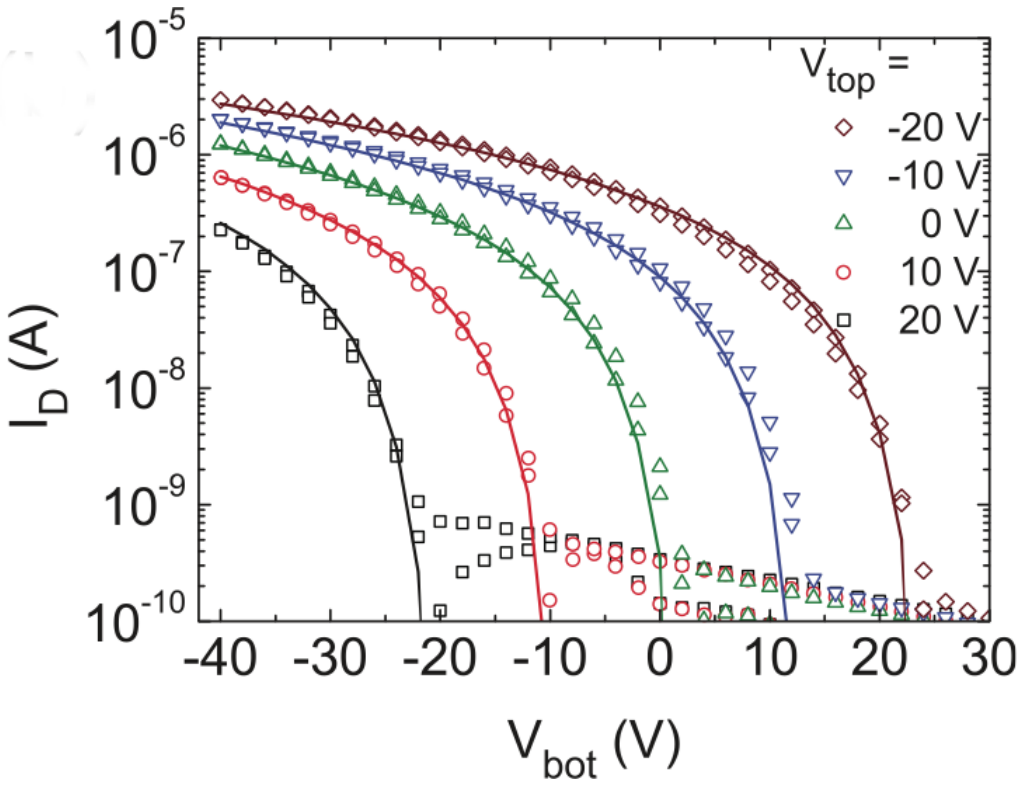

Figure B.4. Modulating the bottom gate threshold voltage by applying a bias to the top gate. Reprinted with permission from the American Institute of Physics Publishing, LLC.: J. Brondijk, M. Spijkman, F. Torricelli, P. Blom, and D. De Leeuw, "Charge transport in dual-gate organic field-effect transistors," *Applied Physics Letters*, vol. 100, no. 2, p. 023308, copyright 2012.

B.4 Alignment and Placement of 1-Dimensional Structures

Several methods already exist for aligning nanofibers. Most offer alignment without placement (*i.e.*, θ is controlled, but x and y are not). While this does afford some improvement of uniformity, the device yield (defined as the probability of having one electrode pair connecting to one nanofiber) tends to be difficult to control. Some methods offer placement in addition, but at the expense of extra process steps. We will review some of the methods that have been demonstrated for organic nanofibers.

One method to align nanofibers involves moving the contact line of a solution on a substrate. In this "stick and slip" method, the substrate moves relative to the solvent-air interface. As the substrate moves, it stretches the meniscus, which compresses it. Nanofibers near the meniscus are drawn in via capillary flow and stick to the substrate. After sufficient stretching, the meniscus slips. During the slip, the fibers are dragged in the same direction (Figure B.5). The result is periodic rows of aligned nanofibers [134]. The nanofiber density and length can be controlled by adjusting the nanofiber concentration and sticking time, respectively [135].

In a variation named "droplet-pinned crystallization," a drop of solution containing the building block molecules is cast onto a substrate. In certain embodiments, a small piece of silicon is placed in the center to create corners. These corners wick solvent through the capillary effect, which draws the solution toward the center. As the solvent evaporates, molecules are deposited on the substrate. The direction of the receding edge of the solvent dictates the direction of the nanofiber alignment. The result is a circle of nanofibers directed toward the center of the circles [136]. Droplets of different materials (*e.g.*, a p-type and an n-type) can be placed on the same substrate. Patterning electrodes on top of the aligned nanofibers produces logic devices, such as inverters [137] (Figure B.6). While both the droplet-pinned crystallization and stick and slip methods were effective in the lab, scaling them to an industrial level will be difficult.

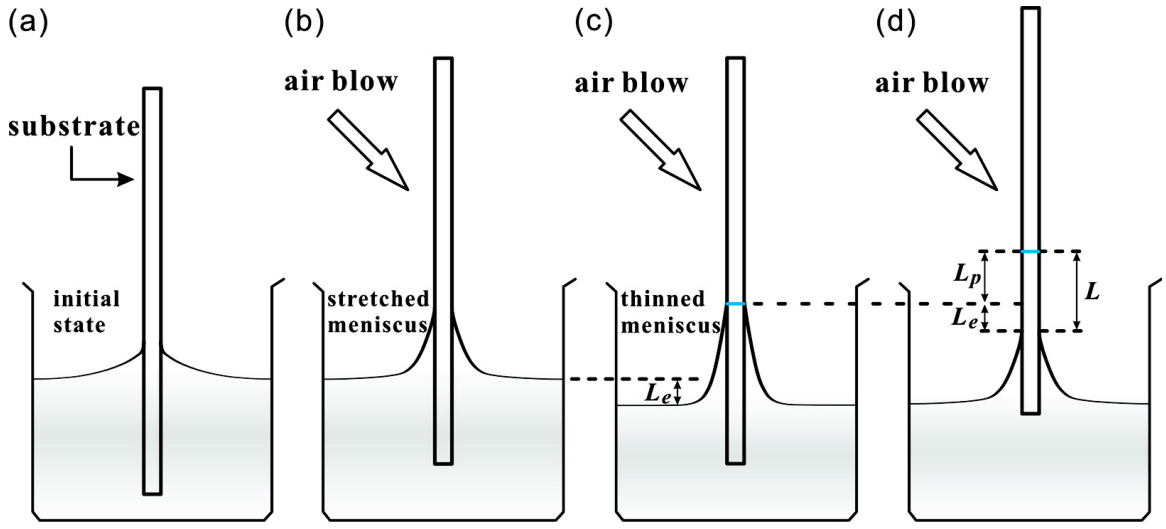

Figure B.5. Overview of the stick and slip process. a) The substrate is placed in a solution containing organic nanofibers. b) The substrate is lifted to stretch the meniscus. c) The substrate is lifted to further stretch the meniscus by a distance of L_e. d) The substrate is lifted once more, by a distance of L_p. This causes the meniscus to slip, leaving a row of aligned nanofibers. Reprinted with permission from the American Chemical Society: N. Liu, Y. Zhou, L. Wang, J. Peng, J. Wang, J. Pei, and Y. Cao, "In situ growing and patterning of aligned organic nanowire arrays via dip coating," *Langmuir*, vol. 25, no. 2, pp. 665-671, copyright 2009.

Electrospinning is another technique widely used for processing organic semiconducting nanofibers, although it is primarily used for polymers. A metal syringe needle is used to deposit the material from solution. A large bias (> 1 kV) is applied between the needle and the substrate. The voltage is large enough to induce charges in the organic materials. These charges respond to the external electric field by elongating the droplet into a nanofiber shape [138]. Patterning the substrate to modify the electric field (*e.g.*, by applying the bias with patterned electrodes) enables alignment to be achieved at a high nanofiber density [139]. Further work could potentially allow this to be a viable technique for organic semiconducting nanofibers based on small molecules.

Microfluidic channels can also be used to align nanofibers and place them in a desired location. The process involves two lithography steps: one to pattern the

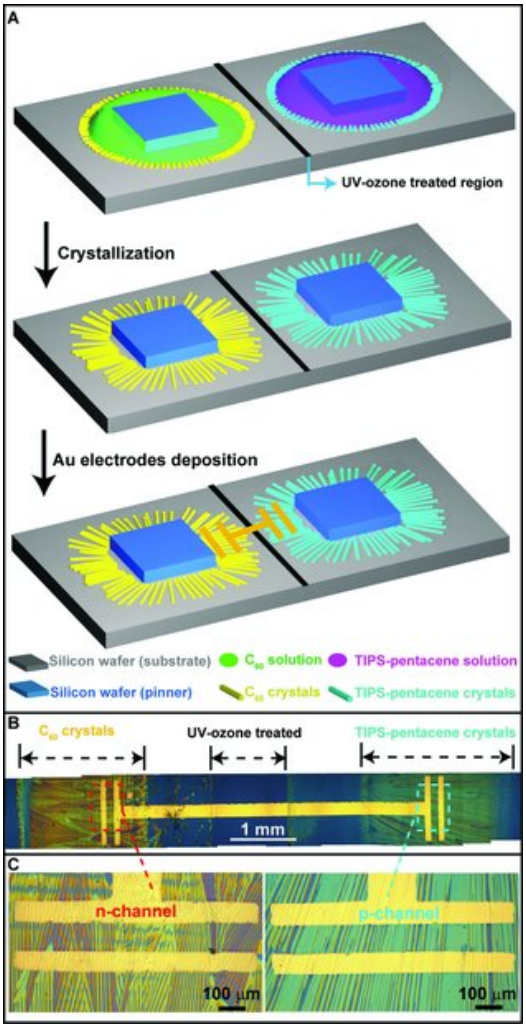

Figure B.6. Overview of the droplet-pinned crystallization process. a) Schematic of the droplet-pinned crystallization process for producing inverters based on organic nanofibers. b and c) Optical images of the nanofibers fabricated using this process. Reprinted with permission from John Wiley and Sons: H. Li, B. C.-K. Tee, G. Giri, J. W. Chung, S. Y. Lee, and Z. Bao, "High- performance transistors and complementary inverters based on solution-grown aligned organic single-crystals," *Advanced Materials*, vol. 24, no. 19, pp. 2588-2591, copyright 2012.

electrodes and one to fabricate the microfluidic channels. A solution containing the semiconducting material is placed in a reservoir and is pulled into the channels by capillary action. As the solution evaporates, the semiconductor is left behind, forming a nanofiber [140]. Nanofibers can be curved by design; they will grow in the shape of the microfluidic channels [141]. This technique was used to create parallel lines of light emitting nanofibers, which emitted highly polarized light [142].

In nanoimprint lithography, the organic semiconductor is deposited on the substrate. Then a hard mold is placed over the top and pressure is applied, which redistributes the soft organic materials into channels cut in the mold. When the mold is removed, the organic semiconductor remains in the desired location [143] (Figure B.7). The process can involve heat [144] or solvent vapor [145] to soften the organic layer. This technique is generally used for polymers; it is unclear if it can be used for small molecules. Additionally, the molds are expensive and can be reused a finite number of times.

A final method for aligning organic nanofibers is the filter-and-transfer technique. A polymer mask is patterned on a porous media. The solution containing the nanofibers is injected through the mask and filter. The nanofibers collect on the media and are aligned by the mask while the solvent passes through the filter. The mask is removed and the nanofibers are transferred to a silicon substrate. Field effect transistors fabricated using this method yielded devices with high electron mobility and good uniformity [113] (Figure B.8). The main drawback of this method is that it requires extra process steps and materials.

B.5 Dielectrophoresis

Among alignment and placement techniques, dielectrophoresis is unique because it offers both alignment and high-accuracy placement without the need for additional process steps (Figure B.9). In this technique, an electric field (typically ac) is applied to a solution containing nanofibers. The electric field induces a dipole in the nanofiber, which enables a Coulombic interaction. Restated, the electric field induces a dipole and then pushes or pulls on it [146].

Dielectrophoresis has been used mainly to align inorganic nanofibers, such as III-V semiconductors [147, 148], ZnO [149], SnO_2 [150], carbon nanotubes [151], etc. In these materials, development is at an advanced stage. Freer *et al.* used dielectrophoresis with a flow cell to produce single nanowire devices with a yield of

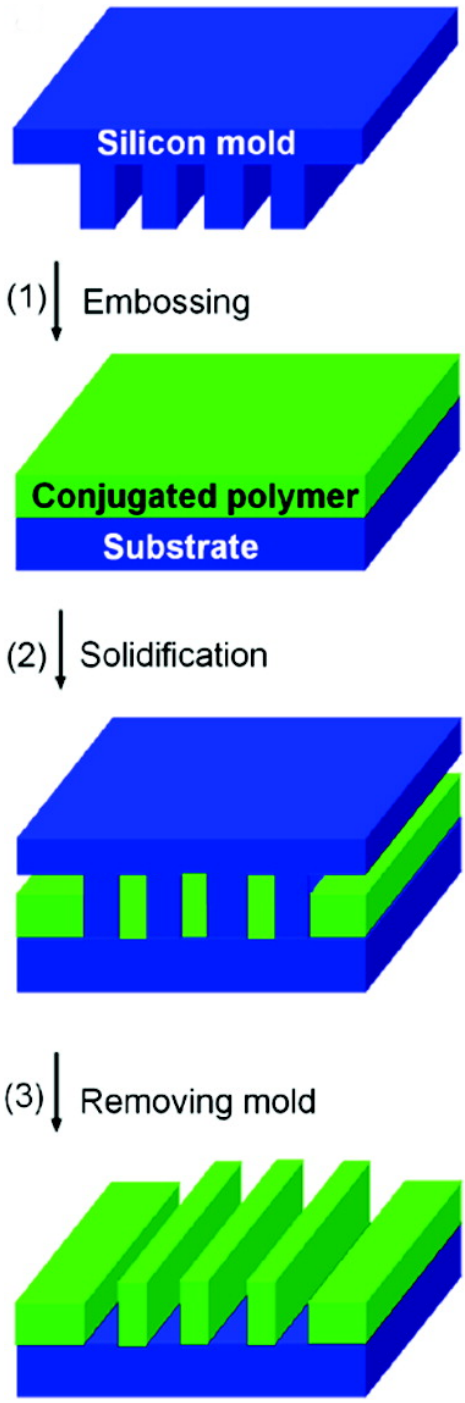

Figure B.7. Overview of the nanoimprint lithography process. Reprinted with permission from the American Chemical Society: Z. Hu, B. Muls, L. Gence, D. A. Serban, J. Hofkens, S. Melinte, B. Nysten, S. Demoustier-Champagne, and A. M. Jonas, "High-throughput fabrication of organic nanowire devices with preferential internal alignment and improved performance," *Nano Letters*, vol. 7, no. 12, pp. 3639-3644, copyright 2007.

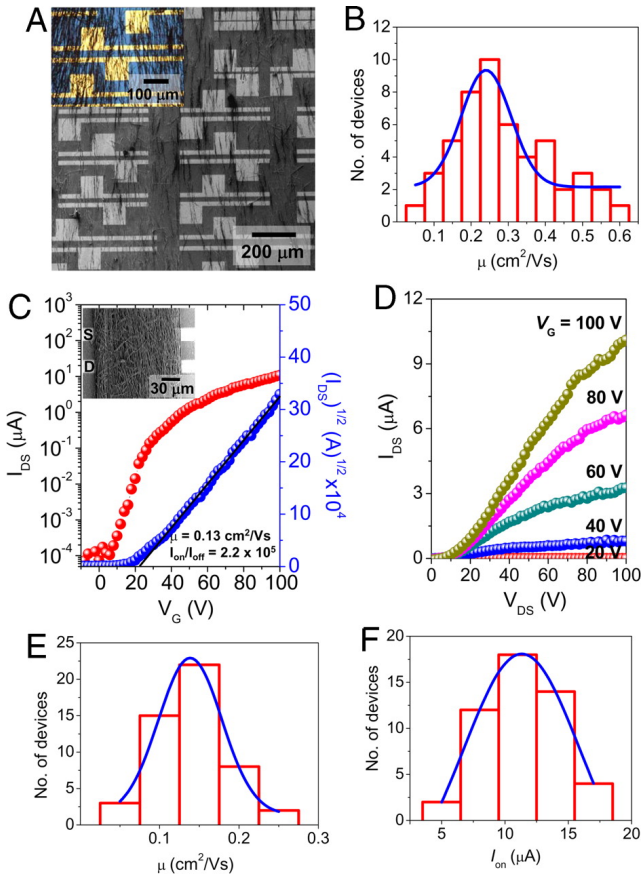

Figure B.8. Field effect transistors fabricated using the filter and transfer process. a) Scanning electron microscopy image of field effect transistors based on nanofibers aligned using the filter and transfer process. b) Histogram of electron mobilities of 50 devices with a low nanofiber density. Transfer (c) and output (d) characteristics for typical devices. Histograms of electron mobility (e) and on current (f) for 50 devices with a high nanofiber density. Reprinted with permission from the National Academy of Sciences: J. H. Oh, H. W. Lee, S. Mannsfeld, R. M. Stoltenberg, E. Jung, Y. W. Jin, J. M. Kim, J.-B. Yoo, and Z. Bao, "Solution-processed, high-performance n-channel organic microwire transistors," *Proceedings of the National Academy of Sciences*, vol. 106, no. 15, pp. 6065-6070, copyright 2009.

98.5%. This is especially astonishing considering the scale they used: over 16,000 electrode pairs were used! Furthermore, they demonstrated precise control over the number of nanowires deposited across a given electrode pair [152]. This technique was also applied to sensors. Gary Hunter's team at the NASA Glenn Research Center developed a process in which nanowires are mixed with a photoresist. This solution is used for dielectrophoresis. Once the solvent is evaporated, the photoresist is patterned

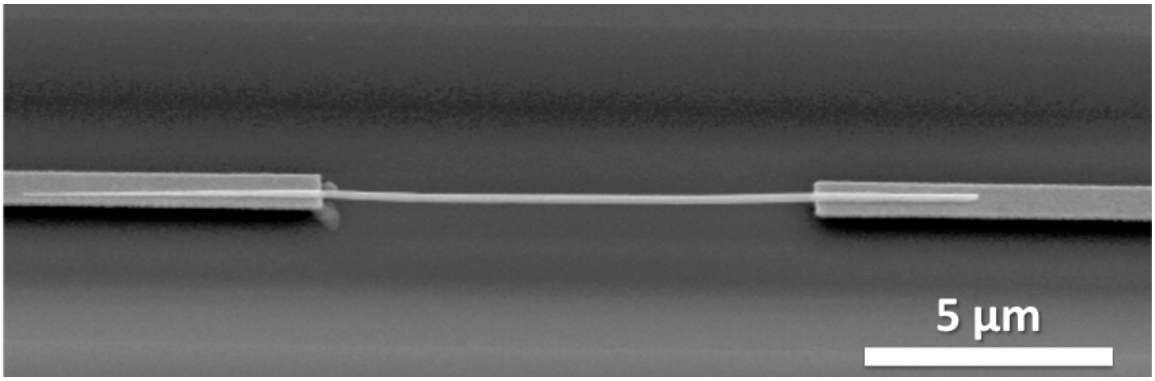

Figure B.9. Scanning electron microscopy image of an InAs nanowire aligned using dielectrophoresis. Reprinted with permission from the American Chemical Society: S. Raychaudhuri, S. A. Dayeh, D. Wang, and E. T. Yu, "Precise semiconductor nanowire placement through dielectrophoresis," *Nano Letters*, vol. 9, no. 6, pp. 2260-2266, copyright 2009.

to expose the portions of the nanowires above the electrodes. Additional metal is deposited to fully encase the nanowire contact in metal. The remaining resist is then stripped, exposing the nanowire within the electrode gap to the environment. The variability, already reduced by the alignment of the nanowires, is further diminished by producing more consistent electrical contacts to the nanowires [153]. With a little extra effort, sensors based on inorganic semiconductors fabricated using dielectrophoresis may become a product.

To fully understand the mechanism, we will analyze the force exerted on a nanofiber by an external electric field. The dielectrophoretic force is given by the following equation:

$$F = c\epsilon_m Re(f_{CM})\nabla E^2 \tag{B.1}$$

where F is the dielectric force, c is a volumetric factor, ϵ_m is the dielectric constant of the medium (*e.g.*, the solvent), f_{CM} is the Clausius-Mossotti factor, and E is the magnitude of the electric field. The Clausius-Mossotti factor is different for the electric field relative to the transverse and longitudinal directions of the nanowire. Along the long axis of a nanofiber, the Clausius-Mossotti factor is given by:

$$f_{cm,long} = \frac{\epsilon_{nf} - \epsilon_m}{\epsilon_m} \tag{B.2}$$

where ϵ_{nf} is the dielectric constant of the nanofiber. In the transverse direction, the factor becomes:

$$f_{cm,trans} = 2\frac{\epsilon_{nf} - \epsilon_m}{\epsilon_{nf} + \epsilon_m} \tag{B.3}$$

Determining the dielectric force exerted on a nanofiber requires calculating the superposition of the transverse and longitudinal forces [147]. Equations B.2 and B.3 highlight the challenge of using dielectrophoresis with organic nanofibers. In both cases, the numerator is $\epsilon_{nf} - \epsilon_m$. Whereas inorganic nanofibers, such as InAs, tend to have relatively high dielectric constants (>10), those of organic semiconductors tend to be lower. The diminished dielectric constants of organic nanofibers decrease the dielectrophoretic force exerted upon them. Further complicating the matter is that the dielectric constants of many organic materials are not reported in the literature, or are disputed. These issues make selecting organic semiconductors for dielectrophoretic alignment a major challenge.

Nevertheless, a few researchers succeeded in aligning organic nanofibers using dielectrophoresis, with the first demonstration in 2004 [154] (Figure B.10). While there are some examples of nanofibers being aligned from solution [155], assembly of aligned nanofibers on the electrodes was also demonstrated [156]. This enables nanofibers that are not long enough to bridge the electrode gap to form working devices while minimizing n and ℓ. However, no application of this process to sensors using organic nanofibers has been performed.

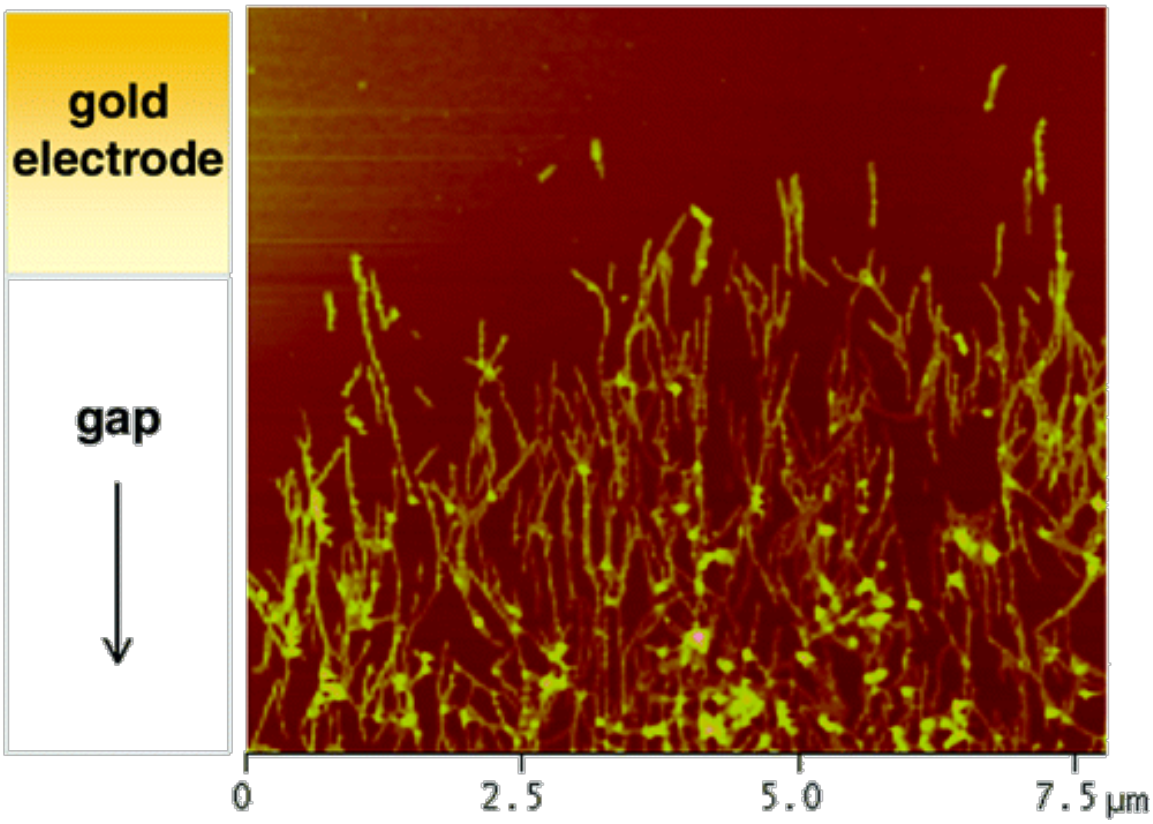

Figure B.10. Atomic force microscopy image of organic nanofibers aligned using dielectrophoresis. Reprinted with permission from the American Chemical Society: B. W. Messmore, J. F. Hulvat, E. D. Sone, and S. I. Stupp, "Synthesis, self-assembly, and characterization of supramolecular polymers from electroactive dendron rodcoil molecules," *Journal of the American Chemical Society*, vol. 126, no. 44, pp. 14452-14458, copyright 2004.

APPENDIX C

CURRICULUM VITA

C.1 Education

- Ph. D., Materials Science and Engineering, University of Utah, 2015.
- M. S., Engineering Management Systems, Union Graduate College, 2009.
- B. S., Electrical Engineering, Union College, 2008.
- B. S., Mathematics, Union College, 2008.

C.2 Work Experience

- Technical Advisor, *Vaporsens*, January 2011-Present.
- Visiting Technologist, *NASA Glenn Research Center*, July 2015
- Visiting Technologist, *NASA Ames Research Center*, May 2014-July 2014.
- Visiting Technologist, *NASA Glenn Research Center*, May 2013-July 2013.
- Cost Engineer, *GE Energy*, May 2008-May 2009.
- Technician II Intern, *Idaho National Laboratory*, June 2007-September 2007.
- Co-Op Process Development Engineer, *IBM*, June 2006-September 2006.

C.3 Publications

13. **B. R. Bunes**, G. M. Berger, A. Biaggia-Labiosa, and L. Zang, "Improved conductivity and uniformity of devices using organic nanofibers aligned by dielectrophoresis," *in preparation.*

12. C. Wang, H. Huang, **B. R. Bunes**, N. Wu, M. Xu, X. Yang, and L. Zang, "Trace detection of RDX, HMX, and PETN explosives using a fluorescence spot sensor," *in preparation.*

11. B. Redd, **B. R. Bunes**, P. Slattum, and L. Zang, "Algorithm to optimize integer preprocessing parameters for sensor signal classification: Examples in explosives and narcotics vapor detection," *in preparation.*

10. C. Wang, **B. R. Bunes**, M. Xu, N. Wu, X. Yang, D. E. Gross, J. S. Moore, and L. Zang, "One-step growth of organic donor-acceptor nanofibril composites for selective alkane vapor detection," *in preparation.*

9. Y. Zhang, M. Xu, **B. R. Bunes**, N. Wu, D. E. Gross, J. S. Moore, and L. Zang, "Oligomer-coated carbon nanotube chemiresistive sensors for selective detection of nitroaromatic explosives," *ACS Applied Materials & Interfaces*, vol. 7, no.14, pp. 7471-7475, 2015.

8. S. Chen, C. Wang, **B. R. Bunes**, Y. Li, C. Wang, and L. Zang, "Enhancement of visible-light-driven photocatalytic H_2 evolution from water over g-C_3N_4 through combination with perylene diimides aggregates," *Applied Catalysis A*, vol. 498, pp. 63-68, 2015.

7. **B. R. Bunes**, M. Xu, Y. Zhang, D. E. Gross, A. Saha, D. L. Jacobs, X. Yang, J. S. Moore, and L. Zang, "Photodoping and enhanced visible light absorption in single-walled carbon nanotubes functionalized with a wide band gap oligomer," *Advanced Materials*, vol. 27, no. 1, pp. 162-167, 2014.

6. L. Li, D. L. Jacobs, **B. R. Bunes**, H. Huang, X. Yang, and L. Zang, "Anomalous high photovoltages observed in shish kebab-like organic p-n junction nanostructures," *Polymer Chemistry*, vol. 5, pp. 309-313, 2014.

5. L. Li, D. L. Jacobs, Y. Che, H. Huang, **B. R. Bunes**, X. Yang and L. Zang, "Poly(3-hexylthiophene) nanofiber networks for enhancing the morphology stability of polymer solar cells," *Organic Electronics*, vol. 14, no. 5, pp. 1383-1390, 2013.

4. M. Xu, **B. R. Bunes**, and L. Zang, "Paper-based vapor detection of hydrogen peroxide: Colorimetric sensing with tunable interface," *ACS Applied Materials & Interfaces*, vol. 3, no. 3, pp. 642-647, 2011.

3. Y. Che, H. Huang, M. Xu, C. Zhang, **B. R. Bunes**, X. Yang, and L. Zang, "Interfacial engineering of organic nanofibril heterojunctions into highly photoconductive materials," *Journal of the American Chemical Society*, vol. 133, no. 4, pp. 1087-1091, 2011.

2. Z. Zhang, Y. Che, R. Smaldone, M. Xu, **B. R. Bunes**, J. S. Moore, and L. Zang, "Reversible dispersion and release of carbon nanotubes using foldable oligomers," *Journal of the American Chemical Society*, vol. 132, no. 40, pp. 14113-14117, 2010.

1. C. Zhang, Y. Che, X. Yang, **B. R. Bunes**, and L. Zang, "Organic nanofibrils based on linear carbazole trimer for explosive sensing," *Chemical Communications*, vol. 46, pp. 5560-5562, 2010.

C.4 Conference Presentations

11. **B. R. Bunes**, T. Knowlton, D. L. Jacobs, P. Slattum, and L. Zang, "Dual gate architecture for high sensitivity, high selectivity chemical-sensing field effect transistors," *IEEE Sensors*, Valencia, ES, November 2014.

10. **B. R. Bunes**, M. Xu, Y. Zhang, D. E. Gross, A. Saha, D. L. Jacobs, X. Yang, J. S. Moore, and L. Zang, "Enhanced visible light absorption and charge separation in carbon nanotubes functionalized with a wide band gap oligomer for improved

photovoltaic cells," *Commercialization of Micro- and Nanosystems*, Salt Lake City, UT, October 2014.

9. **B. R. Bunes**, D. L. Jacobs, P. Slattum, T. Knowlton, and L. Zang, "A dual-gate field effect transistor for chemical vapor detection," *nanoUtah*, Salt Lake City, UT, October 2013.

8. B. Rollins and **B. R. Bunes**, "Sensitive, light weight, ultra-portable point detector," *NAVEOD Workshop*, Washington, DC, October 2012.

7. **B. R. Bunes**, M. Xu, Y. Zhang, Z. Zhang, D. E. Gross, X. Yang, J. S. Moore, and L. Zang, "Photoresponse of field effect transistors based on a single-walled carbon nanotube/polymer composite," *nanoUtah*, Salt Lake City, UT, October 2012.

6. H. Huang, Y. Che, L. Li, M. Xu, **B. R. Bunes**, X. Yang, and L. Zang, "Interfacial engineering of organic nanofibril heterojunctions into highly photoconductive materials and beyond," *221st Meeting of the Electrochemical Society*, Seattle, WA, May 2012.

5. **B. R. Bunes**, M. Xu, H. Huang, and L. Zang, "Vapor detection of peroxide-based explosives on paper substrates," *National Security Innovation Competition*, Colorado Springs, CO, April 2012.

4. **B. R. Bunes**, M. Xu, Z. Zhang, D. E. Gross, R. A. Smaldone, Y. Che, X. Yang, J. S. Moore, and L. Zang, "Optoelectronic properties of carbon nanotube/polymer composites," *nanoUtah*, Salt Lake City, UT, October 2011.

3. **B. R. Bunes**, M. Xu, H. Huang, and L. Zang, "Low cost sensors for improvised explosive devices," *nanoUtah*, Salt Lake City, UT, October 2011.

2. **B. R. Bunes**, M. Xu, H. Huang, and L. Zang, "Low-cost, portable detection of peroxide-based explosive devices," *National Security Innovation Competition*, Colorado Springs, CO, April 2011.

1. H. Huang, M. Xu, C. Zhang, **B. R. Bunes**, Y. Che, and L. Zang, "A nanofiber-based heterojunction approach for high photoconductivity in organic nanofibers," *nanoUtah*, Salt Lake City, UT, October 2010.

With five additional works presented prior to joining the University of Utah.

C.5 Patents

2. **B. R. Bunes** and L. Zang, "Dual-gate field effect transistor for chemical sensing," U-5819 (2014) (provisional).

1. L. Zang, **B. R. Bunes**, and M. Xu, "Multimode micro-electrode chip integrated with nanofibers for multitarget trace vapor detection of explosives," US1256096 (2012).

C.6 Awards and Honors

- Best Paper Award (Gas Sensors Track), IEEE Sensors Conference, 2014.
- Space Technology Research Fellowship, NASA, 2012.
- Finalist, National Security Innovation Competition, 2011, 2012.
- Integrative Graduate Education and Research Traineeship, NSF, 2010.
- Honorable Mention, NSF GRFP, 2009.
- Wayne Brown Fellowship, University of Utah College of Engineering, 2009.

C.7 Professional Activities

- Reviewer: *ACS Applied Materials & Interfaces*, *Advanced Materials*, *Advanced Electronic Materials*

- Organizing Committee: *nanoUtah 2012*
- Graduate Student Advisory Council, 2011-2014
- Institute of Electrical and Electronics Engineers
    1) Electron Device Society
    2) Nanotechnology Council
    3) Sensors Council
- Sigma Xi (Research Honor Society)
- Tau Beta Pi (Engineering Honor Society)
- Eta Kappa Nu (Electrical Engineering Honor Society)
- Golden Key Honour Society

REFERENCES

[1] V. Gain. (2013, July) Global explosives trace detection technologies market to reach $830m in 2013, says new visiongain report. [Online]. Available: https://www.visiongain.com/Press_Release/441/Global-explosive-trace-detection-%28ETD%29-technologies-market-to-reach-830M-in-2013-says-new-Visiongain-report

[2] BCC Research. (2008, July) Drug testing: Technologies and global markets. [Online]. Available: http://www.bccresearch.com/market-research/pharmaceuticals/drug-testing-technology-markets-phm013e.html

[3] S. Ives. (2014, December) Global market for mass transit security to grow 76 percent by 2018. [Online]. Available: http://www.securitysystemsnews.com/article/global-market-mass-transit-security-grow-76-percent-2018

[4] IMS Research. (2011, September) Global explosives detection market reached $1.84 billion in 2010. [Online]. Available: http://www.asmag.com/showpost/12160.aspx

[5] University of Utah Technology and Venture Commercialization Office, October 2014, unpublished.

[6] J. C. Buzby and J. Hyman, "Total and per capita value of food loss in the United States," *Food Policy*, vol. 37, no. 5, pp. 561–570, 2012.

[7] W. Thorson, "Gas sensing for the real world," in *DOE Sensors Workshop*, 2012.

[8] C. Lourenço and C. Turner, "Breath analysis in disease diagnosis: Methodological considerations and applications," *Metabolites*, vol. 4, no. 2, pp. 465–498, 2014.

[9] PR Newswire. (2014, August) Drug testing market: Alcohol/breath analyzer, saliva testers and biosensor industry worth $7 billion by 2020. [Online]. Available: http://www.prnewswire.com/news-releases/drug-testing-market-alcoholbreath-analyzer-saliva-testers-and-biosensor-industry-worth-7-billion-by-2020-271227071.html

[10] K. G. Furton and L. J. Myers, "The scientific foundation and efficacy of the use of canines as chemical detectors for explosives," *Talanta*, vol. 54, no. 3, pp. 487–500, 2001.

[11] R. J. Harper, J. R. Almirall, and K. G. Furton, "Identification of dominant odor chemicals emanating from explosives for use in developing optimal training aid combinations and mimics for canine detection," *Talanta*, vol. 67, no. 2, pp. 313–327, 2005.

[12] I. Gazit and J. Terkel, "Explosives detection by sniffer dogs following strenuous physical activity," *Applied Animal Behaviour Science*, vol. 81, no. 2, pp. 149–161, 2003.

[13] E. de Hoffman and V. Stroobant, *Mass Spectrometry: Principles and Applications*, 3rd ed. John Wiley and Sons, 2007.

[14] R. Ewing, D. Atkinson, G. Eiceman, and G. Ewing, "A critical review of ion mobility spectrometry for the detection of explosives and explosive related compounds," *Talanta*, vol. 54, no. 3, pp. 515 – 529, 2001.

[15] Associated Press. (2009, May) TSA scraps airport screening program. [Online]. Available: http://www.nbcnews.com/id/30875442/ns/travel-news/t/tsa-scraps-airport-screening-program/

[16] Mr. Ryan Harris and Mr. Ryan Ussing, U.S. Army Utah Proving Ground, Dugway, UT, private correspondence., August 2011.

[17] "U.S. handheld and trace explosives detection markets," Frost and Sullivan, San Antonio, TX, Market Report, March 2009.

[18] C. V. Raman and K. S. Krishnan, "A new type of secondary radiation," *Nature*, vol. 121, no. 3048, pp. 501–502, 1928.

[19] X. Zhu, H. Suhr, and Y. Shen, "Surface vibrational spectroscopy by infrared-visible sum frequency generation," *Physical Review B*, vol. 35, no. 6, p. 3047, 1987.

[20] B. H. Hokr, J. N. Bixler, G. D. Noojin, R. J. Thomas, B. A. Rockwell, V. V. Yakovlev, and M. O. Scully, "Single-shot stand-off chemical identification of powders using random raman lasing," *Proceedings of the National Academy of Sciences*, vol. 111, no. 34, pp. 12 320–12 324, 2014.

[21] M. Li, H. X. Tang, and M. L. Roukesm, "Ultra-sensitive NEMS-based cantilevers for sensing, scanned probe and very high-frequency applications," *Nature Nanotechnology*, vol. 2, no. 2, pp. 114–120, 2007.

[22] N. V. Lavrik, M. J. Sepaniak, and P. G. Datskos, "Cantilever transducers as a platform for chemical and biological sensors," *Review of Scientific Instruments*, vol. 75, no. 7, pp. 2229–2253, 2004.

[23] H. Lang, M. Baller, R. Berger, C. Gerber, J. Gimzewski, F. Battiston, P. Fornaro, J. Ramseyer, E. Meyer, and H. Güntherodt, "An artificial nose based on a micromechanical cantilever array," *Analytica Chimica Acta*, vol. 393, no. 1–3, pp. 59–65, 1999.

[24] C. Cumming, C. Aker, M. Fisher, M. Fok, M. la Grone, D. Reust, M. Rockley, T. M. Swager, E. Towers, and V. Williams, "Using novel fluorescent polymers as sensory materials for above-ground sensing of chemical signature compounds emanating from buried landmines," *Geoscience and Remote Sensing, IEEE Transactions on*, vol. 39, no. 6, pp. 1119–1128, 2001.

[25] Q. Zhou and T. M. Swager, "Method for enhancing the sensitivity of fluorescent chemosensors: Energy migration in conjugated polymers," *Journal of the American Chemical Society*, vol. 117, no. 26, pp. 7017–7018, 1995.

[26] T. M. Swager, "The molecular wire approach to sensory signal amplification," *Accounts of Chemical Research*, vol. 31, no. 5, pp. 201–207, 1998.

[27] J. R. Stetter and J. Li, "Amperometric gas sensors - a review," *Chemical Reviews*, vol. 108, no. 2, pp. 352–366, 2008.

[28] M. Baldigowski. (2011) The pros and cons of electrochemical sensors. [Online]. Available: http://www.safetyandhealthmagazine.com/articles/the-pros-and-cons-of-electrochemical-sensors-2

[29] R. Rahman and P. Servati, "Efficient analytical model of conductivity of CNT/polymer composites for wireless gas sensors," *Nanotechnology, IEEE Transactions on*, vol. 14, no. 1, pp. 118–129, 2015.

[30] M. S. Freund and N. S. Lewis, "A chemically diverse conducting polymer-based electronic nose," *Proceedings of the National Academy of Sciences*, vol. 92, no. 7, pp. 2652–2656, 1995.

[31] M. Bernabei, K. Persaud, S. Pantalei, E. Zampetti, and R. Beccherelli, "Large-scale chemical sensor array testing biological olfaction concepts," *Sensors Journal, IEEE*, vol. 12, no. 11, pp. 3174–3183, 2012.

[32] P.-C. Chen, G. Shen, and C. Zhou, "Chemical sensors and electronic noses based on 1-d metal oxide nanostructures," *Nanotechnology, IEEE Transactions on*, vol. 7, no. 6, pp. 668–682, 2008.

[33] C. Sun, K. R. G. Karthik, S. S. Pramana, L. H. Wong, J. Zhang, H. Yizhong, C. H. Sow, N. Mathews, and S. G. Mhaisalkar, "The role of tin oxide surface defects in determining nanonet FET response to humidity and photoexcitation," *Journal of Materials Chemistry C*, vol. 2, pp. 940–945, 2014.

[34] F. Tian, L. Zhao, X.-Y. Xue, Y. Shen, X. Jia, S. Chen, and Z. Wang, "DFT study of CO sensing mechanism on hexagonal WO_3 surface: The role of oxygen vacancy," *Applied Surface Science*, vol. 311, pp. 362 – 368, 2014.

[35] J. Cho, X. Li, Z. Gu, and P. Kurup, "Recognition of explosive precursors using nanowire sensor array and decision tree learning," *Sensors Journal, IEEE*, vol. 12, no. 7, pp. 2384–2391, 2012.

[36] H. Meixner and U. Lampe, "Metal oxide sensors," *Sensors and Actuators B: Chemical*, vol. 33, no. 1–3, pp. 198–202, 1996.

[37] S. Iijima, "Helical microtubules of graphitic carbon," *Nature*, vol. 354, no. 6348, pp. 56–58, 1991.

[38] T. W. Odom, J.-L. Huang, P. Kim, and C. M. Lieber, "Atomic structure and electronic properties of single-walled carbon nanotubes," *Nature*, vol. 391, no. 6662, pp. 62–64, 1998.

[39] R. Saito, M. Fujita, G. Dresselhaus, and M. Dresselhaus, "Electronic structure of chiral graphene tubules," *Applied Physics Letters*, vol. 60, no. 18, pp. 2204–2206, 1992.

[40] J. Li, Y. Lu, Q. Ye, M. Cinke, J. Han, and M. Meyyappan, "Carbon nanotube sensors for gas and organic vapor detection," *Nano Letters*, vol. 3, no. 7, pp. 929–933, 2003.

[41] F. Wang and T. M. Swager, "Diverse chemiresistors based upon covalently modified multiwalled carbon nanotubes," *Journal of the American Chemical Society*, vol. 133, no. 29, pp. 11 181–11 193, 2011.

[42] J. Chen, M. A. Hamon, H. Hu, Y. Chen, A. M. Rao, P. C. Eklund, and R. C. Haddon, "Solution properties of single-walled carbon nanotubes," *Science*, vol. 282, no. 5386, pp. 95–98, 1998.

[43] M. Holzinger, J. Abraham, P. Whelan, R. Graupner, L. Ley, F. Hennrich, M. Kappes, and A. Hirsch, "Functionalization of single-walled carbon nanotubes with (R-)oxycarbonyl nitrenes," *Journal of the American Chemical Society*, vol. 125, no. 28, pp. 8566–8580, 2003.

[44] P. Qi, O. Vermesh, M. Grecu, A. Javey, Q. Wang, H. Dai, S. Peng, and K. J. Cho, "Toward large arrays of multiplex functionalized carbon nanotube sensors for highly sensitive and selective molecular detection," *Nano Letters*, vol. 3, no. 3, pp. 347–351, 2003.

[45] A. Popa, J. Li, and A. C. S. Samia, "Hybrid platinum nanobox/carbon nanotube composites for ultrasensitive gas sensing," *Small*, vol. 9, no. 23, pp. 3928–3933, 2013.

[46] B. R. Bunes, M. Xu, Y. Zhang, D. E. Gross, A. Saha, D. L. Jacobs, X. Yang, J. S. Moore, and L. Zang, "Photodoping and enhanced visible light absorption in single-walled carbon nanotubes functionalized with a wide band gap oligomer," *Advanced Materials*, vol. 27, no. 1, pp. 162–167, 2015.

[47] R. H. Baughman, A. A. Zakhidov, and W. A. de Heer, "Carbon nanotubes–the route toward applications," *Science*, vol. 297, no. 5582, pp. 787–792, 2002.

[48] K. S. Novoselov, A. K. Geim, S. V. Morozov, D. Jiang, Y. Zhang, S. V. Dubonos, I. V. Grigorieva, and A. A. Firsov, "Electric field effect in atomically thin carbon films," *Science*, vol. 306, no. 5696, pp. 666–669, 2004.

[49] F. Schedin, A. K. Geim, S. V. Morozov, E. W. Hill, P. Blake, M. I. Katsnelson, and K. S. Novoselov, "Detection of individual gas molecules adsorbed on graphene," *Nature Materials*, vol. 6, no. 9, pp. 652–655, 2007.

[50] X. Huang, Z. Yin, S. Wu, X. Qi, Q. He, Q. Zhang, Q. Yan, F. Boey, and H. Zhang, "Graphene-based materials: Synthesis, characterization, properties, and applications," *Small*, vol. 7, no. 14, pp. 1876–1902, 2011.

[51] K. F. Mak, C. Lee, J. Hone, J. Shan, and T. F. Heinz, "Atomically thin MoS_2: A new direct-gap semiconductor," *Physical Review Letters*, vol. 105, no. 13, p. 136805, 2010.

[52] F. K. Perkins, A. L. Friedman, E. Cobas, P. Campbell, G. Jernigan, and B. T. Jonker, "Chemical vapor sensing with monolayer MoS_2," *Nano Letters*, vol. 13, no. 2, pp. 668–673, 2013.

[53] K. Lee, R. Gatensby, N. McEvoy, T. Hallam, and G. S. Duesberg, "High-performance sensors based on molybdenum disulfide thin films," *Advanced Materials*, vol. 25, no. 46, pp. 6699–6702, 2013.

[54] X. Huang, Z. Zeng, and H. Zhang, "Metal dichalcogenide nanosheets: Preparation, properties and applications," *Chemical Society Reviews*, vol. 42, no. 5, pp. 1934–1946, 2013.

[55] C. K. Chiang, C. Fincher Jr, Y. Park, A. Heeger, H. Shirakawa, E. Louis, S. Gau, and A. G. MacDiarmid, "Electrical conductivity in doped polyacetylene," *Physical Review Letters*, vol. 39, no. 17, p. 1098, 1977.

[56] C. W. Tang, "Two-layer organic photovoltaic cell," *Applied Physics Letters*, vol. 48, no. 2, pp. 183–185, 1986.

[57] C. W. Tang and S. VanSlyke, "Organic electroluminescent diodes," *Applied Physics Letters*, vol. 51, no. 12, pp. 913–915, 1987.

[58] A. Tsumura, H. Koezuka, and T. Ando, "Macromolecular electronic device: Field-effect transistor with a polythiophene thin film," *Applied Physics Letters*, vol. 49, no. 18, pp. 1210–1212, 1986.

[59] V. Coropceanu, J. Cornil, D. A. da Silva Filho, Y. Olivier, R. Silbey, and J.-L. Brédas, "Charge transport in organic semiconductors," *Chemical Reviews*, vol. 107, no. 4, pp. 926–952, 2007.

[60] T. Sakanoue and H. Sirringhaus, "Band-like temperature dependence of mobility in a solution-processed organic semiconductor," *Nature Materials*, vol. 9, no. 9, pp. 736–740, 2010.

[61] C. Wang, H. Dong, W. Hu, Y. Liu, and D. Zhu, "Semiconducting π-conjugated systems in field-effect transistors: A material odyssey of organic electronics," *Chemical Reviews*, vol. 112, no. 4, pp. 2208–2267, 2011.

[62] P. Stallinga, "Electronic transport in organic materials: Comparison of band theory with percolation/(variable range) hopping theory," *Advanced Materials*, vol. 23, no. 30, pp. 3356–3362, 2011.

[63] G. Horowitz, "Field-effect transistors based on short organic molecules," *Journal Materials Chemistry*, vol. 9, no. 9, pp. 2021–2026, 1999.

[64] S. Olthof, S. Mehraeen, S. K. Mohapatra, S. Barlow, V. Coropceanu, J.-L. Brédas, S. R. Marder, and A. Kahn, "Ultralow doping in organic semiconductors: Evidence of trap filling," *Physical Review Letters*, vol. 109, no. 17, p. 176601, 2012.

[65] J. Takeya, M. Yamagishi, Y. Tominari, R. Hirahara, Y. Nakazawa, T. Nishikawa, T. Kawase, T. Shimoda, and S. Ogawa, "Very high-mobility organic single-crystal transistors with in-crystal conduction channels," *Applied Physics Letters*, vol. 90, no. 10, p. 102120, 2007.

[66] A. B. Chwang and C. D. Frisbie, "Temperature and gate voltage dependent transport across a single organic semiconductor grain boundary," *Journal of Applied Physics*, vol. 90, no. 3, pp. 1342–1349, 2001.

[67] C. Reese and Z. Bao, "High-resolution measurement of the anisotropy of charge transport in single crystals," *Advanced Materials*, vol. 19, no. 24, pp. 4535–4538, 2007.

[68] Z. Liu, H. A. Becerril, M. E. Roberts, Y. Nishi, and Z. Bao, "Experimental study and statistical analysis of solution-shearing processed organic transistors based on an asymmetric small-molecule semiconductor," *Electron Devices, IEEE Transactions on*, vol. 56, no. 2, pp. 176–185, 2009.

[69] J. A. Lim, H. S. Lee, W. H. Lee, and K. Cho, "Control of the morphology and structural development of solution-processed functionalized acenes for high-performance organic transistors," *Advanced Functional Materials*, vol. 19, no. 10, pp. 1515–1525, 2009.

[70] W. Zhang, J. Smith, S. E. Watkins, R. Gysel, M. McGehee, A. Salleo, J. Kirkpatrick, S. Ashraf, T. Anthopoulos, M. Heeney *et al.*, "Indacenodithiophene semiconducting polymers for high-performance, air-stable transistors," *Journal of the American Chemical Society*, vol. 132, no. 33, pp. 11 437–11 439, 2010.

[71] H. Yan, Z. Chen, Y. Zheng, C. Newman, J. R. Quinn, F. Dötz, M. Kastler, and A. Facchetti, "A high-mobility electron-transporting polymer for printed transistors," *Nature*, vol. 457, no. 7230, pp. 679–686, 2009.

[72] H. Pan, Y. Li, Y. Wu, P. Liu, B. S. Ong, S. Zhu, and G. Xu, "Low-temperature, solution-processed, high-mobility polymer semiconductors for thin-film transistors," *Journal of the American Chemical Society*, vol. 129, no. 14, pp. 4112–4113, 2007.

[73] H. Sirringhaus, T. Kawase, R. Friend, T. Shimoda, M. Inbasekaran, W. Wu, and E. Woo, "High-resolution inkjet printing of all-polymer transistor circuits," *Science*, vol. 290, no. 5499, pp. 2123–2126, 2000.

[74] L.-L. Chua, R. H. Friend, and P. K. Ho, "Organic double-gate field-effect transistors: Logic-AND operation," *Applied Physics Letters*, vol. 87, no. 25, p. 253512, 2005.

[75] S. W. Thomas, G. D. Joly, and T. M. Swager, "Chemical sensors based on amplifying fluorescent conjugated polymers," *Chemical Reviews*, vol. 107, no. 4, pp. 1339–1386, 2007.

[76] L. Chen, D. W. McBranch, H.-L. Wang, R. Helgeson, F. Wudl, and D. G. Whitten, "Highly sensitive biological and chemical sensors based on reversible fluorescence quenching in a conjugated polymer," *Proceedings of the National Academy of Sciences*, vol. 96, no. 22, pp. 12 287–12 292, 1999.

[77] J.-S. Yang and T. M. Swager, "Fluorescent porous polymer films as TNT chemosensors: Electronic and structural effects," *Journal of the American Chemical Society*, vol. 120, no. 46, pp. 11 864–11 873, 1998.

[78] T. Naddo, Y. Che, W. Zhang, K. Balakrishnan, X. Yang, M. Yen, J. Zhao, J. S. Moore, and L. Zang, "Detection of explosives with a fluorescent nanofibril film," *Journal of the American Chemical Society*, vol. 129, no. 22, pp. 6978–6979, 2007.

[79] Y. Che and L. Zang, "Enhanced fluorescence sensing of amine vapor based on ultrathin nanofibers," *Chemical Communications*, no. 34, pp. 5106–5108, 2009.

[80] D. Chaudhuri, D. Li, Y. Che, E. Shafran, J. M. Gerton, L. Zang, and J. M. Lupton, "Enhancing long-range exciton guiding in molecular nanowires by h-aggregation lifetime engineering," *Nano Letters*, vol. 11, no. 2, pp. 488–492, 2010.

[81] Y. Che, D. E. Gross, H. Huang, D. Yang, X. Yang, E. Discekici, Z. Xue, H. Zhao, J. S. Moore, and L. Zang, "Diffusion-controlled detection of trinitrotoluene: Interior nanoporous structure and low highest occupied molecular orbital level of building blocks enhance selectivity and sensitivity," *Journal of the American Chemical Society*, vol. 134, no. 10, pp. 4978–4982, 2012.

[82] Y. Che, H. Huang, M. Xu, C. Zhang, B. R. Bunes, X. Yang, and L. Zang, "Interfacial engineering of organic nanofibril heterojunctions into highly photoconductive materials," *Journal of the American Chemical Society*, vol. 133, no. 4, pp. 1087–1091, 2010.

[83] Y. Che, X. Yang, G. Liu, C. Yu, H. Ji, J. Zuo, J. Zhao, and L. Zang, "Ultrathin n-type organic nanoribbons with high photoconductivity and application in optoelectronic vapor sensing of explosives," *Journal of the American Chemical Society*, vol. 132, no. 16, pp. 5743–5750, 2010.

[84] J. Hu, T. W. Odom, and C. M. Lieber, "Chemistry and physics in one dimension: Synthesis and properties of nanowires and nanotubes," *Accounts of Chemical Research*, vol. 32, no. 5, pp. 435–445, 1999.

[85] A. Puretzky, D. Geohegan, X. Fan, and S. Pennycook, "In situ imaging and spectroscopy of single-wall carbon nanotube synthesis by laser vaporization," *Applied Physics Letters*, vol. 76, no. 2, pp. 182–184, 2000.

[86] J. Kong, A. M. Cassell, and H. Dai, "Chemical vapor deposition of methane for single-walled carbon nanotubes," *Chemical Physics Letters*, vol. 292, no. 4, pp. 567–574, 1998.

[87] J. R. Sanchez-Valencia, T. Dienel, O. Gröning, I. Shorubalko, A. Mueller, M. Jansen, K. Amsharov, P. Ruffieux, and R. Fasel, "Controlled synthesis of single-chirality carbon nanotubes," *Nature*, vol. 512, no. 7512, pp. 61–64, 2014.

[88] Z. Zhang, Y. Che, R. A. Smaldone, M. Xu, B. R. Bunes, J. S. Moore, and L. Zang, "Reversible dispersion and release of carbon nanotubes using foldable oligomers," *Journal of the American Chemical Society*, vol. 132, no. 40, pp. 14 113–14 117, 2010.

[89] R. Martel, T. Schmidt, H. Shea, T. Hertel, and Ph. Avouris, "Single-and multi-wall carbon nanotube field-effect transistors," *Applied Physics Letters*, vol. 73, no. 17, pp. 2447–2449, 1998.

[90] V. Derycke, R. Martel, J. Appenzeller, and Ph. Avouris, "Carbon nanotube inter- and intramolecular logic gates," *Nano Letters*, vol. 1, no. 9, pp. 453–456, 2001.

[91] Y. Geng, M. Y. Liu, J. Li, X. M. Shi, and J. K. Kim, "Effects of surfactant treatment on mechanical and electrical properties of CNT/epoxy nanocomposites," *Composites Part A: Applied Science and Manufacturing*, vol. 39, no. 12, pp. 1876–1883, 2008.

[92] D. E. Hill, Y. Lin, A. M. Rao, L. F. Allard, and Y.-P. Sun, "Functionalization of carbon nanotubes with polystyrene," *Macromolecules*, vol. 35, no. 25, pp. 9466–9471, 2002.

[93] M. J. O'Connell, P. Boul, L. M. Ericson, C. Huffman, Y. Wang, E. Haroz, C. Kuper, J. Tour, K. D. Ausman, and R. E. Smalley, "Reversible water-solubilization of single-walled carbon nanotubes by polymer wrapping," *Chemical Physics Letters*, vol. 342, no. 3, pp. 265–271, 2001.

[94] H. Gui, J. K. Streit, J. A. Fagan, A. R. Hight Walker, C. Zhou, and M. Zheng, "Redox sorting of carbon nanotubes," *Nano Letters*, 2015.

[95] H. W. Lee, Y. Yoon, S. Park, J. H. Oh, S. Hong, L. S. Liyanage, H. Wang, S. Morishita, N. Patil, Y. J. Park *et al.*, "Selective dispersion of high purity semiconducting single-walled carbon nanotubes with regioregular poly(3-alkylthiophene)s," *Nature Communications*, vol. 2, p. 541, 2011.

[96] N. M. Dissanayake and Z. Zhong, "Unexpected hole transfer leads to high efficiency single-walled carbon nanotube hybrid photovoltaic," *Nano Letters*, vol. 11, no. 1, pp. 286–290, 2011.

[97] C. Zhang, Y. Che, X. Yang, B. R. Bunes, and L. Zang, "Organic nanofibrils based on linear carbazole trimer for explosive sensing," *Chemical Communications*, vol. 46, no. 30, pp. 5560–5562, 2010.

[98] Y. Zhang, M. Xu, B. R. Bunes, N. Wu, D. E. Gross, J. S. Moore, and L. Zang, "Oligomer-coated carbon nanotube chemiresistive sensors for selective detection of nitroaromatic explosives," *ACS Applied Materials & Interfaces*, vol. 7, no. 14, pp. 7471–7475, 2015.

[99] J. Janata, "Thirty years of CHEMFETs – a personal view," *Electroanalysis*, vol. 16, no. 22, pp. 1831–1835, 2004.

[100] ——, "Potentiometric microsensors," *Chemical Reviews*, vol. 90, no. 5, pp. 691–703, 1990.

[101] J. Janata and M. Josowicz, "Conducting polymers in electronic chemical sensors," *Nature Materials*, vol. 2, no. 1, pp. 19–24, 2003.

[102] M. C. Tanese, D. Fine, A. Dodabalapur, and L. Torsi, "Interface and gate bias dependence responses of sensing organic thin-film transistors," *Biosensors and Bioelectronics*, vol. 21, no. 5, pp. 782–788, 2005.

[103] A.-M. Andringa, C. Piliego, I. Katsouras, P. W. Blom, and D. M. d. Leeuw, "NO_2 detection and real-time sensing with field-effect transistors," *Chemistry of Materials*, vol. 26, no. 1, pp. 773–785, 2013.

[104] A. Das, R. Dost, T. Richardson, M. Grell, J. J. Morrison, and M. L. Turner, "A nitrogen dioxide sensor based on an organic transistor constructed from amorphous semiconducting polymers," *Advanced Materials*, vol. 19, no. 22, pp. 4018–4023, 2007.

[105] A. N. Sokolov, M. E. Roberts, and Z. Bao, "Fabrication of low-cost electronic biosensors," *Materials Today*, vol. 12, no. 9, pp. 12–20, 2009.

[106] M. E. Roberts, A. N. Sokolov, and Z. Bao, "Material and device considerations for organic thin-film transistor sensors," *Journal of Materials Chemistry*, vol. 19, no. 21, pp. 3351–3363, 2009.

[107] J. Janata and M. Josowicz, "Organic semiconductors in potentiometric gas sensors," *Journal of Solid State Electrochemistry*, vol. 13, no. 1, pp. 41–49, 2009.

[108] K. Domanskỳ, D. L. Baldwin, J. W. Grate, T. B. Hall, J. Li, M. Josowicz, and J. Janata, "Development and calibration of field-effect transistor-based sensor array for measurement of hydrogen and ammonia gas mixtures in humid air," *Analytical Chemistry*, vol. 70, no. 3, pp. 473–481, 1998.

[109] V. Podzorov, E. Menard, A. Borissov, V. Kiryukhin, J. Rogers, and M. Gershenson, "Intrinsic charge transport on the surface of organic semiconductors," *Physical Review Letters*, vol. 93, no. 8, p. 086602, 2004.

[110] B. G. Streetman and S. Banerjee, *Solid State Electronic Devices*, 6th ed. Upper Saddle River, NJ: Pearson Prentice Hall, 2000.

[111] M. Jagota and N. Tansu, "Conductivity of nanowire arrays under random and ordered orientation configurations," *Scientific Reports*, vol. 5, p. 10219, 2015.

[112] Q. Zhang, H. Li, M. Poh, F. Xia, Z.-Y. Cheng, H. Xu, and C. Huang, "An all-organic composite actuator material with a high dielectric constant," *Nature*, vol. 419, no. 6904, pp. 284–287, 2002.

[113] J. H. Oh, H. W. Lee, S. Mannsfeld, R. M. Stoltenberg, E. Jung, Y. W. Jin, J. M. Kim, J.-B. Yoo, and Z. Bao, "Solution-processed, high-performance n-channel organic microwire transistors," *Proceedings of the National Academy of Sciences*, vol. 106, no. 15, pp. 6065–6070, 2009.

[114] Y. Liu, J.-H. Chung, W. K. Liu, and R. S. Ruoff, "Dielectrophoretic assembly of nanowires," *The Journal of Physical Chemistry B*, vol. 110, no. 29, pp. 14 098–14 106, 2006.

[115] D. E. Gross and J. S. Moore, "Arylene–ethynylene macrocycles via depolymerization–macrocyclization," *Macromolecules*, vol. 44, no. 10, pp. 3685–3687, 2011.

[116] T. Ebbesen, H. Lezec, H. Hiura, J. Bennett, H. Ghaemi, and T. Thio, "Electrical conductivity of individual carbon nanotubes," *Nature*, vol. 382, no. 54 – 56, 1996.

[117] S. Okada and A. Oshiyama, "Curvature-induced metallization of double-walled semiconducting zigzag carbon nanotubes," *Physical Review Letters*, vol. 91, no. 21, p. 216801, 2003.

[118] H. Qiu, Z. Shi, L. Guan, L. You, M. Gao, S. Zhang, J. Qiu, and Z. Gu, "High-efficient synthesis of double-walled carbon nanotubes by arc discharge method using chloride as a promoter," *Carbon*, vol. 44, no. 3, pp. 516–521, 2006.

[119] M. S. Arnold, A. A. Green, J. F. Hulvat, S. I. Stupp, and M. C. Hersam, "Sorting carbon nanotubes by electronic structure using density differentiation," *Nature Nanotechnology*, vol. 1, no. 1, pp. 60–65, 2006.

[120] J. A. Rogers, Z. Bao, K. Baldwin, A. Dodabalapur, B. Crone, V. Raju, V. Kuck, H. Katz, K. Amundson, J. Ewing *et al.*, "Paper-like electronic displays: Large-area rubber-stamped plastic sheets of electronics and microencapsulated electrophoretic inks," *Proceedings of the National Academy of Sciences*, vol. 98, no. 9, pp. 4835–4840, 2001.

[121] K. Myny, E. van Veenendaal, G. H. Gelinck, J. Genoe, W. Dehaene, and P. Heremans, "An 8-bit, 40-instructions-per-second organic microprocessor on plastic foil," *Solid-State Circuits, IEEE Journal of*, vol. 47, no. 1, pp. 284–291, 2012.

[122] H. Marien, M. S. Steyaert, E. van Veenendaal, and P. Heremans, "A fully integrated ADC in organic thin-film transistor technology on flexible plastic foil," *Solid-State Circuits, IEEE Journal of*, vol. 46, no. 1, pp. 276–284, 2011.

[123] K. Myny, M. J. Beenhakkers, N. A. van Aerle, G. H. Gelinck, J. Genoe, W. Dehaene, and P. Heremans, "Unipolar organic transistor circuits made robust by dual-gate technology," *Solid-State Circuits, IEEE Journal of*, vol. 46, no. 5, pp. 1223–1230, 2011.

[124] S. C. Mannsfeld, B. C. Tee, R. M. Stoltenberg, C. V. H. Chen, S. Barman, B. V. Muir, A. N. Sokolov, C. Reese, and Z. Bao, "Highly sensitive flexible pressure

sensors with microstructured rubber dielectric layers," *Nature Materials*, vol. 9, no. 10, pp. 859–864, 2010.

[125] E. Cantatore, T. C. Geuns, G. H. Gelinck, E. van Veenendaal, A. F. Gruijthuijsen, L. Schrijnemakers, S. Drews, and D. M. de Leeuw, "A 13.56-mhz rfid system based on organic transponders," *Solid-State Circuits, IEEE Journal of*, vol. 42, no. 1, pp. 84–92, 2007.

[126] J. Zaumseil and H. Sirringhaus, "Electron and ambipolar transport in organic field-effect transistors," *Chemical Reviews*, vol. 107, no. 4, pp. 1296–1323, 2007.

[127] A. Wang, I. Kymissis, V. Bulović, and A. I. Akinwande, "Tunable threshold voltage and flatband voltage in pentacene field effect transistors," *Applied Physics Letters*, vol. 89, no. 11, p. 112109, 2006.

[128] J. Takeya, T. Nishikawa, T. Takenobu, S. Kobayashi, Y. Iwasa, T. Mitani, C. Goldmann, C. Krellner, and B. Batlogg, "Effects of polarized organosilane self-assembled monolayers on organic single-crystal field-effect transistors," *Applied Physics Letters*, vol. 85, no. 21, pp. 5078–5080, 2004.

[129] S. Kobayashi, T. Nishikawa, T. Takenobu, S. Mori, T. Shimoda, T. Mitani, H. Shimotani, N. Yoshimoto, S. Ogawa, and Y. Iwasa, "Control of carrier density by self-assembled monolayers in organic field-effect transistors," *Nature Materials*, vol. 3, no. 5, pp. 317–322, 2004.

[130] R. P. Ortiz, A. Facchetti, and T. J. Marks, "High-k organic, inorganic, and hybrid dielectrics for low-voltage organic field-effect transistors," *Chemical Reviews*, vol. 110, no. 1, pp. 205–239, 2010.

[131] S. Olthof, S. Singh, S. K. Mohapatra, S. Barlow, S. R. Marder, B. Kippelen, and A. Kahn, "Passivation of trap states in unpurified and purified C_{60} and the influence on organic field-effect transistor performance," *Applied Physics Letters*, vol. 101, no. 25, p. 253303, 2012.

[132] T. Fujimoto, M. M. Matsushita, and K. Awaga, "Dual-gate field-effect transistors of octathio [8] circulene thin-films with ionic liquid and SiO_2 gate dielectrics," *Applied Physics Letters*, vol. 97, no. 12, p. 123303, 2010.

[133] J. B. Koo, C. H. Ku, J. W. Lim, and S. H. Kim, "Novel organic inverters with dual-gate pentacene thin-film transistor," *Organic Electronics*, vol. 8, no. 5, pp. 552–558, 2007.

[134] C. Zhang, X. Zhang, X. Zhang, X. Fan, J. Jie, J. C. Chang, C.-S. Lee, W. Zhang, and S.-T. Lee, "Facile one-step growth and patterning of aligned squaraine nanowires via evaporation-induced self-assembly," *Advanced Materials*, vol. 20, no. 9, pp. 1716–1720, 2008.

[135] N. Liu, Y. Zhou, L. Wang, J. Peng, J. Wang, J. Pei, and Y. Cao, "In situ growing and patterning of aligned organic nanowire arrays via dip coating," *Langmuir*, vol. 25, no. 2, pp. 665–671, 2009.

[136] H. Li, B. C. Tee, J. J. Cha, Y. Cui, J. W. Chung, S. Y. Lee, and Z. Bao, "High-mobility field-effect transistors from large-area solution-grown aligned C_{60} single crystals," *Journal of the American Chemical Society*, vol. 134, no. 5, pp. 2760–2765, 2012.

[137] H. Li, B. C.-K. Tee, G. Giri, J. W. Chung, S. Y. Lee, and Z. Bao, "High-performance transistors and complementary inverters based on solution-grown aligned organic single-crystals," *Advanced Materials*, vol. 24, no. 19, pp. 2588–2591, 2012.

[138] D. Li and Y. Xia, "Electrospinning of nanofibers: Reinventing the wheel?" *Advanced Materials*, vol. 16, no. 14, pp. 1151–1170, 2004.

[139] D. Li, Y. Wang, and Y. Xia, "Electrospinning of polymeric and ceramic nanofibers as uniaxially aligned arrays," *Nano Letters*, vol. 3, no. 8, pp. 1167–1171, 2003.

[140] M. Hamedi, K. Tvingstedt, R. H. Karlsson, and O. Ingana s, "Bridging dimensions in organic electronics: Assembly of electroactive polymer nanodevices from fluids," *Nano Letters*, vol. 9, no. 2, pp. 631–635, 2009.

[141] A. M. Hung and S. I. Stupp, "Simultaneous self-assembly, orientation, and patterning of peptide-amphiphile nanofibers by soft lithography," *Nano Letters*, vol. 7, no. 5, pp. 1165–1171, 2007.

[142] C. De Marco, E. Mele, A. Camposeo, R. Stabile, R. Cingolani, and D. Pisignano, "Organic light-emitting nanofibers by solvent-resistant nanofluidics," *Advanced Materials*, vol. 20, no. 21, pp. 4158–4162, 2008.

[143] Z. Hu, B. Muls, L. Gence, D. A. Serban, J. Hofkens, S. Melinte, B. Nysten, S. Demoustier-Champagne, and A. M. Jonas, "High-throughput fabrication of organic nanowire devices with preferential internal alignment and improved performance," *Nano Letters*, vol. 7, no. 12, pp. 3639–3644, 2007.

[144] N. Stutzmann, T. A. Tervoort, D. J. Broer, H. Sirringhaus, R. H. Friend, and P. Smith, "Microcutting materials on polymer substrates," *Advanced Functional Materials*, vol. 12, no. 2, pp. 105–109, 2002.

[145] N. E. Voicu, S. Ludwigs, E. J. Crossland, P. Andrew, and U. Steiner, "Solvent-vapor-assisted imprint lithography," *Advanced Materials*, vol. 19, no. 5, pp. 757–761, 2007.

[146] R. Martinez-Duarte, "Microfabrication technologies in dielectrophoresis applications – a review," *Electrophoresis*, vol. 33, no. 21, pp. 3110–3132, 2012.

[147] S. Raychaudhuri, S. A. Dayeh, D. Wang, and E. T. Yu, "Precise semiconductor nanowire placement through dielectrophoresis," *Nano Letters*, vol. 9, no. 6, pp. 2260–2266, 2009.

[148] T. Kim, S. Lee, N. Cho, H. Seong, H. Choi, S. Jung, and S. Lee, "Dielectrophoretic alignment of gallium nitride nanowires (GaN NWs) for use in device applications," *Nanotechnology*, vol. 17, no. 14, p. 3394, 2006.

[149] C. S. Lao, J. Liu, P. Gao, L. Zhang, D. Davidovic, R. Tummala, and Z. L. Wang, "ZnO nanobelt/nanowire schottky diodes formed by dielectrophoresis alignment across Au electrodes," *Nano Letters*, vol. 6, no. 2, pp. 263–266, 2006.

[150] A. Biaggi-Labiosa, F. Solá, M. Lebrón-Colón, L. Evans, J. Xu, G. Hunter, G. Berger, and J. González, "A novel methane sensor based on porous SnO_2 nanorods: Room temperature to high temperature detection," *Nanotechnology*, vol. 23, no. 45, p. 455501, 2012.

[151] S. Shekhar, P. Stokes, and S. I. Khondaker, "Ultrahigh density alignment of carbon nanotube arrays by dielectrophoresis," *ACS Nano*, vol. 5, no. 3, pp. 1739–1746, 2011.

[152] E. M. Freer, O. Grachev, X. Duan, S. Martin, and D. P. Stumbo, "High-yield self-limiting single-nanowire assembly with dielectrophoresis," *Nature Nanotechnology*, vol. 5, no. 7, pp. 525–530, 2010.

[153] G. Hunter, R. Vander Wal, L. Evans, J. Xu, G. Berger, M. Kullis, and A. Biaggi-Labiosa, "Nanostructured material sensor processing using microfabrication techniques," *Sensor Review*, vol. 32, no. 2, pp. 106–117, 2012.

[154] B. W. Messmore, J. F. Hulvat, E. D. Sone, and S. I. Stupp, "Synthesis, self-assembly, and characterization of supramolecular polymers from electroactive dendron rodcoil molecules," *Journal of the American Chemical Society*, vol. 126, no. 44, pp. 14 452–14 458, 2004.

[155] V. Duzhko, J. Du, C. A. Zorman, and K. D. Singer, "Electric field patterning of organic nanoarchitectures with self-assembled molecular fibers," *The Journal of Physical Chemistry C*, vol. 112, no. 32, pp. 12 081–12 084, 2008.

[156] Y. Shoji, M. Yoshio, T. Yasuda, M. Funahashi, and T. Kato, "Alignment of photoconductive self-assembled fibers composed of π-conjugated molecules under electric fields," *Journal of Materials Chemistry*, vol. 20, no. 1, pp. 173–179, 2010.